



## Application of electrochemical impedance spectroscopy to commercial Li-ion cells: A review



Nina Meddings<sup>a,1</sup>, Marco Heinrich<sup>b,1</sup>, Frédéric Overney<sup>c</sup>, Jong-Sook Lee<sup>d,\*\*\*</sup>, Vanesa Ruiz<sup>e</sup>, Emilio Napolitano<sup>e</sup>, Steffen Seitz<sup>b</sup>, Gareth Hinds<sup>a</sup>, Rinaldo Raccichini<sup>a,\*</sup>, Miran Gaberšček<sup>f,\*\*</sup>, Juyeon Park<sup>a,\*\*\*</sup>

<sup>a</sup> National Physical Laboratory, Hampton Road, Teddington, TW11 0LW, United Kingdom

<sup>b</sup> Physikalisch-Technische Bundesanstalt (PTB), Braunschweig, D 38116, Germany

<sup>c</sup> Federal Institute of Metrology METAS, Bern, 3003, Switzerland

<sup>d</sup> School of Materials Science and Engineering, Chonnam National University, Gwangju, 61186, South Korea

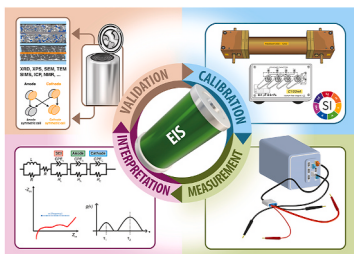
<sup>e</sup> European Commission, Joint Research Centre (JRC), Directorate for Energy, Transport & Climate, Energy Storage Unit, Westerduinweg 3, NL-1755 LE, Petten, the Netherlands

<sup>f</sup> Department of Materials Chemistry, National Institute of Chemistry, Hajdrihova 19, 1000, Ljubljana, Slovenia

### HIGHLIGHTS

- Comprehensive evaluation of EIS-based techniques for investigation of commercial LIBs.
- In-depth report and analysis of a large number of papers dealing with commercial LIBs.
- Critical assessment of the state-of-the-art for EIS calibration and measurement.
- Critical assessment of the state-of-the-art for EIS interpretation and validation.
- Critical review of both standard and new, physics-based equivalent circuit models.

### GRAPHICAL ABSTRACT



### ARTICLE INFO

#### Keywords:

Lithium-ion battery

EIS

Interpretation

Validation

Metrology

Degradation

### ABSTRACT

Electrochemical impedance spectroscopy (EIS) is a widely applied non-destructive method of characterisation of Li-ion batteries. Despite its ease of application, there are inherent challenges in ensuring the quality and reproducibility of the measurement, as well as reliable interpretation and validation of impedance data. Here, we present a focus review summarising best metrological practice in the application of EIS to commercial Li-ion cells. State-of-the-art methods of EIS interpretation and validation are also reported and examined to highlight the benefits and drawbacks of the technique.

\* Corresponding author.

\*\* Corresponding author.

\*\*\* Corresponding author.

\*\*\*\* Corresponding author.

E-mail addresses: [jongsook@jnu.ac.kr](mailto:jongsook@jnu.ac.kr) (J.-S. Lee), [rinaldo.raccichini@npl.co.uk](mailto:rinaldo.raccichini@npl.co.uk) (R. Raccichini), [miran.gaberscek@ki.si](mailto:miran.gaberscek@ki.si) (M. Gaberšček), [juyeon.park@npl.co.uk](mailto:juyeon.park@npl.co.uk) (J. Park).

<sup>1</sup> These authors contributed equally.

## 1. Introduction

The internal impedance of a battery is an important characteristic that has a direct effect on its operating voltage, rate capability and efficiency, and can also affect its practical capacity. In practical terms, impedance is the opposition to current flow through the battery, leading to overpotentials during charge and discharge. Impedance generally increases as a function of cell ageing due to degradation of the electrode materials, electrolyte, and electrical contacts within the cell [1]. Characterising impedance, therefore, is integral in defining battery operational boundaries, estimating performance and tracking state of health (SOH) and state of function (SOF) [2,3].

Commercial Li-ion batteries (LIBs) are complex systems consisting of many components: each cell contains a cathode, anode, current collectors, separator and electrolyte, as well as electrical contacts. These components each give rise to various sources of impedance, including resistive, capacitive and inductive contributions, both electrical and electrochemical in nature [1]. Additional impedance sources and effects arise when cells are combined to form modules and packs, which has been the subject of several studies [4–11]. However, since the present review focuses on commercial cell-level impedance, modules and packs are not discussed here. The aim of this review paper is to report and evaluate the state-of-the-art in how to measure, interpret and validate impedance of commercial Li-ion cells. We would like to point out that, in this paper, the terms battery and cell are used interchangeably to describe a single unit of commercially available battery product.

Electrochemical impedance spectroscopy (EIS) is a powerful and widely used non-invasive test method for characterisation of LIBs [12]. As a non-destructive technique, EIS can be used at various points throughout a battery's lifetime as a diagnostic or prognostic tool: for quality assurance [13–16]; for state estimation [17] including (i) state of charge (SOC) [18–27], (ii) SOH [8,25,28–34], (iii) SOF [35]; for monitoring of internal temperature [36–42]; and for characterisation for second-life applications [30,43–45].

The measurement approach typically consists of applying a sinusoidal current (galvanostatic mode, GEIS) or voltage (potentiostatic mode, PEIS) of a certain amplitude and frequency, and measuring the amplitude and phase shift of the output voltage or current, respectively [46]. This procedure is repeated for a number of frequencies, typically in the kHz to mHz range, thereby generating a characteristic impedance spectrum. In this way, it is possible to probe processes with different time constants within the battery. Features on the resulting Nyquist plot (where the imaginary part of the impedance is plotted against the real part) and/or Bode plot (where either magnitude and phase, or real and imaginary parts, are plotted as a function of frequency) enable parameterisation of the resistance, capacitance, and inductance of the various cell components and processes [47]. Fig. 1 shows an idealised Nyquist plot for a commercial LIB. The inductive behaviour observed in the upper frequency range of the spectrum can be an artefact of the measurement system (wires connecting the cell to the measuring device) [48,49], but may also stem from the geometry of the cell and cell windings [50]. The high-frequency intercept with the real axis, when the inductance effect is properly subtracted [51], corresponds to the sum of internal ohmic resistances, including the electrolyte, active material, current collectors and electrical (metallic) contacts. The arcs appearing in the mid-frequency range are primarily due to the electrochemical processes occurring at the electrode/electrolyte interfaces inside the cell, which combine resistive and capacitive effects. At each electrode, lithium transport through the solid electrolyte interphase (SEI) occurs in parallel with dielectric polarisation, and lithium (de-)intercalation occurs in parallel with double layer (dis)charging [52]. Thus there are contributions from at least four different processes (anode charge transfer, anode SEI, cathode charge transfer, cathode SEI). However, some research works suggest a possible additional contribution of the current collector/active material contacts in commercial cells [53,54]. In the context of commercial cells, the low-frequency tail mainly reflects

solid state lithium ion diffusion in the active material of the cell electrodes [52,55], although other diffusion aspects (e.g., diffusion in electrolyte-filled pores within the electrodes [56,57] and concentration gradients within the separator [58]) have been considered. Interpretation of EIS spectra is discussed in more detail in section 3.2.

Identifying the relative contribution of the different features in the impedance spectrum as a function of operating conditions can aid in the design and development of batteries [59–64]. However, since EIS of commercial cells relies on two-electrode measurements, detailed attribution of the features can be ambiguous. Similar time constants for any of the various interfacial electrochemical processes occurring at the two electrodes will result in merged mid-frequency arcs in the Nyquist plot [65], making it difficult to distinguish between them. Incorporation of a third, (micro-)reference electrode into modified commercial cells has been reported in order to deconvolute the responses of the anode and cathode [32,66–68], but requires great care in interpretation of data, and is not yet employed as a mass-production solution [69]. Insights into the contribution of charge transfer, SEI and particle-to-particle resistances can be gained by examining how spectra change as a function of SOC and temperature [48,70–72] (varying the electrolyte concentration can also be helpful [73], but this is only possible in lab-scale cells). It can also be helpful to correlate impedance changes with differential capacity analysis [74]. Additionally, impedance measurements in lab-scale three-electrode half cells [53,55,60,75–87], or symmetric two-electrode cells [32,88–92], using electrode samples harvested from commercial cells, can be used to validate and guide interpretation of commercial cell measurements. This is discussed in more detail in the Postmortem analysis section (Section 3.3.2).

Since typically the impedance spectrum of a cell, and the contribution of each of the different processes described above, varies as a function of temperature, SOC and SOH, EIS is a powerful tool for understanding and estimating battery performance under different operating conditions [74,93–99], as required for battery management and control strategies [100–104]. For example, EIS measurements can be used to determine the parameters of equivalent circuit models developed to describe and predict the behaviour of LIBs [27,52,57,71,85,93,103,105–117]. Note that the effects on impedance of temperature, SOC

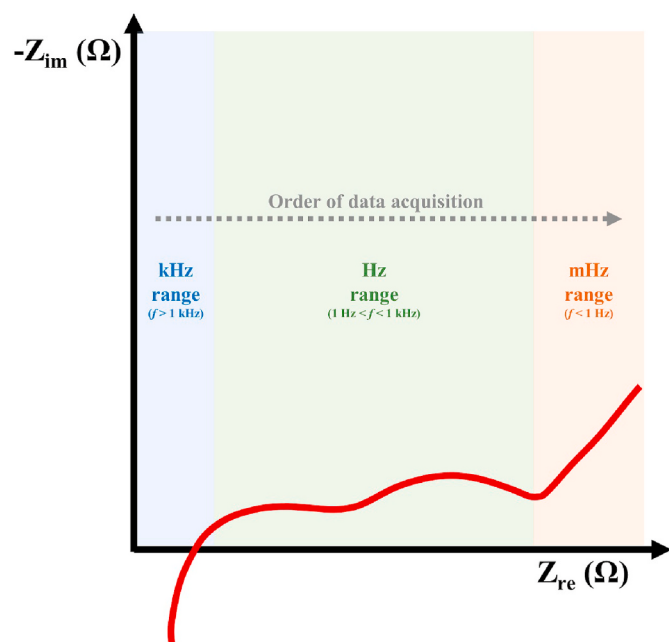


**Fig. 1.** Graphical representation of a typical Li-ion cell EIS measurement presented in a complex impedance plot (i.e., Nyquist plot).  $f$  is the frequency and, the order of data acquisition refers to the order in which frequencies are typically interrogated.

and SOH can, however, be complex, and decoupling them is a challenge for the application of EIS measurements, requiring careful design of experiments, measurements and analysis [13,118–121]. In addition, relationships between impedance and operating parameters may change depending on the level of ageing, which must be accounted for in modelling/estimation [4,94,122].

Clearly, the usefulness of EIS measurements for state estimation depends on the exact relationships between the impedance spectra and the variable in question. For some cell chemistries, such as those with  $\text{LiNi}_x\text{Mn}_y\text{Co}_z\text{O}_2$ -based (NMC) cathodes, there is a clear relationship between impedance and SOC, for example; but for others, particularly those with  $\text{LiFePO}_4$ -based (LFP) cathodes, estimation can be much more challenging [123]. The same may be true for SOH [124]. Impedance contributions from individual cell components/processes, or at particular frequencies, may show a clearer/stronger correlation to SOC, SOH/SOF or remaining useful life than the overall cell impedance [35, 120,123,125–129,133]. Individual impedance contributions may also correlate more strongly than total impedance with ‘sudden death’ (i.e. rapid capacity fade) of cells [127,130–132]. The challenge in using impedance data for sudden death prediction (or avoidance), however, is whether early warning signals can be identified in the measurements, in addition to impedance changes that happen concurrently with rapid capacity fade. Rapid capacity fade is often preceded by lithium plating on the anode, which has been associated with certain changes in the impedance spectra; thus detection of plating via EIS may be helpful as an advance indicator for sudden death [134,135].

With regard to cell ageing, EIS has been widely used to study degradation and degradation mechanisms of commercial LIBs during cycling and calendar ageing [70,75,90,98,122,129,136–147] and to understand the impact of different cycling/storage conditions, including temperature [79,80,127,148–155], rate of cell charge/discharge (C-rate) [81,125,156–162], charging protocol [100,163–165], overcharge/discharge [82,166–168], SOC/depth of discharge (DOD) [169–173] and other storage/operating conditions [174–186], as well as manufacturing factors such as electrode misalignment [54], time required for cell formation [187,188], cell bracing [189], and application of external pressure [190]. The information gained from these studies is clearly relevant for several aspects, including design and development of cells and materials, battery management and control strategies, and extrapolation of accelerated ageing tests to real-world conditions. Generally, the number of reference tests in a cycle or calendar life test should be low enough to avoid additional stress caused by the characterisation itself, but still provide sufficient performance data to allow adequate evaluation of ageing effects [172,191]. Compared to other, destructive, techniques, EIS allows degradation to be studied as it evolves, avoids the risk of spurious results arising from sample damage during cell disassembly [192], and reduces the technical effort required, thus reducing time and costs [65].

Whilst indispensable for a thorough understanding of cell impedance, conventional EIS measurements require specialised equipment [12] and are beyond the capability of most on-board battery management systems [193], although there is also great interest in on-board impedance measurements for state estimation [194]. Approaches for on-board impedance spectroscopy (for cells used in an electric vehicle) are generally based on time domain methods (see Section 3.1), involving either actively generated current pulses or measured current and voltage signals that result from operating the vehicle. Consequently, the frequency range is intrinsically limited to frequencies within the frequency spectrum of the current transient drawn from the cell [194].

The requirement for specialised equipment may be seen as a disadvantage of EIS measurements. In addition, the strong dependence of impedance on temperature (and other state variables), whilst useful on one hand, means that control, or at least knowledge, of the conditions under which measurements are taken is important. Where control is not possible, extrapolation to other conditions may be possible via modeling, provided the test conditions are known [31]. The time required to

collect data at the low frequencies required to probe diffusional processes within the cell may also be seen as a drawback of conventional EIS, particularly in a commercial setting, where testing is often restricted to DC internal resistance (DCiR) measurement, despite the more limited information this provides. However, fast measurement of full impedance spectra can be enabled via the use of multi-sine methods [195], whilst time domain methods also offer a potential solution [196]. These methods are discussed in more detail in the Measurement section (Section 3.1).

Beyond EIS, another useful impedance-based method of analysis is electrical impedance tomography (EIT). EIT is a tomographic imaging method which reconstructs the spatial resistivity distribution in an object under test using voltage-current data measured at the surface [197]. Widely used in biomedical and other applications, EIT has recently been applied to LIBs [197]. Although it has lower spatial resolution compared to conventional tomographic imaging techniques such as computed tomography (CT), it has the advantage of higher temporal resolution [197]. An additional interesting analogue to EIS is thermal impedance spectroscopy, which has been reported as a cost-efficient method for determining the thermal parameters of LIBs [198–202]. However, despite the intriguing scientific concepts of these latter impedance-based methods, these techniques are beyond the scope of the present review.

As noted above, the aim of this review is to report and evaluate the state-of-the-art in how to obtain, interpret and validate impedance measurements on commercial LIBs. We conducted a literature search to identify papers mentioning impedance in the context of commercial LIBs, which yielded over 250 papers in which EIS measurements on commercial cells are reported. These papers were analysed in terms of the purpose/application of the EIS measurements and the type of cell being measured. Fig. 2 presents the results of this analysis. Fig. 2a shows that the most common applications of EIS measurements for commercial LIBs have been to characterise and understand degradation (degradation mechanisms and/or factors affecting ageing/degradation) and performance (for example, to identify the main contributions to impedance as a function of SOC and/or temperature). In terms of cell size and capacity (see Fig. 2b and c), there has been a focus on relatively small cells, with over half of studies investigating cells under 3 Ah capacity, and only a fifth of studies measuring EIS of cells over 20 Ah capacity. Accordingly, almost half of studies have investigated cylindrical cells, whilst less than 15 % have measured prismatic cells. In line with commercial application, there has been an increasing focus in recent years on cells with NMC chemistry, which were measured in over a third of studies conducted since 2015; over the same period, LFP cells were measured in around a quarter of studies (see Fig. 2d). Fig. 2e includes an analysis of the types of impedance measurements conducted; these are discussed in more detail in the Measurement section (Section 3.1). An interactive table containing more detailed information for each of the studies analysed is provided as supplementary material.

The remainder of this review is structured as follows. Section 2 outlines key concepts in impedance metrology, including traceability to the international system of units. The sources of uncertainty associated with LIB impedance measurements are also discussed. Section 3 focuses on EIS measurement, interpretation and validation in relation to commercial LIBs. It begins with a discussion of various measurement techniques for obtaining EIS spectra and some of the key considerations that should be borne in mind when making measurements. Next, the widely practiced method for interpreting EIS, namely equivalent circuit modelling, is critically reviewed in view of the validity of the underlying physics, and its usefulness in the context of commercial LIBs. Finally, approaches for validation, of both the measurement themselves, and the conclusions drawn from them, are discussed, including a review of complementary analytical techniques. Section 4 summarises and provides an outlook for the application of EIS to commercial LIBs.

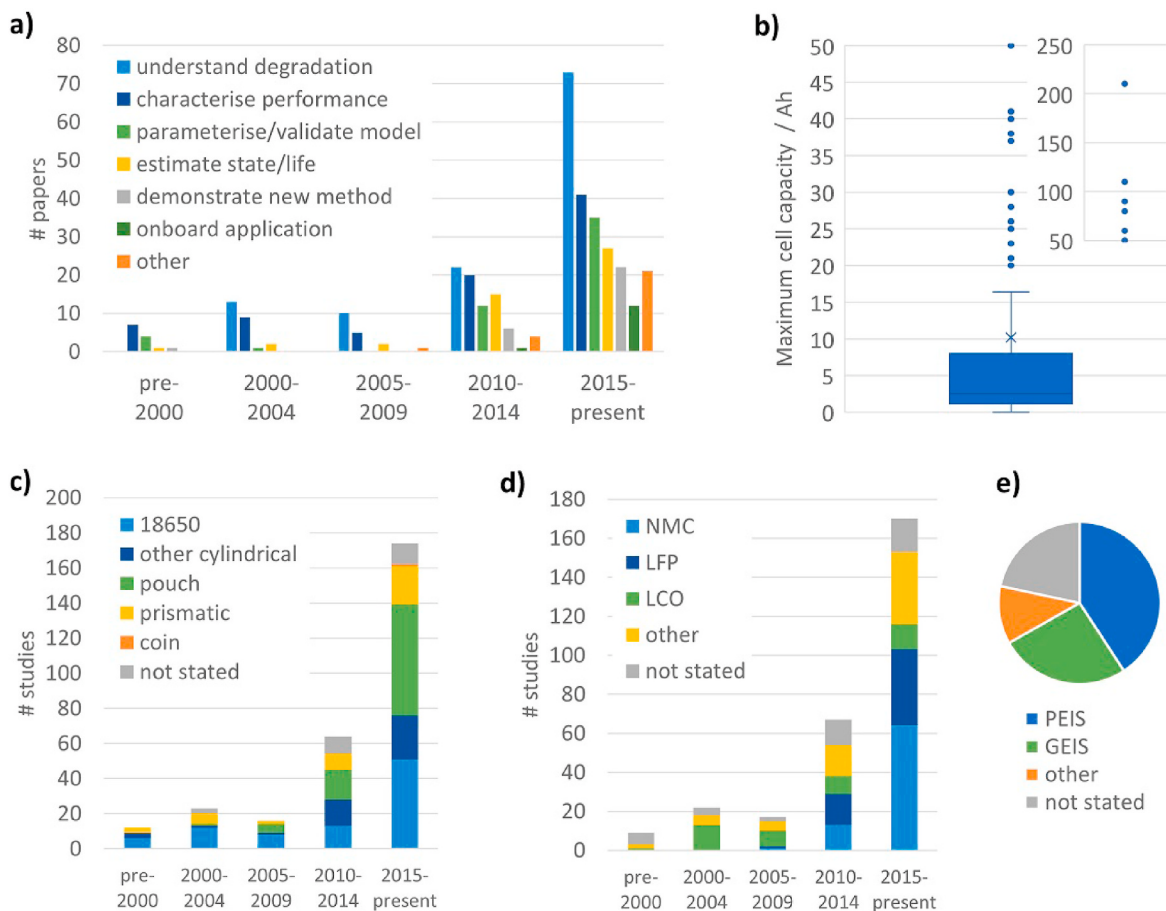


**Fig. 2.** Analysis of papers reporting EIS measurements on commercial LIBs according to: (a) purpose/application of the EIS measurements (note that individual papers may be counted in more than one category); (b) maximum cell capacity investigated; (c) cell format investigated (where a paper measured more than one cell format, the measurement of each format is counted as a separate ‘study’); (d) cell chemistry investigated (where a paper measured more than one type of cell chemistry, the measurement of each chemistry is counted as a separate ‘study’); (e) type of impedance measurement conducted (where a paper applied more than one type of measurement, each type is counted as a separate ‘study’).

## 2. Impedance metrology and calibration

The ability of EIS measurements to effectively characterise the performance of LIBs (as described in the Introduction) largely relies on the accurate measurement of the battery’s impedance over a wide frequency range. The traceability of the impedance measurement is therefore a prerequisite to any interpretation of EIS results.

As represented in Fig. 3a,<sup>2</sup>, metrological traceability is “the property of a measurement result whereby the result can be related to a reference through a documented unbroken chain of calibrations, each contributing to the measurement uncertainty” [205]. In short, a traceable impedance measurement ensures that the quantity is measured in the international system of units (SI) [206].

In this section, the definitions and terminology related to electrical impedance are first briefly introduced. Then, a critical analysis of the realisation of the different impedance scales is presented and the different Calibration and Measurement Capabilities (CMCs) are reviewed. Finally, the influencing factors involved in uncertainty evaluation of impedance measurement of LIBs are examined.

As represented in Fig. 3b, when a current  $I$  flows from terminal 1 to terminal 2 of a given impedance network, a voltage drop  $V$  is generated

between the two terminals. The two terminal (2T) impedance of the element is then defined by the ratio  $Z = V/I$ . If the current has an angular frequency  $\omega$  (i.e.  $I = \hat{I}e^{j\omega t+\varphi_I}$ , using phasor notation with  $j = \sqrt{-1}$ ) and the response of the impedance network is linear, the voltage drop has the same angular frequency (i.e.  $V = \hat{V}e^{j\omega t+\varphi_V}$ ) and the impedance is then given by:

$$Z = \frac{\hat{V}e^{j\omega t+\varphi_V}}{\hat{I}e^{j\omega t+\varphi_I}} = |Z|e^{j\varphi} \\ = \Re(Z) + j\Im(Z) = Z' + jZ'' \quad (1)$$

where  $\varphi = \varphi_V - \varphi_I$  is the phase shift between the voltage and the current. The impedance is a complex number and can be represented either in polar representation or by its projection to a Cartesian coordinate system, as represented in Eq. (1). When the phase shift  $\varphi$  is close to zero, the impedance is mainly resistive and the current flowing through it is dissipating energy. When the phase shift is close to  $\pm 90^\circ$ , the impedance is mainly reactive (purely inductive if  $\varphi = 90^\circ$  and purely capacitive if  $\varphi = -90^\circ$ ); almost no energy is dissipated by the current flow but some reactive power loss can exist.

The electromagnetic field associated with the current and the voltage extends around the impedance element and can interact with metallic parts or with other currents flowing nearby, making the measured impedance unstable and ill-defined. To avoid such a situation, the impedance element is generally placed in a metallic box acting as an electromagnetic shield, or Faraday cage. DC heaters should be used for

<sup>2</sup> Even where commercial instruments are identifiable this does not imply recommendation or endorsement by the authors, nor does it imply that the equipment identified is necessarily the best available for the purpose.

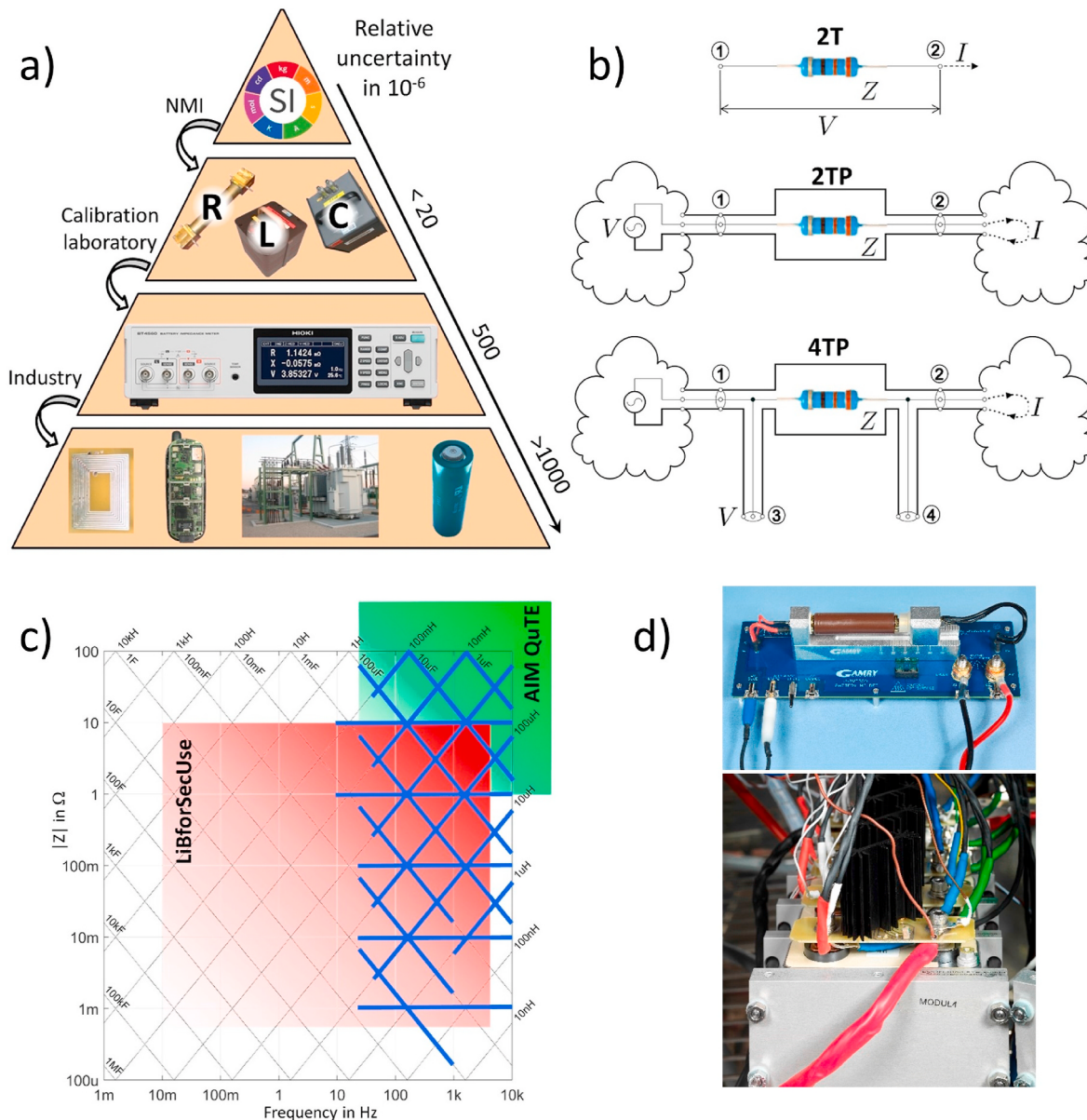


**Fig. 3.** a) Typical traceability chain of impedance measurement. The impedance meter measuring impedance at industry level has to be calibrated regularly using reference impedance standards. Values of the reference impedance standards are determined in terms of SI units realised at the level of the National Metrology Institute (NMI). Typical relative uncertainties required at the different steps of the traceability chain are represented on the right. b) Definition of an impedance as a two terminal (2T), two terminal-pair (2 TP) or four terminal-pair (4 TP) standard. c) Reactance chart representing the Calibration and Measurement Capabilities (CMCs) of NMIs. Most of the CMCs apply to impedance values located along the axis of the impedance plane (blue lines) i.e. either pure resistance, pure capacitance or pure inductance. The green rectangle represents the impedance and frequency ranges for which traceability has been improved through the AIM QuTE project [203]. The red rectangle highlights the impedance and frequency ranges of interest for impedance spectroscopy of Li-ion cells (LiBforSecUse project [204]). d) Two different examples of real-world measurement setups used for impedance spectroscopy of LIBs.

temperature control. Terminals 1, 2 and the shield form what is called a two terminal-pair (2 TP) configuration [207,208] (see the middle part in Fig. 3b). The impedance is then given by the ratio of the voltage measured between terminal 1 and the shield to the current flowing out of terminal 2 and returning to the shield under the condition that the voltage between terminal 2 and the shield is zero.

In this configuration, the measured voltage drop  $V$  is not solely due to the impedance element but also to the contact resistances inevitably present between the impedance element and the measuring instruments. Therefore, this definition is only suitable for the measurement of relatively high impedance values.

When low impedance values have to be measured or high accuracy is required, the impedance must be defined by adding two supplementary

terminal-pairs to the network. This leads to the so-called four terminal-pair definition (4 TP) [207,209] of impedance standards as represented in the bottom part of Fig. 3b. The impedance is then defined by the ratio of the voltage measured at terminal-pair 3 (also called the high potential port or HP) to the current flowing out of terminal-pair 2 (also called the low current port or LC) with the condition of zero voltage at terminal-pair 4 (also called the low potential port or LP) and no current flowing through ports HP and LP. There is no specific condition applied to terminal-pair 1 (also called the high current port or HC). Therefore,

$$Z_{4\text{TP}} = \frac{V_3}{I_2} \quad V_4 = 0 \quad I_4 = 0, I_3 = 0 \quad (2)$$

The four terminal-pair definition can be used for any value of impedance. Despite being conceptually complex and requiring specific active circuitry to guarantee the voltage and current conditions, the four terminal-pair definition is commonly employed in commercial impedance meters when ultimate accuracy is targeted. When the measured quantity is defined in different ways (e.g., two-terminal electronic components), a carefully designed fixture or adapter becomes necessary [210,211]. A supplementary uncertainty component then has to be added to account for the weakness of the impedance definition. Depending on the measuring setup, this component could become the dominant term of the whole uncertainty budget.

## 2.1. Realisation of impedance scales

The primary role of impedance metrology is the realisation of the different units of impedance and their associated scales: the ohm ( $\Omega$ ), the farad (F) and the henry (H). These three units are related to each other through the second (s) [206]:  $1 \Omega = 1 \text{ H/s} = 1 \text{ s/F}$  and therefore, one unit can be chosen as starting point for the realisation of the other two using different dedicated AC bridges [212].

Over time, different units have been used as the starting point [213, 214]. Early in the 20th century, a calculable mutual inductor [215] was used to realise the henry. Later on, the calculable capacitor was preferred [216] since its value can be deduced from a single mechanical dimension with great accuracy. Since the 1990s, with the advent of electrical quantum standards, a new representation of the volt and the ohm has been based on conventional values of the Josephson and von Klitzing constants [217]. The farad and the henry can then be deduced from the conventional ohm. With the redefinition [218] of the International System of Units, this representation of the resistance units has underpinned the SI realisation of the ohm since May 20th, 2019.

National Metrology Institutes (NMIs) have deployed large efforts to develop and improve measuring instruments and secondary impedance standards needed to maintain the different impedance scales [219]. The resulting CMCs of selected NMIs are represented in Fig. 3c for the impedance and frequency domain of interest for impedance spectroscopy of Li-ion cells. Until recently, most of the CMCs concerned impedance values located along one axis of the impedance plane, i.e. either pure resistance, pure capacitance or pure inductance (represented by the blue lines), leaving a large part of the impedance plane with no clear and accurate traceability.

The situation is now changing and a new generation of impedance bridges [220–223] and impedance standards have been developed to improve the traceability of impedance calibration over the whole complex plane. Recently, within the framework of the AIM QuTE project [203], a first comparison of impedance standards having phase angle of either  $\pm 30^\circ$  or  $\pm 60^\circ$  have been performed [224]. Also, a new impedance simulator [225] has been developed to calibrate LCR-meters over the whole complex plane in the frequency range from 50 Hz to 20 kHz and in the impedance range from  $1 \Omega$  to  $10 \text{ M}\Omega$  (green rectangle in Fig. 3c).

Despite these recent improvements, there is still a large range of impedance values that is not covered by any CMCs, and is therefore not properly traceable to SI units, especially in the impedance and frequency ranges of interest for impedance spectroscopy of commercial Li-ion cells. One of the objectives of the LiBforSecUse project [204] is to address this issue and to extend impedance traceability to low impedance values at low frequencies (the red rectangle in Fig. 3c).

## 2.2. Measuring impedance of LIBs

When impedance measurements are performed in an industrial environment, the ideal conditions required to obtain the highest level of accuracy cannot always be realised. The device under test (DUT) may be not configured as a four terminal-pair standard and shielding may not be possible. The measuring system itself may not be designed with coaxial cables and excessively long cables may be required to connect the DUT

to the measuring instrument. A home-made test fixture may need to be used to connect the DUT to the measuring instrument. These measuring conditions are specific to each situation (see Fig. 3d) and have to be carefully considered to avoid the measured impedance deviating significantly from the impedance of the DUT.

There are some basic concepts that can be followed to avoid detrimental effects on the measurement accuracy. The general technique that is most widely used is the Open/Short/Load (OSL) compensation procedure [226]. This procedure allows a significant reduction of the measurement error related to the test fixture, test leads or other additional measurement accessory [227]. However, this is only possible at the expense of having to conduct three supplementary measurements:

1. open admittance measurement,  $Y_o = 1/Z_o$ , carried out by replacing the DUT with a zero admittance standard;
2. short impedance measurement,  $Z_s$ , obtained by replacing the DUT with a zero impedance standard;
3. load measurement,  $Z_{\text{REF}}^m$ , performed with a known reference impedance standard  $Z_{\text{REF}}$ .

The effective impedance of the DUT,  $Z_{\text{DUT}}$ , is then obtained from its measured value,  $Z_{\text{DUT}}^m$ , using the following equation [226]:

$$Z_{\text{DUT}} = Z_{\text{REF}} \frac{(1 - Z_{\text{REF}}^m Y_o)(Z_{\text{DUT}}^m - Z_s)}{(1 - Z_{\text{DUT}}^m Y_o)(Z_{\text{REF}}^m - Z_s)} \quad (3)$$

In the specific case of commercial Li-ion cells the range of interest is mainly below  $0.1 \Omega$  at frequencies lower than a few tens of kHz. Open compensation is therefore less critical because  $|Z_{\text{REF}}^m Y_o|$  and  $|Z_{\text{DUT}}^m Y_o|$  are usually much less than 1. Therefore, Eq. (3) can be reduced to

$$Z_{\text{DUT}} = \frac{Z_{\text{REF}}}{(Z_{\text{REF}}^m - Z_s)} (Z_{\text{DUT}}^m - Z_s) \quad (4)$$

and the dominant correction term is the measured short impedance  $Z_s$ .

A value of  $|Z_s|$  significantly different from zero may indicate the presence of magnetic coupling between the different parts of the measuring setup. Indeed, measurement of the low impedance of commercial LIBs implies the use of a relatively large current (order of 1 A or higher) flowing along the high current (HC) and low current (LC) cables. The magnetic field associated with this measuring current can interact with other parts of the measuring setup and can especially induce electromotive force in the loop formed by the high potential (HP) and low potential (LP) cables. If current equalised coaxial cables [228] cannot be used, the undesirable magnetic field generated by the go-and-return currents can be minimised using twisted-pair wires for the HC and LC cables [229]. Moreover, the size of the pick-up loop can be minimised by also using twisted-pair wires for the HP and LP cables.

The use of Eq. (4) also implies that the measurements of  $Z_{\text{REF}}^m$  and  $Z_s$  have to be carried out using the same setup as that used for the DUT measurement, i.e. the same cables in the same geometry. If the reference impedance is defined as a 4 TP standard but the measuring system does not allow the realisation of the 4 TP definition, correction of the reference value,  $Z_{\text{REF}}$ , may need to be applied and a supplementary uncertainty component added to the reference value uncertainty. Finally, if the geometry of the setup has to be significantly modified for the different measurements, the effect of the variation of the geometry on the measured value has to be evaluated and uncertainty components added accordingly.

## 3. EIS measurement, interpretation and validation

### 3.1. Measurement techniques

As discussed in the Introduction, conventional EIS measurements involve applying a sinusoidal perturbation in either potentiostatic or galvanostatic mode. Three basic requirements of valid EIS

measurements are linearity, causality and stationarity. Electrochemical systems are inherently non-linear, but application of a sufficiently small perturbation ensures that their response remains within the pseudo-linear regime. This means that the response has the same frequency as the perturbation, i.e. it has negligible contributions from higher harmonics which are typically generated in non-linear systems; then, as in the time domain, the frequency-dependent impedance can be calculated by using Ohm's law [47] and PEIS and GEIS should yield identical results [230]. For testing of many electrochemical systems, including lab-scale cells, PEIS is typically used, with a voltage perturbation ca. 5–25 mV (peak), as this generally ensures linearity of the current response [47]. Indeed, as shown in Fig. 2e, over 40% of the studies on commercial Li-ion cells identified in our literature search also used PEIS, typically with a perturbation of 5–10 mV (although often not stated whether a peak, peak-to-peak or rms value). However, commercial batteries have much lower impedance than lab-scale cells, typically in the mΩ range [99], due to the much larger electrode areas. This means that small input voltage perturbations will lead to large output current flows. Voltage control in such a situation tests the specification of most commercial potentiostats [231] and may result in a poor signal-to-noise ratio [196]. On the other hand, applying a current perturbation in the

0.1–1 A range, and measuring a voltage response of a few mV, is well within the capability of most instruments. For this reason, GEIS may give more accurate EIS measurements of commercial cells [231], though, as noted, PEIS has frequently been used, and has been shown to produce comparable results [119,232] (Fig. 4a).

Using a higher current perturbation (relative to cell capacity) can improve signal to noise ratio [2]; however, care is needed to ensure that the response remains in the linear regime, and that the internal temperature of the cell is not affected significantly by larger current amplitudes, particularly for impedance measurements at low ambient temperatures [57,93]. For example, in Ref. [93], cell impedance and cell surface temperature (as an indicator of internal temperature) were measured as a function of applied current perturbation in preliminary tests to identify a suitable perturbation value.

As already mentioned in Section 2, a well-defined measurement setup is important to minimise variations between measurements. In Ref. [99], for example, a variation in the cell ohmic resistance of up to 10% was observed over ten EIS measurements involving different cell holders and/or removal and reinsertion of the cell into the same holder. As discussed in the Introduction, EIS measurements at different values of cell SOC, temperature and number of cycles can yield important

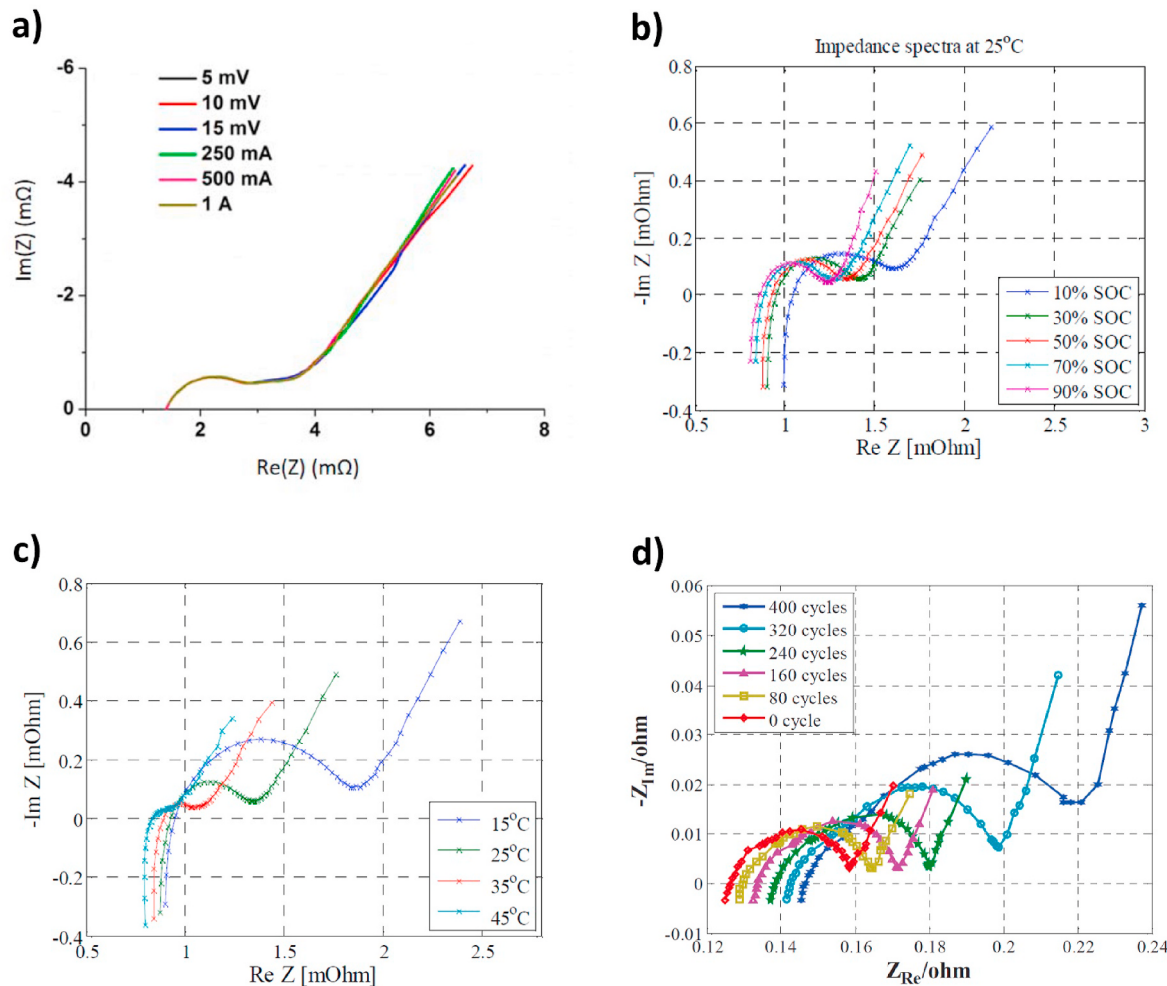


**Fig. 4.** (a) Comparison of impedance spectra of a commercial 8 Ah prismatic lithium iron phosphate battery obtained with different potentiostatic or galvanostatic excitation signal amplitudes in the 1 kHz - 10 mHz frequency range at 23 °C. Inductive effects at high frequencies not shown in the original figure (Reproduced from [119]). (b) Variation with SOC of the impedance spectrum of a Kokam  $\text{LiCoO}_2\text{-LiMn}_{0.33}\text{Ni}_{0.33}\text{Co}_{0.33}\text{O}_2\text{||carbon}$  pouch cell (nominal capacity 53 Ah) collected at 25 °C in the 2 kHz - 10 mHz frequency range with a 10 mV perturbation (Reproduced from [233]). (c) Variation with temperature of the impedance spectrum of a Kokam  $\text{LiCoO}_2\text{-LiMn}_{0.33}\text{Ni}_{0.33}\text{Co}_{0.33}\text{O}_2\text{||carbon}$  pouch cell (nominal capacity 53 Ah) at SOC 50% (frequency range and voltage perturbation as in (b)) (Reproduced from [233]). (d) EIS spectra (perturbation = 20 mV) of Sanyo's UR14500P lithium cobalt oxide battery (nominal capacity 0.8 Ah) collected at SOC 50% and 25 °C in the 1 kHz - 100 mHz frequency range, after selected cycles at 1C. (Reproduced from [34]). Note that the x- and y-axes in b, c, d have different scales; the arcs are much more depressed than they appear.

information. Variation of impedance spectra as a function of these parameters are illustrated in Fig. 4 b, c, and d respectively, for different commercial LIBs. In the case of SOC, measurements are typically taken by first fully charging (or discharging) the cell using a constant-current constant-voltage (CCCV) protocol, then discharging (or charging) at constant current to a desired value of SOC, measuring EIS and repeating this process for each of the required SOC values. However, it is worth noting that in some cases the measured impedance of a cell can depend on whether the previous step was a charge or discharge, as a result of open circuit voltage (OCV) hysteresis [21,234]. In order to fulfil the condition of stationarity, a sufficient rest period should be allowed following each partial discharge for the cell to reach steady state [234, 235]. Note that even after a steady OCV has been reached (defined in terms of a maximum rate of change in potential, e.g. 5 mV/h, or maximum residual current value during the constant voltage step if SOC setting is achieved via a CCCV protocol), continued relaxation (e.g. of slow diffusional processes in the cell) can lead to changes in the measured impedance spectrum [236]. The time taken for the measured impedance to stabilise may depend on the cell chemistry and format, as well as the SOC, temperature, current/protocol used for SOC setting, and region of interest in the impedance spectrum [196,236–238]. One study of several different cell types found that a rest period of 4 h was generally adequate (subsequent changes in measured EIS spectra were within acceptable limits) [239]; others have found that much shorter (15–90 min) [93] or longer (up to 100 h) [94,234,236,237] rest times are necessary. Although it is an essential part of the measurement protocol, only half of the studies identified in our literature search stated the allowed rest period after SOC setting. Amongst these, ca. 40% allowed 1 h or less, ca. 40% allowed 1–4 h, and ca. 20% allowed more than 4 h. In most cases, however, the basis for the choice was not explicitly stated.

A rest period is also required if the temperature of the cell is adjusted, to allow the cell to reach thermal equilibrium [39,71,74,93,232,240], though this rest period may be short if a slow temperature ramp rate has been applied [238]. It is important to remember that the internal cell temperature, which is the relevant one, may differ from that measurable at the cell surface. Another consideration is the order in which different temperatures are applied, in order to minimise degradation-induced changes in the impedance [190]. Moreover, the adjustment of SOC is affected by temperature, since the capacity of a cell depends on temperature. Thus, if investigating impedance as a function of both SOC and temperature, it may be advantageous to adjust the SOC of the cell first, and measure impedance at different temperatures for a given SOC (before returning to the original temperature, adjusting the SOC, and repeating this process) [57,241]. Although this procedure is more time consuming than the alternative (adjusting the temperature and measuring impedance at different SOC values for a given temperature), it improves the comparability of the impedance measurements. Otherwise, SOC adjustment can be made with reference to separate discharge curves measured at each of the temperatures in question.

In terms of the EIS measurement itself, consideration should be given to the number and spacing of sampled frequencies required to resolve each of the features and to estimate parameter values reliably [93]; higher sampling rates, however, particularly in the lower frequency range, will increase the duration of the test. Similarly, selection of the number of periods measured at each frequency, as well as the delay allowed for a periodic steady-state to be achieved after a current or voltage perturbation is applied, involves a trade-off between accuracy and measurement time. Thus preliminary tests are indispensable for establishing appropriate measurement parameters [93,238].

GEIS may be performed at zero net current condition (also called stationary EIS or SEIS), or with AC current perturbations superimposed on an applied DC current (known as dynamic EIS or DEIS). Similarly, PEIS can be performed at open circuit voltage or with an applied DC bias. The vast majority of the studies identified in our literature search took the former measurement approach, with no DC current or potential bias. The main advantage of this approach is that, subject to the

precautions outlined above, the battery under test fulfils the stationarity condition for valid impedance measurements. On the other hand, applying a DC current during GEIS allows the impedance of the battery during continuous charge or discharge to be investigated, which may be useful as an *operando* impedance technique. Impedance measured during DEIS may be lower than that measured during SEIS due to the non-linearity of the charge transfer reactions (i.e. the Butler-Volmer relationship between current and overpotential) (see Fig. 5A) [242]. Note that the impedance measurement itself, which is obtained from the small AC perturbation superimposed on the DC bias, can, and should, still fulfill the linearity condition; however, the measured impedance value may depend non-linearly on the applied DC current. Not only the magnitude of the DC current but also its direction can have an influence on the measured impedance due to asymmetry of the charge transfer reactions. Impedance has been found to be lower during charge than during discharge (see Fig. 5A) [74,243,244]. During dynamic EIS, however, the SOC of the cell will be different at the start and end of the measurement [95,242], which can lead to significant errors in the low frequency components of the spectrum if unaddressed. One approach is to compensate deviations at low frequencies through the use of a 3D Nyquist plot, including a time axis in addition to real and imaginary impedance. The impedance spectrum at a specific SOC point can then be estimated by interpolation [245–247]. Another approach involves continuous measurements at a single frequency across a full SOC range during charge or discharge. This process is repeated at other selected frequencies and the impedance spectrum extracted by interpolation [243]. Alternatively, changes in SOC during the course of the measurement can be minimised by reducing the measurement time, either by using a multi-sine approach (as described later in this section), or simply by omitting very low frequency measurements, although this of course has implications for the ability to probe slow diffusional processes within the cell. Note that the differences between static and dynamic EIS will be more pronounced at lower test temperatures (due to greater sensitivity to temperature differences generated by Joule heating), whilst for temperatures above 25 °C they may be negligible [95].

Hybrid EIS is a modified form of GEIS in which the applied current is continuously adjusted to match a user-specified value of the measured potential. At each frequency, the cell voltage is measured and the current is adjusted until the measured voltage agrees with the desired one. For low-impedance systems, this can improve the signal-to-noise ratio of impedance measurements [250]. However, hybrid GEIS has not been as widely applied as PEIS or GEIS to commercial LIBs, with relatively few studies using this method [4,94,131,172,251].

Total harmonic distortion (THD) analysis can be used to assess any non-linearities in the measured system response. The THD factor for a measured signal is the ratio of the combined root mean square (RMS) magnitude of all its  $n$ th-order harmonic components ( $Y_n$  with  $n \geq 2$ ), which are due to non-linearities in the response, to the RMS magnitude of the fundamental frequency component ( $Y_1$ ). The THD factor increases with the non-linearity of the response. It is calculated for each frequency of the applied sinusoidal signal (analogously to the impedance) and can be plotted versus the frequency of the applied signal, indicating, for a given amplitude of applied signal, the frequency range over which linearity can be assumed and EIS measurements are valid [248, 252–254]. Note that the degree of non-linearity may vary depending on the SOC of the cell [255].

Indeed, Non-Linear Frequency Response Analysis (NFRA) involves application of relatively large currents (e.g. 1.5–3C) to deliberately excite higher harmonics in the battery's voltage response. The resulting harmonic amplitudes (usually the second and third, individually or combined, as these provide the largest contributions) can be analysed as a function of frequency to obtain additional dynamic information about the cell (see Fig. 5B) [256–258]. However, the measured response is always input amplitude-dependent and results can depend strongly on cell type and specification [259], restricting the technique to locally comparative analysis. In contrast, Non-Linear EIS (NLEIS) applies only

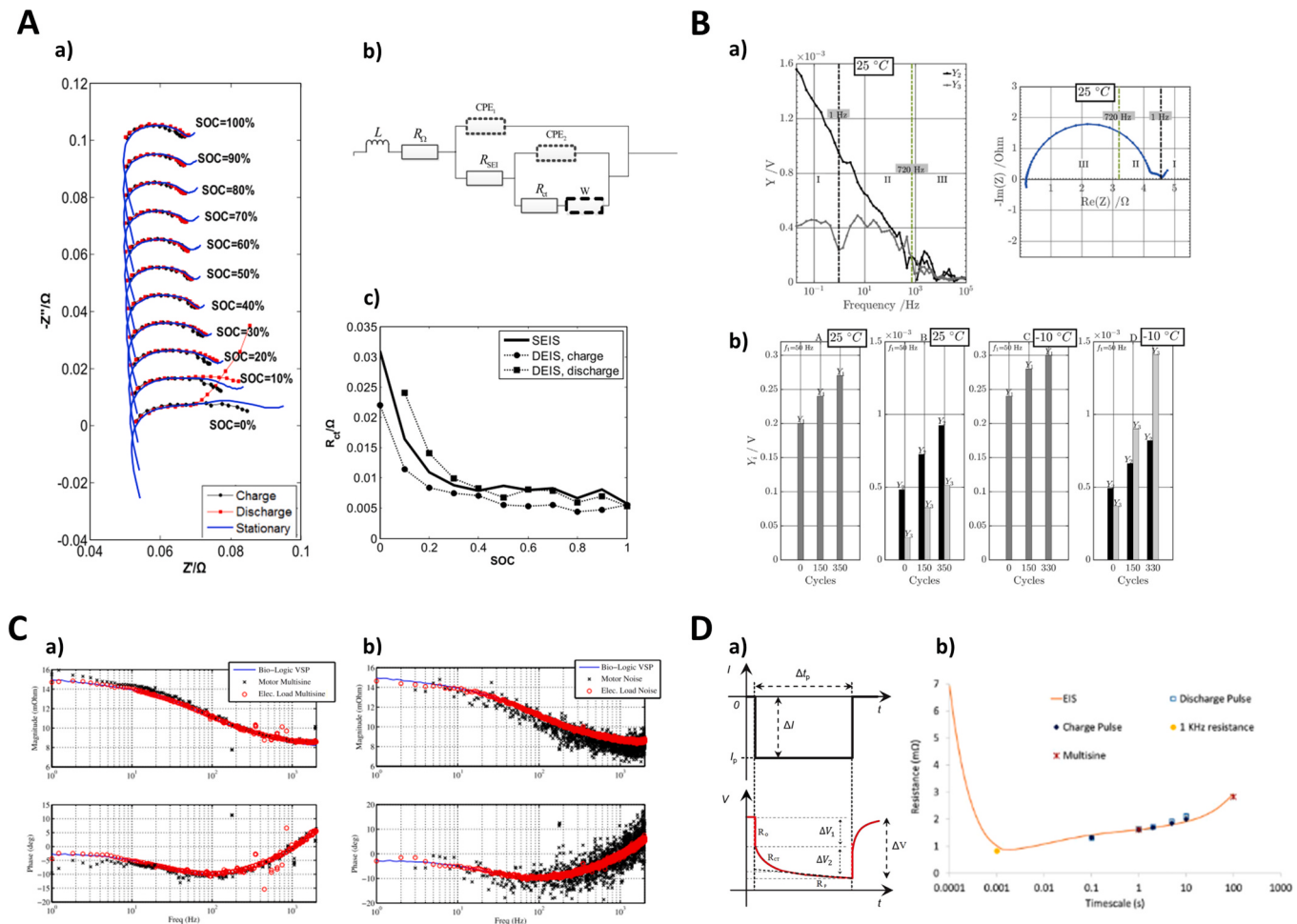


**Fig. 5.** (A) (a) impedance spectra of a commercial NMC 18650 cell (nominal capacity 2.2 Ah) at different SOC, measured using SEIS and DEIS during charge and discharge. Data collected at 20 °C in the 10 kHz - 100 mHz frequency range with a 10 mA perturbation (SEIS) and in the 1 kHz - 1 Hz frequency range with  $I_{DC} = 1$  A,  $I_{AC} = 10$  mA (DEIS). Note that the imaginary part of impedance is artificially shifted by  $0.1 \times \text{SOC } \Omega$  as a function of SOC, for visualisation purposes. (b) Equivalent circuit model used to fit the spectra. (c) Comparison of the fitted parameter  $R_{ct}$  obtained from SEIS and DEIS measurements, as a function of SOC. (Reproduced from [243]). (B) (a) Correlation of the non-linear frequency response spectrum (left) and impedance spectrum (right) of a NMC111||graphite pouch cell (nominal capacity 0.3 Ah). (b) Intensities of the fundamental frequency response  $Y_1$  (from EIS), and higher harmonic responses ( $Y_2$  and  $Y_3$ , from NFRA) for cells aged at 25 °C (panels A and B) and at -10 °C (panels C and D). An increase in the ratio  $Y_3/Y_2$  is observed in the NFRA results for cells aged at -10 °C, which was correlated via *ex situ* analysis to lithium plating. In contrast, EIS results of cells aged at -10 °C and at 25 °C show similar qualitative behaviour. Data collected at 25 °C in the frequency range 10 kHz - 0.02 Hz (NFRA) and 1 MHz - 0.02 Hz (EIS) with a current perturbation of 1.5C (NFRA) and 0.16C (EIS). (Reproduced from [248]). (C) Measured impedance spectra (Bode plot) of an A123 Systems LFP 26650 cell (nominal capacity 2.3 Ah), obtained using single-sine EIS with a commercial measurement system vs. excitation of a low cost electronic load and a motor test rig using multisine (a) and broadband noise (b) approaches, for online applications. Data collected at ambient temperature (18 °C–21 °C) in the 2 kHz–1 Hz frequency range with an applied current of  $IDC = 150$  mA,  $IAC = 130$  mA (peak-to-peak). (Reproduced from [249]). (D) (a) Schematic of a cell voltage response to a DC current pulse, highlighting different contributions at different pulse times. (b) Measured impedance modulus/“total resistance” of a commercial LFP||graphite pouch cell (nominal capacity 20 Ah), obtained at 25 °C using different AC and DC measurement techniques and plotted vs. timescale of the measurement, showing that values (approximately) agree when measurement timescales match. EIS measured in the frequency range 100 kHz - 0.01 Hz with a current perturbation of C/20. Pulse tests carried out with a pulse amplitude of 5C and 10 s duration. Note that ‘multisine’ here refers to a pulsed multisine method; see ref. [2] for details. (Reproduced and adapted from [2]).

moderately larger excitation currents than conventional EIS (e.g. C/3), such that the battery’s response remains in the ‘weakly non-linear’ regime ( $\text{THD} \ll 1$ ) [244,252]. In this case, the response remains input-independent and higher order harmonics in the measured signal can be used to calculate meaningful “higher order impedance” spectra, akin to the first order (linear) impedance, from the same experimental data set. However, the small amplitude of the higher order harmonics requires very good measurement capability, and may be distorted by circuitry contributions at frequencies above a certain value (e.g. 10 Hz) [252]. Non-linear techniques have been used to elucidate degradation mechanisms [252] and in the identification of lithium plating (see Fig. 5B) and SOH estimation of LIBs [248,259]. With larger permissible current perturbations, problems with low signal-to-noise ratio may be

avoided [260], though care should be taken to avoid damaging the cell and enhancing ageing, especially at extreme SOC values and low temperatures [259]. Sensitivity of higher harmonic responses to underlying electrochemical processes can provide richer information and improve model parameter identification [252]. However, this requires more sophisticated analysis, and a lack of experience in these relatively new techniques means there is currently no unique, standardised methodology and no common implementation in commercial instruments/software [259–261].

As discussed in the Introduction, EIS measurements are commonly made using the “single-sine” method in which individual frequencies are measured sequentially. A disadvantage of this approach is the time it takes to acquire a full spectrum, particularly if probing of solid-state

diffusion processes within the cell is required. These processes are usually very slow and thus require time-consuming measurements at very low frequencies  $<1$  mHz [262]. If measurements are averaged over several periods at each frequency, measurement times to acquire a complete spectrum of several hours - even days in extreme cases - can result. This can bring the steady state condition of the battery under test into question, and there may also be current drift in the measurement equipment [263]. One way to address this is to measure multiple frequencies at the same time, known as the “multi-sine” method [195,264]. Steps must be taken to ensure similar completion times for all frequencies and to keep the overall amplitude of the perturbation, given by the sum of the individual sine wave amplitudes, small in order to maintain good stability and linearity [195,265]. That said, methods to estimate linear response functions from non-linearly excited systems have been proposed [255]. Compared to the single-sine method, signal-to-noise ratio is typically lower for multi-sine EIS since the excitation is defined for all the frequencies and therefore each frequency is less excited than in single-sine mode [266] (see Fig. 5C). Odd random phase EIS, a multi-sine based technique designed to allow evaluation of the linearity, stationarity and noise level of the measured impedance, has been applied to commercial NCA electrodes [121].

In multi-sine EIS, the time domain response of the system is measured, and then the impedance spectrum, which is the frequency response function of the system, is obtained through mathematical (e.g. Fourier) transformation. Other time domain and wideband methods have also been developed [196,267] in which the excitation signal is an arbitrarily shaped current (e.g. step function, rectangular pulse/Gaussian/sinc pulse [196], pseudo-random binary sequence [17,32,52,268] or broadband noise [249], see Fig. 5C) that simultaneously excites multiple frequencies. Fourier, Laplace or other transformations are used to obtain the impedance spectrum from the time domain response [34, 40,237,269]. Achieving a sufficiently high signal-to-noise ratio can be an issue with time domain approaches involving a current step or pulse [17]; however, both the pulse duration and the current amplitude (typically on the order of 1C) can be tuned to optimise this, with the trade-off being limits to the measurable frequency range and the linearity of the system, respectively [270]. A combination of frequency and time domain measurements, covering high and low frequency ranges respectively, may be advantageous [55,263,271]. Time domain methods extend to passive impedance spectroscopy, which has been proposed as an online diagnostic tool for electric vehicles. Passive approaches are based on current and voltage signals that result from operating the vehicle, without the need for an additional excitation; a recent summary was provided by Liebhart et al. [194].

AC impedance measurements at a single frequency (e.g. 1 kHz) are commonly used for quality assurance and cell matching during battery manufacture, along with DCiR measurement [2]. Such measurements are rapid and can identify cell-to-cell variances and deviations from manufacturing thresholds. Single-frequency AC measurements have also been applied for internal temperature estimation and health monitoring [41,173,272–276]. However, the particular frequency corresponding to any given feature in the overall impedance spectrum will be highly dependent on the cell specification, and therefore the frequency needs to be chosen according to the particular battery; preliminary full-spectrum EIS measurements can be used to guide selection [2,50]. DCiR measurements involve some form of step current (applied current pulse, current interrupt, or current switch) and the ohmic resistance of the cell is given by the instantaneous voltage drop:  $\Delta V / \Delta I$ . The measured value, however, is dependent on the data sampling rate, and in the case of an applied current pulse, may also be affected by the rise times of the test equipment [2,277,278]. After the initial instantaneous drop, further voltage drop is due to resistance associated with charge transfer and, at longer times, diffusional processes in the cell. Measurements at different time points/pulse durations (analogous to AC measurements at different frequencies) will therefore give different values for “total” cell resistance, depending on the extent to which those processes are being

probed [2,94] (see Fig. 5D). Values will also depend on the amplitude of the applied current pulse/step, due to non-linearity of the electrochemical processes, as well as increased Joule heating and changes in SOC during tests with higher amplitudes [2,94,278]. Pulse power characterisation (PPC) tests, with specified pulse durations and amplitudes, are commonly defined in standards and manuals [279–281]. Correlation between resistance values obtained from EIS measurements and from PPC tests will depend on all of the aforementioned factors (see Fig. 5D) [2,278].

### 3.2. Interpretation

Even when reliable EIS measurements can be obtained, their interpretation, in a manner that can provide useful guidance on battery design and performance prediction, remains a significant challenge. By far the most widely used approach is Equivalent Circuit Modelling (ECM), whereby the response of the cell is analytically parameterised in terms of electrical circuit elements representing different physical and chemical processes in the battery. This approach can rapidly generate broad insights into cell performance but suffers from the limitation that such models are difficult to validate with respect to experimentally measurable parameters and often lead to unnecessary over-parameterisation.

Impedance has also been numerically simulated from the governing physical equations such as the Butler-Volmer equation, drift-diffusion equations, and conservation of mass and charge [282,283]. The use of this latter approach has increased in traction in recent years with the help of commercial tools [252,284–286], and can help understanding and discovery of underlying physics in LIBs, as well as supporting development of physics-based ECMs, which can be more conveniently implemented for LIBs.

In the following sections, we will discuss some physics-based concepts implemented in conventional ECM studies. Finally, a fully integrated physics-based ECM, still simplified enough for practical battery impedance analysis, is introduced and discussed.

#### 3.2.1. Distribution of relaxation times

Attribution of specific features in an ECM to physical quantities associated with different parts of the LIB requires an a priori knowledge of the underlying processes in the LIB. Distribution of Relaxation Times (DRT) has been recommended as a method that assists in developing a specific ECM that is physically meaningful and is less likely to be over-parameterised. This method of analysis transforms the impedance data from the frequency to the time domain via the following equation:

$$Z_{\text{pol}}(\omega) = R_{\text{pol}} \int_0^{\infty} \frac{g(\tau)}{1 + j\omega\tau} d\tau \quad (5)$$

where  $R_{\text{pol}}$  is the total ‘polarisation’ resistance of the considered impedance spectrum,  $g(\tau)$  the distribution of relaxation times,  $j$  the imaginary unit,  $\omega$  the angular frequency and  $\tau$  the time constant of the exponential relaxation. Polarisation is used to represent different processes leading to the overpotentials during current flow in electrochemical cells, i.e. ohmic, activation, and concentration polarisations. Note that  $Z = R/(1+j\omega\tau)$  is the Laplace transform of the voltage exponential relaxation in an  $R||C$  circuit, where the relaxation time constant  $\tau = RC$ . The relaxation time  $\tau$  defines the time until the effect of an impulse on the system has subsided to  $1/e$  of its initial value, with  $e$  being Euler’s number. Two sequential exponential relaxation processes are represented by the second order Voigt-type circuit element [287] consisting of two series  $R||C$  circuits shown in Fig. 6a. The transformation for the real processes is shown schematically in Fig. 6b where capacitors are substituted by constant phase elements (CPEs).

In general, the DRT method is a suitable option for electrochemical energy storage systems presenting [262]:

- 1) low impedance signal
- 2) a large number of possible rate limiting processes
- 3) overlap of the anode and cathode contributions

Although the development of the DRT technique was carried out by Schweißler and Wagner in the early 20th century [288,289], nowadays DRT is considered as a valuable tool for the analysis of both fuel cells [290] and LIBs [55,237,251,291,292]. Another advantage for the use of DRT is the free availability and usability of tools (e.g. Matlab® [293] using the Optimization toolbox [294]) such as that developed by Wan et al. [295].

In general, considering that one of the most beneficial aspects of DRT is its broad applicability (independent of the system under analysis), some researchers have specifically highlighted that erroneous measurement data points could have a significant impact on the resulting DRT, while noise has a minor effect [262,298]. Therefore, it is recommended to delete erroneous data points prior to DRT analysis [262]. Improved DRT mathematical algorithms for LIBs were also investigated by several research groups [295,299]. Another improvement has been presented by Schmidt and Ivers-Tiffée, who combined DRT with a pulse-fitting method and have been able to analyse polarisation losses at frequencies down to 0.01 mHz [237].

For commercial Li-ion cells, DRT is mainly used to distinguish overlapping processes in order to predefine a suitable ECM. Such processes appear as separate peaks in the DRT plot (Fig. 6a and b). The distinct processes derived from DRT analysis can be correlated with SOC [53,55], temperature [70,300], SOH [56] or other system variables. In addition, knowledge of the number of underlying processes can be used to set up advanced physics-based ECMs of LIBs [70]. However, particular care should be taken because the number of processes identified by the DRT algorithm highly depends on the magnitude of the

regularisation parameters [301]. Therefore, accurate selection of parameters is the basis of a proper DRT evaluation [262,302].

Even with suitable values for the regularisation parameters, the outcome of an LIB DRT analysis can be affected by inductive and diffusional components. Based on Eq. (5), the analysis is often limited to the impedance arcs representing the charge transfer reaction together with double layer capacitance and SEI films [70,292]. Recently, Danzer proposed an alternative strategy of analysis using a more comprehensive DRT in which inductive and diffusional impedance signals are taken into account [303]. Concerning diffusion processes, Song and Bazant introduced the mathematical principles for the Distribution of Diffusion Times (DDT), which they suggested for use in conjunction with DRT where there is a strong contribution from diffusion processes [304].

### 3.2.2. Conventional equivalent circuit modelling

ECMs are typically applied to EIS data by interconnecting electrical circuit elements and adjusting their parameters in order to minimise the difference between measured and simulated impedance spectra. ECMs are nowadays frequently used because they are easy to set up and have low computational cost compared to elaborate physico-chemical models (e.g., a Newman-type model) [112,252,282,284–286,305]. Therefore, they are suitable for application in Battery Management Systems (BMSs). Furthermore, the analysis of various states of an LIB can be easily carried out by evaluating the change of fitting parameters due to changes in, for example, the SOC, SOH or temperature. To this end, some research groups have developed SOH and temperature dependent circuit elements [102,233,306]. A good overview of the techniques used to identify parameters of ECMs is given by Fleischer et al. [307]. The main drawback of ECMs, and in particular those that are most elaborate, is the lack of the exact correlation between the circuit elements and the physical and chemical processes occurring in the LIB. This, in spite of the

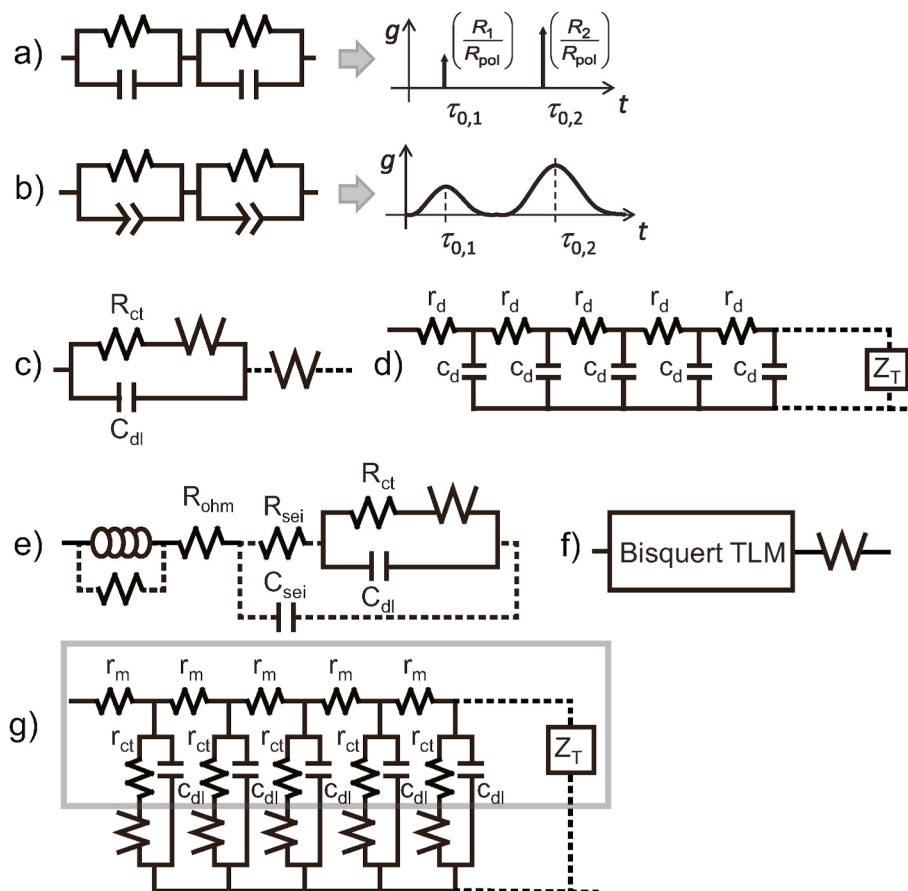


**Fig. 6.** a) Second order Voigt-type circuit element consisting of two  $R||C$  circuit elements for ideally capacitive processes and corresponding DRT where  $g(t)$  consist of Dirac pulses. b) Two fractional order Voigt-type circuit elements or  $R||Q$  circuit elements for real processes with DRT as general distribution function (reproduced and adapted from [55]). c) Randles circuit. The Warburg element,  $W$ , is sometimes alternatively positioned in series as indicated with dashed lines. d) TLM for Warburg element where  $R_d = \Sigma r_d$  and  $C_d = \Sigma c_d$  and terminal impedance  $Z_T$ . e) Hierarchical ladder network with SEI capacitance in parallel with Randles circuit and additional SEI resistance as proposed in [111,243]. f) Bisquert TLM for the electrochemical reaction of a porous electrode connected to Warburg element [32,251]. g) TLM for porous electrodes where Randles circuit is distributed together with the electrolyte resistance along the pores [47,296,297] (the area marked by the grey outlined rectangle represents the Bisquert TLM reported in f).

apparently excellent fit to the data, can make the interpretation of the identified parameters ambiguous and thus the entire analysis of surprisingly limited use. In this review, therefore, the status of ECM approaches for LIBs is systematically and critically examined.

The basis for the ECMs used today was established by the original work of Kohlrausch [308] and Heaviside [309] at the end of the 19th century. In the same era, Warburg integrated Fick's second law and identified the 45° phase angle which is distinctive for the impedance of diffusion processes [310]. The Randles circuit (see Fig. 6c), introduced in 1947 [311], is probably the most used ECM in the LIB research field. The original Randles circuit represents the charge transfer reaction at the metal-electrolyte interface and the diffusion of a dilute faradaic reactant in the supporting liquid electrolyte. In 1980, Ho et al. [312] applied the Randles circuit to model lithium diffusion in the solid state for the first time. Another important development for the ECM was introduced in the 1960s by de Levie through the adoption of a transmission line model (TLM) for the charge transfer reaction at the distributed metal-electrolyte interface in a porous electrode [313,314] (see the grey outline rectangle in Fig. 6g). The model is often known as the Gerischer model as Gerischer used it to represent the diffusion-reaction process in homogeneous bulk electrolyte [315]. This TLM has been more recently actively developed by Bisquert for finite thickness electrodes [316,317] and thus is also named the Bisquert model [318–320] in commercially available software for graphing and analysis of impedance data [321]. The concept of the CPE was introduced by Cole and Cole in 1941 [322], originally to represent non-ideal  $R$  in the Debye dielectric response.

The most common circuit elements used to simulate the impedance spectra of LIBs are inductors ( $L$ ), resistors ( $R$ ), capacitors ( $C$ ), CPEs ( $Q$ ) and Warburg elements ( $W$ ), where the latter may be either infinite-length or finite-length with an “open” terminal  $Z_T$  (see Fig. 6d) [47, 323,324]. While  $R$ ,  $C$ ,  $L$ , and  $W$  have well-defined electrical circuit analogues, the measured impedance spectrum of a commercial LIB cannot be described using these alone [298] and many research groups have proposed modified ECMs. Firstly, capacitors are generalised as CPEs with  $\alpha < 1$  (see below). Secondly, the selection, and position, of the components may be different. The state-of-the-art ECM could consist of either complex variations of the Randles circuit or TLMs for porous electrodes. Indeed, since different ECMs can produce the same impedance spectrum, choosing a more physics-based ECM is essential for an appropriate interpretation of impedance data. In general, to minimise the risk of over-fitting, it is strongly recommended to reduce to a minimum the number of circuit elements used in the ECM. More or less physics-based and often non-trivial adjustments of ECMs have been extensively reported. Different ECMs for LIBs have been overviewed by Osaka et al. [32], Huang et al. [103], and Choi et al. [325].

In general, ECMs for LIBs are constructed considering three different regions of the complex impedance spectrum [172,326,327] (see also Fig. 1). Each region is assigned to a frequency range as follows:

- 1) High frequency range above 1 kHz: Inductive effects of the connecting wires (and cell windings) modelled with an inductance (and often with a parallel resistor, see below) and a series resistor representing the resistance of electrolyte and electrodes i.e.  $(L||R)R_{\text{ohm}}$  (see Fig. 6e).
- 2) Mid frequency range: Series connections of parallel networks of resistor and capacitor (or CPE) used to model charge transfer reactions and double layer effects at anodes, cathodes and solid electrolyte interphases (SEIs), which are straightforwardly related to DRT analysis (Fig. 6a and b).
- 3) Low frequency range: Diffusion processes modelled with Warburg elements,  $W$ , which in connection to the mid frequency responses modelled as  $R||C$  or  $R||Q$ , have two different variations as shown in Fig. 6c.

It has been noted that high frequency inductive effects often exhibit a

non-ideal behaviour [28,103,111,243], which can be described by a resistor in parallel with the  $L$  element [103,111,243] (see Fig. 6e) or by a non-ideal  $L$  (using a CPE with negative  $\alpha$  deviating from  $-1$  [28]). It should be pointed out that the  $R$  parallel to  $L$  does not contribute to the DC cell resistance.

In the mid frequency region of the LIB Nyquist plot, strongly overlapping arcs represent charge transfer impedance, as shown in Fig. 1 (green area) and Fig. 4 (note that the  $x$ - and  $y$ -axes in Fig. 4b, c, d have different scales; the arcs are much more depressed than they appear). These are attributed to the combined impedance from cathode, anode and also the respective SEI layers, each of which could be modelled as an  $RC$  parallel circuit based on the ideal physical descriptions of charge transfer resistance and double layer capacitance at a planar electrode-electrolyte interface, or a thin SEI film with constant specific conductivity and dielectric constant. In the case of poorly conductive active particles such as LFP, the mid frequency region response is also affected by the presence/absence and quality of electronically conductive coatings [328,329]. In order to satisfactorily fit the overlapping arcs, however, the capacitors are typically replaced with CPEs [18] (Fig. 6b). The CPE is a non-intuitive element that cannot be given a specific physical interpretation in any particular context. It is parameterised by a quantity  $Q$  with units of capacitance and a phase angle  $\alpha$ , and expressed as an impedance  $Z_Q = 1/Q(j\omega)^\alpha$  or complex capacitance  $C_Q^* = Q(j\omega)^{\alpha-1}$  that reduces to a corresponding element  $R$ ,  $C$ ,  $L$ , and  $W$  (infinite length) for  $\alpha = 0, 1, -1$ , and  $1/2$ , respectively. Since the simulated arc of a parallel connection of  $R$  and CPE or  $R||Q$  connection is depressed compared to the semicircle of a  $R||C$  connection, the parallel connection of resistor and CPE is called  $Z_{\text{ARC}}$  or ZARC which denotes an arc-shaped impedance trace. Note that the respective impedance arcs are described by the three parameters,  $R$ ,  $Q$ , and  $\alpha$ , rather than numerous  $R||C$  with distributed  $\tau$  values represented by Eq. (5) of DRT analysis. Models including a parallel connection of resistor and CPE are called fractional order circuit models [330]. The distribution is generally and rather vaguely ascribed to the various inhomogeneities associated with composite battery electrodes, far from the idealised case of the single planar interface.

To fit the diffusion processes in the low frequency range, the Warburg element  $W$  is conventionally used. It is either placed in series with  $R||C$  for the surface charge transfer reaction, which corresponds to simple geometrical consideration, or connected in series to  $R$  but in parallel to  $C$  as in the Randles circuit (Fig. 6c). The effect of this simplification has been analysed by Huang et al. [331]. From a physical point of view placing the Warburg element in parallel with the double layer capacitance is to be preferred because diffusion following the charge transfer reaction at the interface is a parallel process with the charging and discharging of double layers. A hierarchical ladder network [47] has also been suggested where the capacitance of the SEI is placed in parallel with the Randles circuit and SEI resistance as shown in Fig. 6e, for the study of SEI deterioration [111,243], which may be a more physical representation of the processes. However, if impedance contributions from various processes need to be separated (e.g., to reduce the spectrum to its polarisation effects for DRT analysis according to Eq. (5)), Voigt-type modelling of the respective processes (Fig. 6b) and placing the Warburg element in series is recommended [332]. Some research groups generalise the Warburg element as a CPE with  $\alpha$  different from  $-1/2$ , because the measured slope of the diffusion impedance often deviates from the ideal inclination angle of 45°. It should be noted, however, that the low frequency diffusion impedance “tail” in the Nyquist plot often exhibits an inclination higher than 45° (see Fig. 1), which cannot be described by CPE generalisation if a TLM is adopted. Oldenburger et al. [234] have explained this behaviour by the effect of the hysteresis of the OCV curve on the differential capacity (see below), which in turn affects the slope of the diffusion impedance. Other physical explanations have been given by stating that the slope is affected by anisotropic diffusion in the particles and by the particle size distribution [333,334].

It should be noted that the Randles circuit and its variation with the Warburg diffusion element in series assumes charge transfer at a planar interface with one-dimensional diffusion into a homogeneous bulk. The one-dimensional diffusion ( $d$ ) can be equivalently represented by an RC TLM, shown in Fig. 6d, where  $R_d = \Sigma r_d$  and  $C_d = \Sigma c_d$ , due to the analogy between Fick's 2nd law for one-dimensional diffusion and the telegrapher's equations [309].

However, in LIBs, the charge transfer reaction occurs at the surface of active material particles dispersed in the electrode layers, connected by conducting binders, with electrolyte permeating through the pores. Ionic transport through the electrode pores and also possibly electronic transport through the solid network, with resistance  $r_m$  (where 'm' identifies the medium), giving a total resistance  $R_m = \Sigma r_m$ , causes additional, non-negligible resistance with respect to the ohmic resistance of the electrolyte in the separator. This is accompanied by the charge transfer reaction at the individual particles, represented by  $r_{ct}||c_{dl}$ , of a total  $R_{ct} = (\Sigma r_{ct}^{-1})^{-1}$  and  $C_{dl} = \Sigma c_{dl}$ . Current passes through the thickness of the electrode layer in a hierarchical manner, as represented in Fig. 6g (grey rectangle) which is known as the Bisquert model [316,321] or finite-length Gerischer model. The impedance response is characterised by a slope-one high frequency trace, as if an  $R_m C_{dl}$  TLM of  $Z = 1/\sqrt{j\omega \cdot \sqrt{R_m/C_{dl}}}$ , and a semi-circular low frequency response as if  $R_{ct}||C_{dl}$ . The magnitude of the skewed impedance arc is  $\sqrt{R_m R_{ct}} \coth \sqrt{R_m/R_{ct}}$ . With  $R_m \rightarrow 0$  the response becomes  $R_{ct}||C_{dl}$  (see Section 3.2.3). The individual particles may be considered to represent the discrete components in the ladder network when the numbers are sufficiently large, the response of which approaches the continuum limit represented by the telegrapher's equation. In common practice for TLMs for porous electrodes [32,251,335,336],  $C_{dl}$  is replaced by  $Q_{dl}$  to describe the depressed semicircular low frequency arcs (from  $R_{ct}||Q_{dl}$ ), as shown in Fig. 4. (It should be noted that Fig. 4b, c, d are not plotted with isotropic axis scales.). With this modification, modelling predicts that the high frequency slope is reduced to  $Z = 1/\sqrt{(j\omega)^{\alpha} \cdot \sqrt{R_m/Q_{dl}}}$  [337]. Due to the overlapping inductive effects, this feature cannot be directly observed, and thus this model may not be supported by experimental data.

Although the Bisquert TLM is used for the electrochemical reaction of LIBs [32,251,335], diffusion processes described in the Randles circuit are not fully incorporated. Rather, the Warburg element for one-dimensional diffusion is placed outside the Randles circuit in series with the TLM, as for the one-dimensional diffusion into the bulk electrode, as shown in Fig. 6f; this is inconsistent. Randles circuits combining solid-state diffusion with charge transfer should be positioned as distributed elements as shown in Fig. 6g [297,336]. Incorporating the one-dimensional Warburg element into the TLM can be applicable when the diffusion in the active particles is essentially one-dimensional due to the particle geometry or crystallographic anisotropy [333,334]. More generally, three-dimensional diffusion into spherical active material particles should be considered. This will be discussed in detail in the Section 3.2.3.

It should be noted that the apparently excellent description of the data by ECMs, regardless of the different circuit configurations, is due to the ubiquitous replacement of capacitors by CPEs, including those in TLMs. The  $\alpha$  parameters in CPEs represent frequency dispersion over a wide frequency range and thus multiple CPEs with arbitrarily adjustable  $\alpha$  can describe experimental data almost perfectly, and do so equally well for somewhat different positioning of the elements, as long as the data are Kramers-Kronig compliant (see Section 3.3.1). Thus, whilst capacitance effects differing by several orders of magnitude allow the respective processes to be deconvoluted in EIS of commercial LIBs, capacitive parameters cannot be unequivocally derived from models using CPEs.

The variety of ECMs used for LIBs can thus be summarised as different connections of electrical elements which have respective physical meanings. Physics-based arrangements or connections of these

components are recommended and they should be applied to fit the experimental data properly. However, generalisation of the capacitive components into CPEs, with arbitrary adjustment of  $\alpha$  values, often allows different ECMs to describe the experimental data equally well but with different sets of parameters. A common model can also yield totally different fit results from automated multi-variable complex nonlinear fitting, depending on the initial values, weighting methods and optimisation algorithms [321,338–340].

### 3.2.3. Advanced physics-based modelling

As pointed out in the previous section, in spite of the excellent fit of many ECMs with experimental data, the results can be poorly utilised or dubiously interpreted due to over-parameterisation and the presence of multiple CPEs. This aspect is a major drawback of rather phenomenological ECMs in comparison with more fundamental physics-based models, such as pseudo-two-dimensional (P2D) LIB models where the battery impedance response is numerically simulated using physico-chemical parameters in the governing equations, i.e. Butler-Volmer equation and drift-diffusion equations in different phases under mass and charge conservation conditions [252,282–286,305]. The essential physics of these governing equations have been implemented in the ECM of Fig. 6g, which was developed for LIBs almost two decades ago by Barsoukov et al. [47,105,296,341], (see Fig. 7a). In short, the Bisquert TLM for porous electrodes is combined with charging/discharging of three-dimensionally dispersed particles in the manner of a Randles circuit. An in-depth explanation and discussion of the model is reported in the book edited by Barsoukov and Macdonald [47] as well as in the manual of the "Multiple Electrochemical Impedance Spectra Parameterization" or MEISP program [339]. The MEISP program allows users to modify or build models using analytical equations. The Barsoukov model for spherical diffusion and some modified forms have been recently implemented in commercial software for graphing and analysis of impedance data such as ZView® (DX-28, 29 and, 30 models) [321]. Both programs are based on Fortran-coded LEVM [338] by J. R. Macdonald. Recently, a Python-based analyzer, PyPhyEIS, has been developed by T. L. Pham [340]. Unfortunately, the use of this advanced physics-based ECM by the battery research community is still very limited. This situation may be due to the widespread acceptance of the customary practice for ECMs, as critically reviewed in the previous section.

It is to be noted that the Barsoukov model [47,296,339] has theoretical and practical limitations related to the generality of the detailed microscopic parameters in the numerical simulations [252,282–286,305]. Nevertheless, it integrates important LIB physics, i.e., ion-binding or trapping, or intercalation, representing the rate-limiting process in the solid state charge storage [342,343] (Barsoukov et al. named this a 'new phase formation' process, which may cause some confusion in view of materials science for battery materials [344]). This process can be incorporated in the diffusion equation [342], but has not been considered in physics-based battery simulations so far [252,282–286,305]. The physics can, however, be succinctly represented by ECM as indicated by  $z_{ss}$  in Fig. 7a. The implementation is to divide the overall differential battery capacity into  $c_d$  representing faster diffusion and  $c_i$  representing a slower crystallisation or binding reaction with relaxation time  $\tau_i = r_i c_i$ , where in general in LIBs,  $c_i \gg c_d$ . Simulated results from this physics-based ECM are shown in Fig. 7c. The left panel represents the well-known diffusion impedance for the different geometries shown in Fig. 7b [333,334,345] and the right panel shows the effect of including the solid state reaction where the low frequency limiting capacitance  $C_d + C_i$  corresponds to the differential capacity of the LIB as computed from the cell open-circuit voltage,  $V$  vs. SOC. As data in the low frequency limit are generally difficult to obtain using EIS, Barsoukov et al. [47] suggested using the capacitance values from  $V$  vs. SOC as a fixed parameter for ECM analysis. Such comprehensive interpretation of the EIS spectra can be beneficial for the detection of specific features in the case of electrochemical testing and measurements of commercial LIBs.

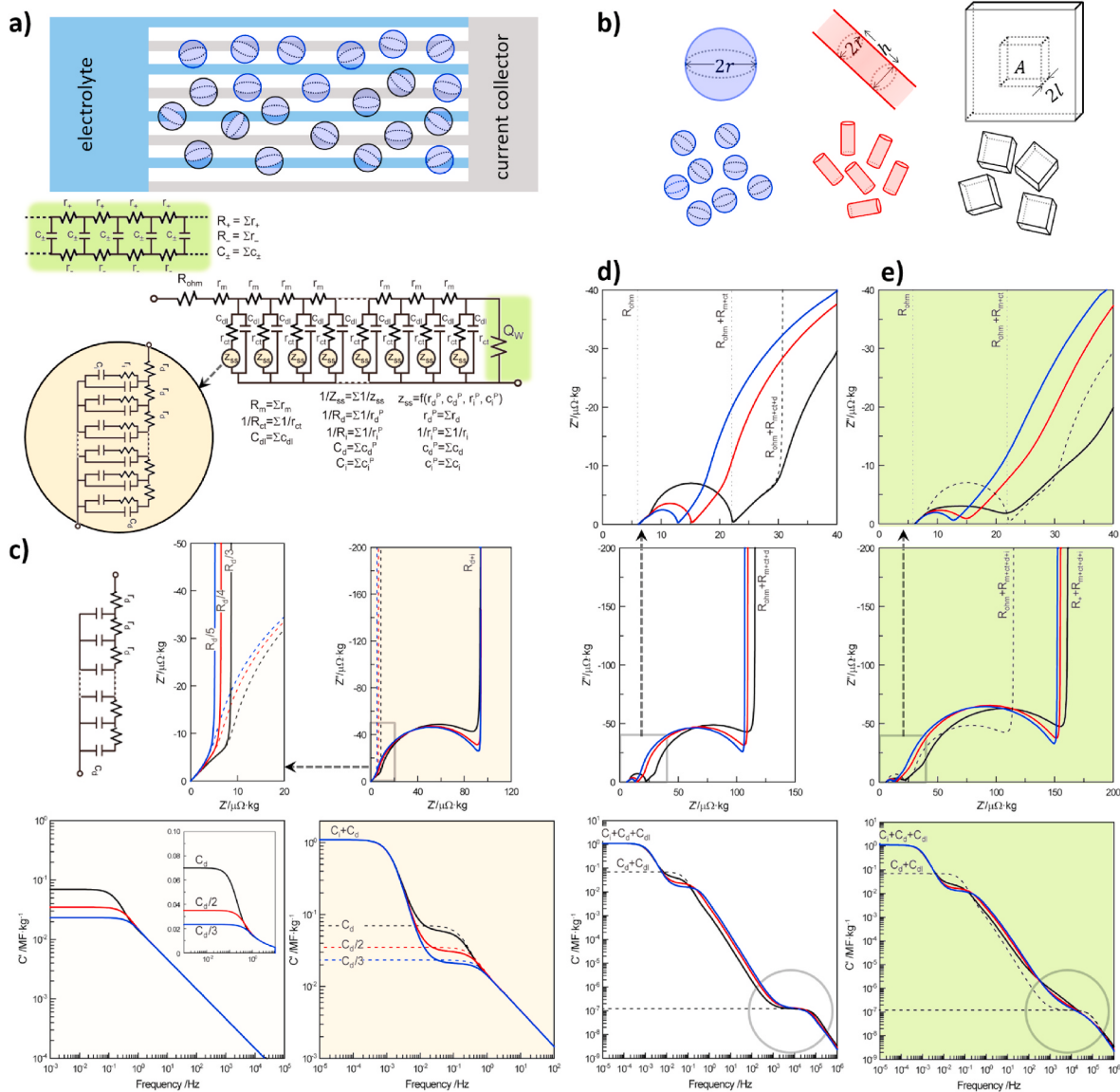


**Fig. 7.** (a) Top, graphical representation of spherical active material particles distributed within a porous battery electrode where the blue and grey colours schematically represent the network of electrolyte pores connected to the separator layer and electronically conducting network connected to the current collector. Bottom, Barsoukov TLM [47,105,296,341] with addition of Warburg element as the terminal impedance,  $Z_T = W$ , highlight green, of the parameter  $Q_W$ , which is CPE coefficient with  $\alpha = 1/2$  [319,320]. ECM for drift-diffusion in liquid electrolyte is also shown where  $R_{\text{ohm}}^{-1} = R_{+}^{-1} + R_{-}^{-1}$ . (b) Active material particle geometry for 3-dimensional (blue), 2-dimensional (red), and 1-dimensional (black outline) diffusion solution where  $r$  and  $l$  represent the respective diffusion length. (c) Complex impedance spectra and capacitance Bode plots for solid state reaction,  $Z_{ss}$  for diffusion only (left column) and for diffusion-intercalation (right column) for spherical (blue), cylindrical (red) and planar geometry (black) for a given amount of active material in the electrode. TLM for 1-dimensional case is indicated. (d) Full spectra of Barsoukov battery impedance model for different diffusion geometry. (e) Full spectra as (d) with the terminal Warburg impedance and diffusion in separator. For (d) and (e) top row presents magnified high frequency region. In (c), (d), and (e) the characteristic capacitive parameters are indicated. Adapted from [340].

Some lack of clarity [333,334] or confusion [47,296,339] exists in ECM parameterisation for different geometries of active material particles. In a recent Python algorithm, PyPhyEIS [340], the impedance function is formulated so that the specific material quantities  $C_d$  and  $C_i$  in  $\text{F}/\text{kg}$  and  $R_i$  in  $\Omega \cdot \text{kg}$ , and thereby the derived diffusivity and intercalation reaction constants,  $D = l^2/(R_d C_d)$  or  $r^2/(R_d C_d)$  and  $\tau_i = R_i C_i$ , are consistently parameterised in a physically meaningful way for all diffusion geometries, as shown in Fig. 7c.

Fig. 7d shows the response of the full Barsoukov TLM, where the Bisquert TLM of the components  $r_m$ ,  $r_{ct}$ , and  $c_{dl}$ , also indicated in Fig. 6f, is combined with the solid state processes  $z_{ss}$  of Fig. 7c. Note that the impedance is given using specific gravimetric units to enable comparison with commercial cells, although  $R_d$ ,  $R_{ct}$ , and  $C_{dl}$  depend on the size of the particles ( $l$  or  $r$ ),  $R_{\text{ohm}}$  depends on the liquid electrolyte

conductivity and separator geometry, and  $R_m$  depends on liquid electrolyte conductivity, porosity, and possibly the electronic network in the electrode composites [47,296,339]. Some of these properties are either unrelated or only indirectly related to the active materials. With the common particle diffusion dimension ( $l$  or  $r$ ) as shown in Fig. 7c, the ratio of the specific surface area ( $\text{cm}^2/\text{g}$ ) is 1:2:3 for the planar, cylindrical, and spherical geometry, respectively, and thus correspondingly varying values of  $C_{dl}$  and  $R_{ct}$  (as 3:2:1 for the latter) can be used in the simulation.

As discussed in the previous section, for a finite medium resistance  $R_m$ , the mid-frequency impedance response exhibits a high frequency inclination of  $45^\circ$  but a semicircular low frequency trace, attributed to  $C_{dl}$  in the TLM of Fig. 7a. The presence of an ideal  $C_{dl}$  is indicated by the plateau (circled) in the capacitance Bode plot in Fig. 7d, bottom. (The

plateau magnitude is also dependent on  $R_m$ ,  $R_{ct}$ ,  $R_{ohm}$  [340].) As already mentioned, however, real EIS responses recorded for commercial LIBs, as in Fig. 1, exhibit often skewed and strongly depressed semicircular traces. This may be one of the reasons why the Barsoukov model has not been widely utilised since the earlier work [296]. Only recently was the model applied to interpret EIS measurements of modified commercial pouch cells containing a lithiated lithium titanate reference electrode [68]; the goodness-of-fit using an ideal  $C_{dl}$  was shown to be rather poor, compared to the conventional analyses using CPEs.

A modified Bisquert TLM has been proposed [319], which explains the high frequency 45° inclination, as observed clearly in experiment [319] and requiring a well-defined  $C_{dl}$  component in the TLM, alongside the generally observed depressed feature. The depressed feature can be simulated by introducing a terminal Warburg impedance  $Z_T = W$ , highlighted green in Fig. 7a. This interfacial impedance plays a unique role as it is connected in series with  $R_m$  but in parallel with  $R_{ct}$  and  $C_{dl}$  [316]. A Warburg-like interfacial impedance is suggested to be a generic feature of many electrochemical cells [319,320]. The physics associated with this component should be further clarified. For example, it has recently been proposed that instead of using  $W$ , one may add an additional parallel current path with resistive elements that represent migration of non-active (i.e. non-lithium) mobile ions [346]. These resistive elements are then coupled to the active ions through an appropriate chemical capacitance of the liquid electrolyte, as indicated by  $r_+$ ,  $r_-$  and  $c_\pm$  for the electrolyte in Fig. 7b. Thus, the physical meaning of  $W$  may be linked to the coupled transport of active and non-active ions in the electrode pores. It has been reported that the diffusion of the electrolyte in the separator layer [346], due to a large capacitance  $c_\pm$  (originating from the large amount of electrolyte contained within the separator), could overlap the low frequency response of diffusion-intercalation in the solid state [286]. In Fig. 7e, compared to Fig. 7d, the low frequency diffusion and intercalation impedance of solid particles are shown to be substantially affected by the diffusion impedance of the solution, indicating further complications in evaluating diffusivity from EIS of LIBs.

The model with up to 11 parameters indicated in Fig. 7a is presently available for simulation and fitting in the PyPhyEIS GitHub platform [340]. It should be emphasised that this ECM succinctly and correctly represents underlying governing equations used in physics-based simulations. Physics underlying the intercalation process can be straightforwardly included in the ECM, even those not yet considered before in the Newman-type simulations.

Overall, the physics-based Barsoukov TLM model is characterised by additive capacitance effects ( $C_i + C_d + C_{dl}$ ). Note that the  $C_{dl}$  contribution may be especially significant in nanostructured active materials. The situation should be clearly distinguished from the additive impedance effects underlying DRT analysis and Voigt-type models (Fig. 6a and b). Although the impedance spectra in Fig. 7d and e appear to be segmentable into different processes, such segments do not exactly correspond to any  $R$  parameters of the ECM in Fig. 7a. Limiting values as indicated by  $R_{m+ct}$ ,  $R_{m+ct+d}$  and  $R_{m+ct+d+i}$  in Fig. 7d can be found by simulation and are also given by somewhat complex analytical expressions of  $R$  and also  $C$  parameters [340]. The individual parameters can be extracted by fitting and used to quantify specific LIB characteristics.

### 3.3. Validation

#### 3.3.1. Kramers-Kronig relations

Reliable interpretation of impedance measurement data is only possible if the data can be validated. Since EIS requires linearity, causality and stationarity, these conditions can be used to formulate mathematical equations that can be applied to the validation of impedance data. Kramers and Kronig derived equations which describe the correlation between the real and imaginary parts of the impedance [347,348]. These first publications on this topic have been reviewed with regard to whether or not the equations were intended to have

general validity [349]. Nowadays, the following equations are used by many research groups and are widely referred to as the Kramers-Kronig relations:

$$Z'(\omega) = Z'(\infty) + \frac{2}{\pi} \int_0^\infty \frac{x Z''(x) - \omega Z''(\omega)}{x^2 - \omega^2} dx \quad (6)$$

and

$$Z''(\omega) = -\frac{2\omega}{\pi} \int_0^\infty \frac{Z'(x) - Z'(\omega)}{x^2 - \omega^2} dx \quad (7)$$

The equations shown above can be used to calculate the real part of the impedance from its imaginary part and vice versa but they can also be formulated in terms of the magnitude of the impedance and its phase. In both cases the calculated values can be compared to the measured ones and the degree of convergence describes the quality of the measurement. Barsoukov and Macdonald pointed out that measuring the magnitude of the impedance and calculating its phase is easier and therefore possible with cheaper measurement devices [47]. Since impedance spectra cannot be measured from 0 Hz to  $\infty$  Hz direct use of equations (6) and (7) is not recommended, but a calculation using direct and inverse Fourier transforms has been presented [350]. Usually, the fact that simple ECMs fulfil the requirements of the Kramers-Kronig relations is sufficient to avoid the issue of incomplete measurement data. If such a model can be fitted to experimental data, the data are assumed to be validated in terms of the Kramers-Kronig relations. This approach, known as the linear Kramers-Kronig transform, was introduced by Agarwal and Orazem [351] and has been extended by Boukamp who added inductive and capacitive behaviour to the model [352]. More recently, the linear Kramers-Kronig transform has been refined in order to avoid ambiguities due to under- and over-fitting [353]. In the same publication, the authors present a short derivation of the fundamental equations and describe how a suitable model order can be determined using a given impedance spectrum. Based on this work the linear Kramers-Kronig test has been automated and improved by Lohmann et al. [269]. In research on impedance spectroscopy on commercial LIBs the Kramers-Kronig relations have only been applied in a minority of publications until now, but their importance has been increasing since the advent of DRT, which is used in an increasing number of studies and requires excellent data quality [55]. The deviation between measured and calculated impedance should be well below 1% [302] which is only possible by careful selection of amplitude for the sinusoidal excitation signal as a trade-off between good signal-to-noise ratio and approximately linear excitation of the non-linear system [354].

#### 3.3.2. Postmortem analysis

As discussed in the Introduction section, since EIS of commercial cells relies on two-electrode measurements, the interpretation of impedance spectra in terms of the underlying contributions from particular cell components and processes can be ambiguous. Measurements in lab-scale cells, using electrode samples harvested from commercial cells, can be used to validate and guide interpretation of commercial cell measurements. Harvesting of electrode samples can be done before or after cell cycling/storage, and in the latter case, can be used to investigate ageing mechanisms, and validate conclusions about these mechanisms drawn from EIS measurements. Ageing of Li-ion cells is a complex process which involves changes in battery parameters related to their usage (cycling ageing) and/or storage (calendar ageing) which can be evaluated through EIS measurements. The deterioration of the battery performance can be mainly attributed to the chemical reactions happening in the various battery components [355] and, despite its complexity, battery degradation has two primary effects at the macroscale: capacity fade (e.g. due to the loss of active material able to store Li) and increased internal resistance/power fading (e.g. due to decreased particle-to-particle contact, growth of surface passivating films, delamination of active materials from current collectors) [65]. To

gain useful insights into Li-ion cell degradation and to validate the interpretation of EIS measurements, several physico-chemical methods of analysis of battery materials obtained from aged cells can be employed. In this section we will focus only on the most relevant techniques used to validate the interpretation of EIS measurements; for a comprehensive review on postmortem analyses of LIBs we suggest the article by Waldmann et al. [356].

In order to perform reliable postmortem analysis of battery materials, particular attention should be paid to the procedure for sampling materials from disassembled cells to obtain representative and reliable results. The various steps generally needed to carry out an exhaustive postmortem analysis are reported in the flowchart of Fig. 8a. It should be pointed out that, when referring to the analysis of aged cells, an analogous assessment must be performed on fresh cells in order to establish a baseline for comparison purposes [82].

**3.3.2.1. Cell inspection and disassembly.** In general, after long-term ageing of an LIB, visual inspection of the specimen is recommended, to observe possible mechanical deformation of the cell enclosure which could be attributed to the generation of excessive amounts of gas and growth of solid side-products during cycling.

Although a small electrolyte leakage might be undetectable by mass loss measurements, visual inspection of the cell could give an indication of electrolyte leakage as it can lead to corrosion of the cell casing or other components. In case of leakage, it is generally not recommended to disassemble the cell, but if deemed necessary, since leakage may evidence phenomena of interest, this should be done with extreme care by a trained (or authorised) operator to avoid any safety incidents, as the presence of leakage elevates the risk of the procedure. Non-destructive investigations, such as X-ray computed tomography (XCT) and neutron diffraction (ND) tomography, can be employed to reveal essential information regarding the cell design, position of safety vents, thickness of various layers, signs of internal failure, thickness of the casing and cutting locations for cell opening [357,358]. It should be mentioned that alternative non-destructive electrochemical methods, such as capacity measurement, cyclic voltammetry and differential capacity analysis [359] can also be used to gain knowledge about ageing mechanisms and to validate EIS measurements.

Prior to cell cutting, a discharge step is required (usually to 0% SOC to ensure personnel safety). It is also important that the cell voltage remains inside the limits of standard operation (identified by the cell manufacturer) to avoid undesired material changes beyond those solely assigned to ageing [356]. The exact definition of the discharge

procedure is especially relevant for the comparison of “fresh” and “cycled” samples and the application of a relatively slow C-rate (e.g. C/20) is generally recommended to ensure comparable sample conditions. Cell cutting can be carried out in various ways depending on the type of cell design; cylindrical cells can be opened by using a pipe tube cutter, a carbide-tip saw tool [360] or, in the case of a more precise cut, a lathe tool [361]. For soft cases such as pouch cells, ceramic scissors are sufficient. However, for hard prismatic cases, drilling might even be required [362] although technical challenges and risk for the operator(s) can arise. It is important in any case to entirely avoid short-circuiting and bending/damaging of the cell to ensure the integrity of the harvested electrodes. To achieve this, the use of specially designed tools is advised; a description of an in-house built tool developed for this purpose has been presented by Pfrang et al. [361]. Information obtained by means of e.g. XCT as mentioned previously is very useful to avoid short-circuiting the cell during disassembly. Opening or disassembling of the cell needs to be carried out under an inert environment to minimise potential safety risks and contamination. Typically an argon-filled glove box is necessary for this, to protect cell components from exposure to O<sub>2</sub>, N<sub>2</sub> and H<sub>2</sub>O.

Extraction of cell components from their enclosure needs to be carried out with care to avoid cross-contamination, mechanical damage, contact with sharp edges, or contamination with metallic debris or fragments generated during the cutting. The welding point of the tabs to the battery case may need to be cut with insulated tools (e.g. ceramic) or to be removed manually. Following this step, anode, separator and cathode can be separated and harvested. To extract the electrolyte, the electrode can be immersed in a specific organic solvent (e.g., CH<sub>2</sub>Cl<sub>2</sub>) [363]. This step must be done quickly as the solvents contained in the electrolyte are highly volatile.

A washing step can also be considered in the case of electrode (anode and cathode) and separator harvesting by using specific solvents (e.g., dimethyl carbonate, DMC, or diethyl carbonate, DEC). A critical aspect to ensure repeatability and comparability of postmortem analysis is the reporting procedure for the washing step which includes, e.g., the amount and type of solvent used, time of exposure applied, temperature. Somerville et al. have found that washing with DMC removes not only the electrolyte salt but also SEI components on the electrode surface [364]. Therefore, the need for a washing step should be evaluated carefully on a case by case basis. After washing, the drying procedure also needs to be reported (e.g. drying in the glove box antechamber or vacuum drying in an oven).

Certain techniques require additional steps in terms of sample

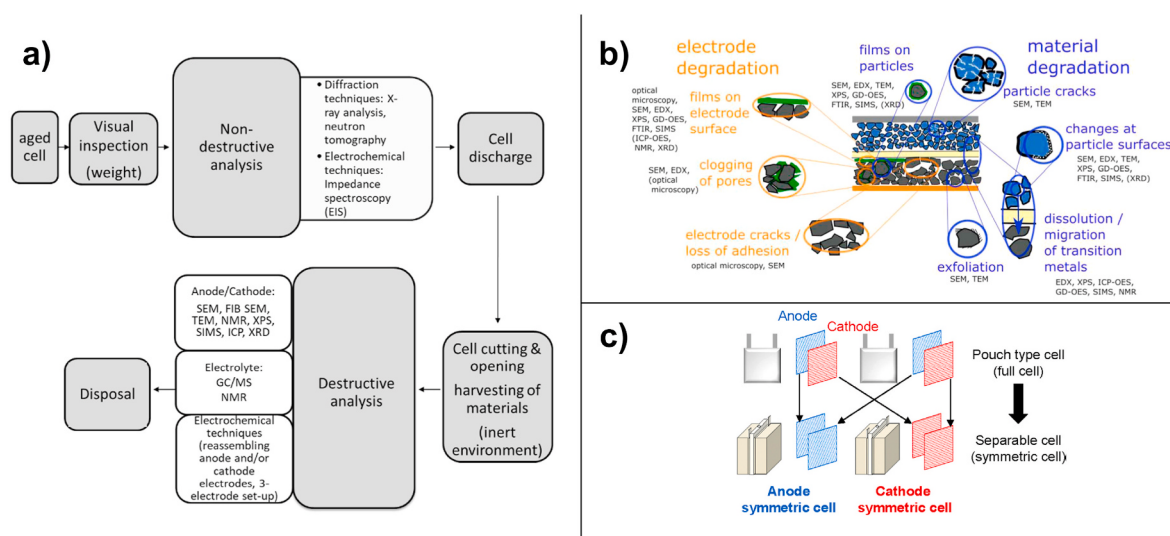


**Fig. 8.** a) Flow chart representation for postmortem analysis of Li-ion cells; b) Physico-chemical techniques used for postmortem analysis of LIB cells (Reproduced from [356]); c) Schematic representation of a Li-ion pouch cell disassembly and symmetric cell reconstruction (Reproduced from [88]).

preparation; in some cases the “intact” electrodes (i.e. electrode samples directly extracted from the cells without any further manipulation) are sufficient, but in other cases the material should be collected by mechanical abrasion of the electrode surface. For example, when performing electrochemical testing on harvested electrodes, usually referred to as lab-scale cell reconstruction, the electrode needs to be cut to an appropriate size/diameter, and one side of the coating needs to be removed (as commercial electrodes are double-side coated) using, for example, N-methyl-2-pyrrolidone (NMP) [154] and water for cathode and anode respectively, by gently rubbing with a cotton bud. It is important to highlight that, since degradation processes do not occur uniformly through the whole electrode foil, multiple sections of the cell need to be harvested to obtain meaningful and representative data. An example of this multiple sampling procedure is reported by Klett et al. [365], where non-uniform electrode ageing (mainly of the graphite electrodes) was observed, showing clear physical differences (even visible to the naked eye) between the central parts of the electrode compared to the outer parts.

Another important aspect, sometimes overlooked when postmortem sampling procedures are described, is the time elapsed between cell disassembly and the actual analysis. This should be minimised to ensure that the electrode samples in contact with electrolyte do not continue reacting. Finally, it should be pointed out that the use of a specific sample holder for transport from the glove box to the equipment of interest is essential to avoid air/moisture contamination of the samples.

**3.3.2.2. Ex situ analysis.** The physicochemical techniques most frequently used for postmortem analysis to validate EIS measurements are summarised below and represented in Fig. 8b.

Surface sensitive methods for electrode and separator analysis:

- Microscopy-based: Optical microscopy, Scanning electron microscopy (SEM), Focused ion beam (FIB)-SEM, Transmission electron microscopy (TEM)
- Spectroscopy-based: Energy dispersive X-ray spectroscopy (EDX), Depth profiling X-ray photoelectron spectroscopy (XPS), Secondary ion mass spectroscopy (SIMS)/Time of Flight SIMS (TOF-SIMS).

Bulk methods for electrode analysis:

- Inductively coupled plasma optical emission spectrometry (ICP-OES), Nuclear magnetic resonance spectroscopy (NMR), X-ray diffraction (XRD).

Surface & bulk methods of analysis:

- Diffraction-based techniques, Fourier transform infrared spectroscopy (FTIR), Glow discharge optical emission spectroscopy depth profiling (GD-OES).

Chemical methods for electrolyte analysis:

- NMR (liquid), Liquid Chromatography coupled with Fourier infrared spectrometry (LC-FTIR), Gas Chromatography (GC) coupled with a thermal conductivity detector (GC-TCD), GC-Mass Spectrometry (GC-MS), GC coupled with a flame ionisation detector (GC-FID) and Ion Chromatography (IC) coupled with Electro Spray Ionisation (ESI).

Diffraction-based techniques (e.g. XRD or ND) are most suited to better understand the solid-state transformations taking place in the active materials of the battery, both in the bulk and, using special experimental set-ups, also in the surface/interface domain [366,367]. XRD and ND techniques are complementary, although in some cases the latter is preferred to the former, e.g. in targeting light elements, specific isotopes or to discriminate between adjacent elements in the periodic table [368,369].

For investigation of Li-ion cell materials, it is strongly recommended to select appropriate X-ray wavelengths for diffraction experiments [370,371]. The choice should be made as a function of (i) chemical composition of the samples and (ii) targeted experimental results.

A Cu sealed anode is the most common X-ray source used for general materials characterisation. However, this source is not the best choice for battery electrode materials [43,372–375]. Mn, Fe, Co and Ni are the main chemical constituents of cathode materials in Li-ion cells, and their interaction with Cu X-ray photons generates low quality diffraction patterns due to absorption and fluorescence issues [371,376], which results in several side effects such as: (i) high background noise, (ii) diminished X-ray penetration into the bulk and (iii) reduced peak-to-background ratio and detection limit. Limited improvements to the collection of diffraction patterns can be obtained, e.g. by using a graphite monochromator or discriminating energy detectors in the path of the diffracted beam. Both approaches can only filter parasitic fluorescence and select X-ray diffracted photons reaching the detector. However, the interaction between Cu X-ray photons and the sample is unchanged and so difficulties related to phase identification and results produced by Rietveld refinement [377,378] arise with a Cu-based X-ray source [376,379,380]. To solve this issue, Co, Mo and, Ag sealed tubes have been proposed as enhanced X-ray sources for the analysis of battery materials [374,381,382]. *Ex situ* postmortem X-ray measurements should be carried out by careful sampling of electrode materials followed by gentle hand-milling action on the harvested material using an agate mortar. These additional steps are strongly recommended to improve X-ray data quality and interpretation, due to the reduction of preferential orientations and micro-absorption issues. The two latter phenomena detrimentally affect the Rietveld method via deviation from correct quantitative phase analysis, calculated density values of each polycrystalline phase and incorrect determination of crystallographic site occupancy by ions, with direct impact on assumptions of ion-migration paths [381,383].

Specific XRD techniques such as Wide-angle X-ray scattering (WAXs), Small Angle X-ray scattering (SAXs), X-ray Reflectivity (XRR) and atomic Pair Distribution Function (PDF) methods are useful tools also for postmortem LIB material characterisation. WAXs measurement is the most widely used of these techniques for battery material characterisation. This method can be performed in both reflection (flat sample; Bragg-Brentano setting) and transmission (capillary or passing through a pouch cell) geometries. WAXs measurements can provide useful crystallographic details and complementary information in support of EIS analysis, helping to identify specific phenomena (e.g. ion migration) which can contribute to the increase of the resistance during battery cell ageing [383,384]. Crystallographic and electrochemical investigation can be combined and enriched with SAXs measurements. The SAXs technique is suited to providing information at the nanoparticle and morphological level. Critical parameters such as nanoparticle distribution, dimension, shape, nanostructure, surface area and porosity can be extracted by means of SAXs measurements of battery electrode materials as reported in Refs. [385–387]. With the XRR technique, information about the correlation of the SEI with battery performance degradation can be acquired [388]. Indications about thickness, surface-interface roughness and density of electrode materials can be also obtained through XRR analysis of electrode components harvested from disassembled cells. However, a special experimental set-up is required to achieve nanometric resolution [388,389]. The atomic PDF technique can take into account the total scattered X-ray information coming from a sample, in the form of small peaks and bumps of the background signal. All of these small halos provide information on short length ordering of atoms, such as coordination environment, distance between neighbouring atoms and local distortions. This level of information is not restricted to the first sphere of coordination, and is complementary to crystal structure information from traditional XRD measurements and Rietveld refinement. In the battery field, PDF methods are used to investigate phases under formation or still in amorphous or high disordered states [389–392].

SEM techniques are also widely applied in postmortem analysis to obtain information about changes in electrode morphology upon cycling. Typically, this provides more information on the anode side

than the cathode side [356,393]. It has been reported that, upon degradation, anode materials (harvested from a small Li-ion pouch cell with a capacity of 0.65 Ah) show an apparent roughness on the surface which can be attributed to a damaged SEI [82]. A thick deposited layer on the anode at the midpoint location in the harvested electrode can be also identified by SEM on cells degraded under constant current conditions [365]. SEM can also provide useful information on the separator. For example, Kwak et al. [62] reported a decrease in separator porosity with storage time. This research work suggests that by-products, originating from side-reactions in the Li-ion cell, can accumulate on the separator surface resulting in poor Li-ion transfer and increased internal resistance of the cell.

XPS measurements are also applied to both cathode and anode to identify the various products generated during cycling of the cell which could contribute to changes in the EIS spectra. The collection and analysis of the XPS spectra of the various electrode samples generally reveal the presence of fluorine (mainly attributed to the polyvinylidene fluoride binder and LiF formed by decomposition of the electrolyte solution) and oxygen-containing species, attributed to carbon-oxygen bonds in carbonates and carboxylates generated by decomposition of electrolyte solvent during cell cycling [139]. In the case of LiFePO<sub>4</sub>-based cells, XPS and EDX were able to identify Fe contamination in the graphite, which occurs when LiPF<sub>6</sub> is used as electrolyte salt at elevated temperatures [394,395]. This Fe contamination in the anode has been correlated to increased impedance [396,397]. For this technique, particular attention should be paid during sample preparation and transportation, as well as in the interpretation of the XPS spectra [398].

As mentioned previously, an electrochemical approach to validate the interpretation of commercial cell impedance measurements consists of reassembly of harvested cathode or anode electrodes in a symmetric two-electrode cell configuration (see Fig. 8c) [32,89,129,251,399]. Applying this cell set-up, the individual contribution of each electrode to the overall Li-ion cell impedance spectrum can be evaluated by a comparison of the commercial cell impedance with that of the symmetric lab-scale cells made of harvested materials [400]. To obtain a proper validation of ageing effects, it is suggested to perform multiple symmetric cell measurements at different conditions (e.g. various SOCs and/or temperatures) using electrodes harvested from aged cells [121, 251].

Although the use of symmetric cells (i) removes any possible EIS distortions coming from a chemically distinct counter or reference electrode [121,401] and (ii) is beneficial in terms of qualitative evaluation of the electrode contributions, reliable quantitative evaluation is not straightforward. Indeed, since symmetric cells are reconstructed from harvested electrodes, fresh electrolyte and uncycled separator are used to acquire the impedance measurements [88]. Moreover, because of the symmetric nature, SOC cannot be varied in this type of cell after assembly [251] and, thus, precision of cell construction (e.g., in terms of sampling and application of harvested electrodes at the same SOC) is essential to obtain reliable validation procedures. Alternatively, the three-electrode half-cell configuration (i.e. where the counter electrode is metallic lithium and a separate, stable electrode is applied as reference electrode) [402] is also used for EIS validation [403]. With this cell configuration, the SOC of the electrode under study can be varied, although the other limitations of the symmetric cell are present. As with full cells, it is important to allow the reconstructed cell to equilibrate after adjusting the SOC [76].

To summarise, performing postmortem analysis to validate the interpretation of EIS measurements of commercial Li-ion cells is a complex and non-trivial task and several factors can affect reliable data collection. The procedure for disassembly of the battery cells is crucial, and all the details need to be comprehensively reported in order to ensure reproducibility and comparability of results. Although many characterisation techniques can be applied, the selection of a suitable set of techniques must be done carefully in order to obtain meaningful

information.

#### 4. Summary, conclusion and outlook

Any interpretation, prediction or evaluation based on impedance spectra relies on the ability to trace the measured impedance values and their uncertainty to a well established common reference: the international system of units. The analysis of CMCs currently proposed by NMIs clearly highlights the need to improve the traceability of impedance measurement, especially in the range of interest for commercial LIBs (i.e. below 0.1 Ω and below 10 Hz). Moreover, a careful uncertainty budget has to be established to take into account measurement conditions (long single-wire cables, home-made test fixtures, etc.) that differ from the ideal conditions required for impedance metrology. Many laboratories and research projects are currently working to address these issues and to improve the reliability of EIS measurement of commercial LIBs [204]. These aspects, if not properly considered, could limit the constructive impact of EIS in understanding the underlying phenomena occurring in commercial LIBs.

A number of measurement techniques are available to obtain the impedance spectra of commercial LIBs. Conventional single-sine EIS is the most commonly applied method for offline impedance measurements. Key considerations include the type (current or voltage) and size of perturbation, in order to maximise signal-to-noise ratio whilst maintaining a linear system response, as well as the procedure for taking measurements at different temperatures and SOCs (including rest periods allowed after adjustment) and the frequency range and resolution for data collection. A well defined measurement system is required to ensure repeatability and reproducibility of results. Various other impedance measurement techniques have been proposed to provide additional information or to overcome some of the measurement challenges of conventional EIS. Dynamic EIS, where the applied perturbation is superimposed on a “baseline” DC current/voltage offset, can be used to investigate dynamic effects of charge/discharge, provided the non-stationarity of the system during the test is minimised/accounted for. Multi-sine EIS, whereby multiple frequencies are excited simultaneously, can be useful for reducing measurement times, though generally at a cost to the signal-to-noise ratio obtainable whilst keeping the overall perturbation amplitude within the linear response regime. The same is true for other time domain techniques, based on non-sinusoidal excitation signals. On the other hand, the non-linear response of the battery, analysed through NFRA/NLEIS, can provide additional information about electrochemical processes. However, this requires more sophisticated interpretation, which is at a relatively early stage of development in the research field. Care is also needed to avoid cell damage with large current perturbations. Whereas conventional EIS requires specialist equipment for signal generation, passive impedance spectroscopy has been proposed as an onboard diagnostic tool for electric vehicles, using only current and voltage signals that result from operating the vehicle, allowing the use of impedance measurements for real-time state estimation and fault detection. Single-frequency EIS measurements have also been proposed for state (temperature) estimation, as well as being commonly used for quality assurance due to their rapidity, but the choice of frequency depends strongly on cell design (especially format). Overall, EIS can be highly effective for understanding and estimating performance of commercial LIBs under different conditions. However, the measurement challenges listed above must be properly considered in order to advance the usefulness of impedance-based techniques in the research field of commercial LIBs. Failure to do so can significantly affect the reliability of EIS measurements and the conclusions drawn from them. Moreover, tests should be properly designed and controlled in order to decouple the effects of different parameters.

A critical insight into the most commonly used methods of interpretation, i.e., ECM and physics-based modelling, to evaluate impedance data from LIBs has been given. Due to their easy application, ECMs are

currently the most widespread option to relate impedance spectra to physical processes and parameters. However, a possible major drawback of applying ECMs to interpret EIS measurements concerns the lack of direct correlation of the ECMs with the physical processes occurring in the battery. Despite the higher level of complexity with respect to ECMs, physics-based models (e.g., the Barsoukov model) are applied increasingly often and are more likely to become the state-of-the-art in the future. In any case, before applying models, validation of the impedance results should be carried out mathematically with the Kramers-Kronig relations in order to check whether the measurements adequately fulfil the criteria of linearity, causality and stationarity.

In terms of attribution of features in the impedance spectrum to particular cell components and processes, validation can be carried out to some extent via postmortem analysis. For such a reason, in this review we have presented some of the most relevant postmortem analysis techniques that can be used to validate, e.g., conclusions about LIB ageing and degradation processes, through the study of the most relevant cell components (anode, cathode and electrolyte). From the analysis carried out, it is clear that selection of a specific technique must be made wisely (targeting each particular case), taking into account that no single technique can provide all the information desired; only through a combination of several techniques can meaningful conclusions be drawn. Of particular importance is the procedure for disassembly of the cell itself. This step, which may be incorrectly regarded as trivial, is actually critical. Careful planning of the sequence of steps requires proper attention and the reporting of steps undertaken needs to be sufficiently detailed to ensure repeatability and reliable interlaboratory comparison. The sampling must also consider the relative position within the cell, to assess the possible - and likely - distribution of local effects. Proper transfer of the harvested samples is essential and needs to avoid contact with air and moisture, to ensure the system analysed is not altered beyond its original harvesting condition. Although the use of non-destructive techniques seems to be preferred to avoid these possible complications, disassembly of the cell may be unavoidable in some cases. A clear example is represented by symmetric cell reconstruction with harvested electrodes, whereby the specific processes occurring at the anode and cathode of the cell can be studied and validated. However, the recent development of *operando* and *in situ* techniques which combine electrochemical and non-electrochemical method of analysis opens up a whole new realm of possibilities which have gained more attention in the research field.

In summary, the methods for measurement, interpretation and validation examined in this review represent the state-of-the-art in the application of EIS to commercial LIBs. With proper consideration of the requirements and limitations associated with specific experimental set-ups, different techniques employed, and proper attention to metrological practice, EIS could be considered as a powerful tool for characterisation of commercial cells.

## Declaration of competing interest

The authors declare that they have no known competing financial interests or personal relationships that could have appeared to influence the work reported in this paper.

## Acknowledgement

Nina Meddings, Marco Heinrich, Frédéric Overney, Vanesa Ruiz, Emilio Napolitano, Steffen Seitz, Gareth Hinds, Rinaldo Raccichini, Miran Gaberšček and Juyeon Park acknowledge the financial support of the European Metrology Programme for Innovation and Research (EMPIR), co-financed by the Participating States and the European Union's Horizon 2020 research and innovation programme, within the project 17IND10-LiBforSecUse. Jong-Sook Lee acknowledges the support of the National Research Foundation (NRF) of Korea funded by the Ministry of Science and ICT (MSIT) (NRF-2018R1A5A1025224). All the

authors thank Dr. Edmund Dickinson (National Physical Laboratory, Teddington, UK) for productive scientific and linguistic discussions.

## Appendix A. Supplementary data

Supplementary data to this article can be found online at <https://doi.org/10.1016/j.jpowsour.2020.228742>.

## References

- [1] K.W. Beard, Linden's Handbook of Batteries, fifth ed., McGraw-Hill Education, 2019.
- [2] A. Barai, K. Uddin, W.D. Widanage, A. McGordon, P. Jennings, A study of the influence of measurement timescale on internal resistance characterisation methodologies for lithium-ion cells, *Sci. Rep.* 8 (1) (2018) 1–13, <https://doi.org/10.1038/s41598-017-18424-5>.
- [3] C. Fleischer, W. Waag, H.-M. Heyn, D.U. Sauer, On-line adaptive battery impedance parameter and state estimation considering physical principles in reduced order equivalent circuit battery models part 2. Parameter and state estimation, *J. Power Sources* 262 (2014) 457–482, <https://doi.org/10.1016/j.jpowsour.2014.03.046>.
- [4] L. Wildfeuer, N. Wassiliadis, C. Reiter, M. Baumann, M. Lienkamp, Experimental characterization of Li-Ion battery resistance at the cell, module and pack level, EVER vol. 2019 (2019), <https://doi.org/10.1109/EVER.2019.8813578>, 14th International Conference on Ecological Vehicles and Renewable Energies 2019) 1–12.
- [5] Y. Tao, J. Ye, X. Li, Q. Zhang, A. Pan, Q. Liao, X. Yang, Ageing study of 26650 type li-ion batteries module at the charge-discharge rates of 1 C, *AIP Conference Proceedings* 2154 (September) (2019), <https://doi.org/10.1063/1.5125355>.
- [6] B.M. Huhsman, J.M. Heinzel, L. Mili, C.T. Love, D.A. Wetze, Investigation into state-of-health impedance diagnosis for 26650 4P1S battery packs, *J. Electrochim. Soc.* 164 (1) (2017) A6401–A6411, <https://doi.org/10.1149/2.063170jes>.
- [7] T. Yokoshima, D. Mukoyama, H. Nara, S. Maeda, K. Nakazawa, T. Momma, T. Osaka, Impedance measurements of kilowatt-class lithium ion battery modules/cubicles in energy storage systems by square-current electrochemical impedance spectroscopy, *Electrochim. Acta* 246 (2017) 800–811, <https://doi.org/10.1016/j.electacta.2017.05.076>.
- [8] K. Takeno, M. Ichimura, K. Takano, J. Yamaki, S. Okada, Quick testing of batteries in lithium-ion battery packs with impedance-measuring technology, *J. Power Sources* 128 (1) (2004) 67–75, <https://doi.org/10.1016/j.jpowsour.2003.09.045>.
- [9] M.J. Brand, M.H. Hofmann, M. Steinhardt, S.F. Schuster, A. Jossen, Current distribution within parallel-connected battery cells, *J. Power Sources* 334 (2016) 202–212, <https://doi.org/10.1016/j.jpowsour.2016.10.010>.
- [10] X. Li, L. Zhang, Y. Liu, A. Pan, Q. Liao, X. Yang, A fast classification method of retired electric vehicle battery modules and their energy storage application in photovoltaic generation, *Int. J. Energy Res.* (2019) 1–8, <https://doi.org/10.1002/er.5083>.
- [11] M. Baumann, L. Wildfeuer, S. Rohr, M. Lienkamp, Parameter variations within Li-Ion battery packs - theoretical investigations and experimental quantification, *J. Energy Storage* 18 (2018) 295–307, <https://doi.org/10.1016/j.est.2018.04.031>.
- [12] A. Barai, K. Uddin, M. Dubarry, L. Somerville, A. McGordon, P. Jennings, I. Bloom, A comparison of methodologies for the non-invasive characterisation of commercial Li-ion cells, *Prog. Energy Combust. Sci.* 72 (2019) 1–31, <https://doi.org/10.1016/j.jpecs.2019.01.001>.
- [13] K. Rumpf, M. Naumann, A. Jossen, Experimental investigation of parametric cell-to-cell variation and correlation based on 1100 commercial lithium-ion cells, *J. Energy Storage* 14 (2017) 224–243, <https://doi.org/10.1016/j.est.2017.09.010>.
- [14] P.S. Attidekou, S. Lambert, M. Armstrong, J. Widmer, K. Scott, P.A. Christensen, A study of 40 Ah lithium ion batteries at zero percent state of charge as a function of temperature, *J. Power Sources* 269 (2014) 694–703, <https://doi.org/10.1016/j.jpowsour.2014.06.064>.
- [15] F.J. Günter, J.B. Habedank, D. Schreiner, T. Neuwirth, R. Gilles, G. Reinhart, Introduction to electrochemical impedance spectroscopy as a measurement method for the wetting degree of lithium-ion cells, *J. Electrochim. Soc.* 165 (14) (2018) A3249–A3256, <https://doi.org/10.1149/2.0081814jes>.
- [16] X. Kong, G.L. Plett, M. Scott Trimboli, Z. Zhang, D. Qiao, T. Zhao, Y. Zheng, Pseudo-kinematical model and impedance diagnosis of micro internal short circuit in lithium-ion cells, *J. Energy Storage* 27 (2020) 101085, <https://doi.org/10.1016/j.est.2019.101085>, July 2019.
- [17] H. Piret, P. Granjon, N. Guillet, V. Cattin, Tracking of electrochemical impedance of batteries, *J. Power Sources* 312 (2016) 60–69, <https://doi.org/10.1016/j.jpowsour.2016.02.006>.
- [18] S. Rodrigues, N. Munichandraiah, A.K. Shukla, AC impedance and state-of-charge analysis of a sealed lithium-ion rechargeable battery, *J. Solid State Electrochem.* 3 (7–8) (1999) 397–405, <https://doi.org/10.1007/s100080050173>.
- [19] S. Rodrigues, N. Munichandraiah, A.K. Shukla, Review of state-of-charge indication of batteries by means of a.c. impedance measurements, *J. Power Sources* 87 (1) (2000) 12–20, [https://doi.org/10.1016/S0378-7753\(99\)00351-1](https://doi.org/10.1016/S0378-7753(99)00351-1).

- [20] J. Xu, C.C. Mi, B. Cao, J. Cao, A new method to estimate the state of charge of lithium-ion batteries based on the battery impedance model, *J. Power Sources* 233 (2013) 277–284, <https://doi.org/10.1016/j.jpowsour.2013.01.094>.
- [21] A. La Rue, P.J. Weddle, M. Ma, C. Hendricks, R.J. Kee, T.L. Vincent, State-of-charge estimation of LiFePO<sub>4</sub>-Li<sub>4</sub>Ti5O<sub>12</sub> batteries using history-dependent complex-impedance, *J. Electrochem. Soc.* 166 (16) (2019) A4041–A4046, <https://doi.org/10.1149/2.0221916jes>.
- [22] A. Cuadras, O. Kanoun, Soc li-ion battery monitoring with impedance spectroscopy, in: 6th International Multi-Conference on Systems, Signals and Devices, SSD, 2009, pp. 1–5, <https://doi.org/10.1109/SSD.2009.4956761>, 2009 (2009).
- [23] J.L. Jespersen, A.E. Tonnesen, K. Nørregaard, L. Overgaard, F. Elefse, Capacity measurements of Li-ion batteries using AC impedance spectroscopy, *World Electric Vehicle Journal* 3 (1) (2009) 127–133, <https://doi.org/10.3390/wevj3010127>.
- [24] F. Leng, C.M. Tan, R. Yazami, M.D. Le, A practical framework of electrical based online state-of-charge estimation of lithium ion batteries, *J. Power Sources* 255 (2014) 423–430, <https://doi.org/10.1016/j.jpowsour.2014.01.020>.
- [25] R. Mingant, J. Bernard, V. Sauvant-Meynot, A. Delaile, S. Mailley, J.L. Hognon, F. Huet, EIS measurements for determining the SoC and SoH of Li-ion batteries, *ECS Transactions* 33 (39) (2011) 41–53, <https://doi.org/10.1149/1.3589920>.
- [26] Y. Sun, Y. Li, M. Yu, Z. Zhou, Q. Zhang, B. Duan, Y. Shang, C. Zhang, Variable fractional order - a comprehensive evaluation indicator of lithium-ion batteries, *J. Power Sources* 448 (October 2019) (2020) 227411, <https://doi.org/10.1016/J.JPOWSOUR.2019.227411>.
- [27] B. Wang, S.E. Li, H. Peng, Z. Liu, Fractional-order modeling and parameter identification for lithium-ion batteries, *J. Power Sources* 293 (2015) 151–161, <https://doi.org/10.1016/j.jpowsour.2015.05.059>.
- [28] R. Xiong, J. Tian, H. Mu, C. Wang, A systematic model-based degradation behavior recognition and health monitoring method for lithium-ion batteries, *Appl. Energy* 207 (2017) 372–383, <https://doi.org/10.1016/j.apenergy.2017.05.124>.
- [29] R. Arunachala, K. Makinejad, S. Athlekar, A. Jossen, J. Garche, Cycle life characterisation of large format lithium-ion cells, 2013 World Electric Vehicle Symposium and Exhibition, EVS (2014) 1–9, <https://doi.org/10.1109/EVS.2013.6914865>, 2014.
- [30] S.F. Schuster, M.J. Brand, C. Campestrini, M. Gleissenberger, A. Jossen, Correlation between capacity and impedance of lithium-ion cells during calendar and cycle life, *J. Power Sources* 305 (2016) 191–199, <https://doi.org/10.1016/j.jpowsour.2015.11.096>.
- [31] X. Wang, X. Wei, H. Dai, Estimation of state of health of lithium-ion batteries based on charge transfer resistance considering different temperature and state of charge, *J. Energy Storage* 21 (2019) 618–631, <https://doi.org/10.1016/j.est.2018.11.020>. August 2018.
- [32] T. Osaka, D. Mukoyama, H. Nara, Review-Development of diagnostic process for commercially available batteries, especially lithium ion battery, by electrochemical impedance spectroscopy, *J. Electrochem. Soc.* 162 (14) (2015) A2529–A2537, <https://doi.org/10.1149/2.0141514jes>.
- [33] M. Galeotti, L. Cinà, C. Giannamico, S. Cordiner, A. Di Carlo, Performance analysis and SOH (state of health) evaluation of lithium polymer batteries through electrochemical impedance spectroscopy, *Energy* 89 (2015) 678–686, <https://doi.org/10.1016/j.energy.2015.05.148>.
- [34] C. Lyu, T. Zhang, W. Luo, G. Wei, B. Ma, L. Wang, SOH Estimation of lithium-ion batteries based on fast time domain impedance spectroscopy, in: Proceedings of the 14th IEEE Conference on Industrial Electronics and Applications, ICIEA, 2019, pp. 2142–2147, <https://doi.org/10.1109/ICIEA.2019.8834119>, 2019.
- [35] R.G. Jungst, G. Nagasubramanian, H.L. Case, B.Y. Liaw, A. Urbina, T.L. Paez, D.H. Dougherty, Accelerated calendar and pulse life analysis of lithium-ion cells, *J. Power Sources* 119–121 (2003) 870–873, [https://doi.org/10.1016/S0378-7753\(03\)00193-9](https://doi.org/10.1016/S0378-7753(03)00193-9).
- [36] R. Koch, A. Jossen, Temperature measurement of large format pouch cells with impedance spectroscopy, in: 28th International Electric Vehicle Symposium and Exhibition 2015, EVS, 2015, pp. 1–9.
- [37] J.P. Schmidt, S. Arnold, A. Loges, D. Werner, T. Wetzel, E. Ivers-Tiffée, Measurement of the internal cell temperature via impedance: evaluation and application of a new method, *J. Power Sources* 243 (2013) 110–117, <https://doi.org/10.1016/j.jpowsour.2013.06.013>.
- [38] L.H.J. Rajmakers, D.L. Danilov, J.P.M. Van Lammeren, M.J.G. Lammers, P.H. L. Notten, Sensorless battery temperature measurements based on electrochemical impedance spectroscopy, *J. Power Sources* 247 (2014) 539–544, <https://doi.org/10.1016/j.jpowsour.2013.09.005>.
- [39] J.G. Zhu, Z.C. Sun, X.Z. Wei, H.F. Dai, A new lithium-ion battery internal temperature on-line estimate method based on electrochemical impedance spectroscopy measurement, *J. Power Sources* 274 (2015) 990–1004, <https://doi.org/10.1016/j.jpowsour.2014.10.182>.
- [40] X. Wang, X. Wei, Q. Chen, J. Zhu, H. Dai, Lithium-ion battery temperature on-line estimation based on fast impedance calculation, *J. Energy Storage* 26 (2019), <https://doi.org/10.1016/j.est.2019.100952>. July.
- [41] H.P.G.J. Beelen, L.H.J. Rajmakers, M.C.F. Donkers, P.H.L. Notten, H.J. Bergveld, A comparison and accuracy analysis of impedance-based temperature estimation methods for Li-ion batteries, *Appl. Energy* 175 (2016) 128–140, <https://doi.org/10.1016/j.apenergy.2016.04.103>.
- [42] P. Haussmann, J. Melbert, Internal cell temperature measurement and thermal modeling of lithium ion cells for automotive applications by means of electrochemical impedance spectroscopy, *SAE International Journal of Alternative Powertrains* 6 (2) (2017), <https://doi.org/10.4271/2017-01-1215>.
- [43] H. Zhou, M.-A. Einarsrud, F. Vullum-Bruer, In situ X-ray diffraction and electrochemical impedance spectroscopy of a nanoporous Li<sub>2</sub>FeSiO<sub>4</sub>/C cathode during the initial charge/discharge cycle of a Li-ion battery, *J. Power Sources* 238 (2013) 478–484, <https://doi.org/10.1016/j.jpowsour.2013.03.193>. Supplement C.
- [44] A. Podias, A. Pfrang, F. Di Persio, A. Kriston, S. Bobba, F. Mathieux, M. Messagie, L. Boon-Brett, Sustainability assessment of second use applications of automotive batteries: ageing of Li-ion battery cells in automotive and grid-scale applications, *World Electric Vehicle Journal* 9 (2) (2018), <https://doi.org/10.3390/wevj9020024>.
- [45] Q. Liao, M. Mu, S. Zhao, L. Zhang, T. Jiang, J. Ye, X. Shen, G. Zhou, Performance assessment and classification of retired lithium ion battery from electric vehicles for energy storage, *Int. J. Hydrogen Energy* 42 (30) (2017) 18817–18823, <https://doi.org/10.1016/j.ijhydene.2017.06.043>.
- [46] J. Li, C. Arbizzani, S. Kjelstrup, J. Xiao, Y. Xia, Y. Yu, Y. Yang, I. Belharouak, T. Zawodzinski, S.T. Myung, R. Raccichini, S. Passerini, Good practice guide for papers on batteries for the Journal of Power Sources, *J. Power Sources* 452 (February) (2020) 227824, <https://doi.org/10.1016/j.jpowsour.2020.227824>.
- [47] E. Barsoukov, J.R. Macdonald (Eds.), *Impedance Spectroscopy: Theory, Experiment, and Applications*, third ed., Wiley, 2018.
- [48] T. Momma, M. Matsunaga, D. Mukoyama, T. Osaka, Ac impedance analysis of lithium ion battery under temperature control, *J. Power Sources* 216 (2012) 304–307, <https://doi.org/10.1016/j.jpowsour.2012.05.095>.
- [49] T.F. Landinger, G. Schwarzerger, A. Jossen, A novel method for high frequency battery impedance measurements, in: 2019 IEEE International Symposium on Electromagnetic Compatibility, Signal and Power Integrity, EMC+SIPI, 2019, pp. 106–110, <https://doi.org/10.1109/ISEMC.2019.8825315>, 2019.
- [50] S. Schindler, M.A. Danzer, Influence of cell design on impedance characteristics of cylindrical lithium-ion cells: a model-based assessment from electrode to cell level, *J. Energy Storage* 12 (2017) 157–166, <https://doi.org/10.1016/j.est.2017.05.002>.
- [51] E.C. Shin, P.A. Ahn, H.H. Seo, J.M. Jo, S.D. Kim, S.K. Woo, J.H. Yu, J. Mizusaki, J. S. Lee, Polarization mechanism of high temperature electrolysis in a Ni-YSZ/YSZ/LSM solid oxide cell by parametric impedance analysis, *Solid State Ionics* 232 (2013) 80–96, <https://doi.org/10.1016/j.ssi.2012.10.028>.
- [52] S.M.M. Alavi, C.R. Birk, D.A. Howey, Time-domain fitting of battery electrochemical impedance models, *J. Power Sources* 288 (2015) 345–352, <https://doi.org/10.1016/j.jpowsour.2015.04.099>.
- [53] T.P. Heins, N. Schlüter, S.T. Ernst, U. Schröder, On the interpretation of impedance spectra of large-format lithium-ion batteries and its application in aging studies, *Energy Technol.* (2019) 1900279doi, <https://doi.org/10.1002/ente.201900279>.
- [54] T.P. Heins, R. Leithoff, N. Schlüter, U. Schröder, K. Dröder, Impedance spectroscopic investigation of the impact of erroneous cell assembly on the aging of lithium-ion batteries, *Energy Technol.* (2019) 1900288, <https://doi.org/10.1002/ente.201900288>.
- [55] J. Illig, J.P. Schmidt, M. Weiss, A. Weber, E. Ivers-Tiffée, Understanding the impedance spectrum of 18650 LiFePO<sub>4</sub>-cells, *J. Power Sources* 239 (2013) 670–679, <https://doi.org/10.1016/j.jpowsour.2012.12.020>.
- [56] X. Zhou, J. Huang, Z. Pan, M. Ouyang, Impedance characterization of lithium-ion batteries aging under high-temperature cycling: importance of electrolyte-phase diffusion, *J. Power Sources* 426 (2019) 216–222, <https://doi.org/10.1016/j.jpowsour.2019.04.040>. April.
- [57] S. Gantenbein, M. Weiss, E. Ivers-Tiffée, Impedance based time-domain modeling of lithium-ion batteries, Part I, *J. Power Sources* 379 (2018) 317–327, <https://doi.org/10.1016/j.jpowsour.2018.01.043>. January.
- [58] J. Landesfeind, D. Pritzl, H.A. Gasteiger, An analysis protocol for three-electrode Li-ion battery impedance spectra: Part I. Analysis of a high-voltage positive electrode, *J. Electrochem. Soc.* 164 (7) (2017) A1773–A1783, <https://doi.org/10.1149/2.0131709jes>.
- [59] J. Xia, K.J. Nelson, Z. Lu, J.R. Dahn, Impact of electrolyte solvent and additive choices on high voltage Li-ion pouch cells, *J. Power Sources* 329 (2016) 387–397, <https://doi.org/10.1016/j.jpowsour.2016.08.100>.
- [60] S. Schindler, M.A. Danzer, A novel mechanistic modeling framework for analysis of electrode balancing and degradation modes in commercial lithium-ion cells, *J. Power Sources* 343 (2017) 226–236, <https://doi.org/10.1016/j.jpowsour.2017.01.026>.
- [61] B. Manikandan, C. Yap, P. Balaya, Towards understanding heat generation characteristics of Li-ion batteries by calorimetry, impedance, and potentiometry studies, *J. Electrochem. Soc.* 164 (12) (2017) A2794–A2800, <https://doi.org/10.1149/2.1811712jes>.
- [62] G. Kwak, J. Park, J. Lee, S. Kim, I. Jung, Effects of anode active materials to the storage-capacity fading on commercial lithium-ion batteries, *J. Power Sources* 174 (2) (2007) 484–492, <https://doi.org/10.1016/j.jpowsour.2007.06.169>.
- [63] R. Petibon, J. Xia, L. Ma, M.K. Bauer, K.J. Nelson, J.R. Dahn, Electrolyte system for high voltage li-ion cells, *J. Electrochem. Soc.* 163 (13) (2016) A2571–A2578, <https://doi.org/10.1149/2.0321613jes>.
- [64] Y. Duan, H. Wu, L. Huang, L. Liu, Y. Zhang, Optimizing current terminals of 18650 lithium-ion power batteries under high discharge current, *Energy Technol.* 5 (9) (2017) 1619–1626, <https://doi.org/10.1002/ente.201700008>.
- [65] J. Vetter, P. Novák, M.R. Wagner, C. Veit, K.C. Möller, J.O. Besenhard, M. Winter, M. Wohlfahrt-Mehrens, C. Vogler, A. Hammouche, Ageing mechanisms in lithium-ion batteries, *J. Power Sources* 147 (1–2) (2005) 269–281, <https://doi.org/10.1016/j.jpowsour.2005.01.006>.
- [66] H. Ge, J. Huang, J. Zhang, Z. Li, Temperature-adaptive alternating current preheating of lithium-ion batteries with lithium deposition prevention,

- J. Electrochim. Soc. 163 (2) (2016) A290–A299, <https://doi.org/10.1149/2.0961602jes>.
- [67] K. Amine, C.H. Chen, J. Liu, M. Hammond, A. Jansen, D. Dees, I. Bloom, D. Vissers, G. Henriksen, Factors responsible for impedance rise in high power lithium ion batteries, *J. Power Sources* 97–98 (2001) 684–687, [https://doi.org/10.1016/S0378-7753\(01\)00701-7](https://doi.org/10.1016/S0378-7753(01)00701-7).
- [68] S.P. Rangarajan, Y. Barsukov, P.P. Mukherjee, In operando impedance based diagnostics of electrode kinetics in Li-ion pouch cells, *J. Electrochim. Soc.* 166 (10) (2019) A2131–A2141, <https://doi.org/10.1149/2.1191910jes>.
- [69] R. Racchini, M. Amores, G. Hinds, Critical review of the use of reference electrodes in Li-ion batteries: a diagnostic perspective, *Batteries* 5 (1) (2019) 12, <https://doi.org/10.3390/batteries5010012>.
- [70] T.P. Heins, N. Schlüter, U. Schröder, Electrode-Resolved monitoring of the ageing of large-scale lithium-ion cells by using electrochemical impedance spectroscopy, *ChemElectroChem* 4 (11) (2017) 2921–2927, <https://doi.org/10.1002/celc.201700686>.
- [71] J. Gomez, R. Nelson, E.E. Kalu, M.H. Weatherspoon, J.P. Zheng, Equivalent circuit model parameters of a high-power Li-ion battery: thermal and state of charge effects, *J. Power Sources* 196 (10) (2011) 4826–4831, <https://doi.org/10.1016/j.jpowsour.2010.12.107>.
- [72] P. Suresh, A.K. Shukla, N. Munichandraiah, Temperature dependence studies of a.c. impedance of lithium-ion cells, *J. Appl. Electrochim.* 32 (3) (2002) 267–273, <https://doi.org/10.1023/A:1015565404343>.
- [73] J.-M. Atebamba, Ž. Moškon, S. Pejovník, M. Gaberšček, On the interpretation of measured impedance spectra of insertion cathodes for lithium-ion batteries, *J. Electrochim. Soc.* 157 (1) (2010) A1218–A1228, <https://doi.org/10.1149/1.3489353>.
- [74] S.S. Zhang, K. Xu, T.R. Jow, Charge and discharge characteristics of a commercial LiCoO<sub>2</sub>-based 18650 Li-ion battery, *J. Power Sources* 160 (2006) 1403–1409, <https://doi.org/10.1016/j.jpowsour.2006.03.037>, 2 SPEC. ISS.
- [75] P. Svens, R. Eriksson, J. Hansson, M. Behm, T. Gustafsson, G. Lindbergh, Analysis of aging of commercial composite metal oxide - Li 4Ti5O12 battery cells, *J. Power Sources* 270 (2014) 131–141, <https://doi.org/10.1016/j.jpowsour.2014.07.050>.
- [76] I. Jiménez Gordon, S. Grugon, A. Débart, G. Pascaly, S. Laruelle, Electrode contributions to the impedance of a high-energy density Li-ion cell designed for EV applications, *Solid State Ionics* 237 (2013) 50–55, <https://doi.org/10.1016/j.ssi.2013.02.016>.
- [77] M. Mastali, M. Parkhondeh, S. Farhad, R.A. Fraser, M. Fowler, Electrochemical modeling of commercial LiFePO<sub>4</sub> and graphite electrodes: kinetic and transport properties and their temperature dependence, *J. Electrochim. Soc.* 163 (13) (2016) A2803–A2816, <https://doi.org/10.1149/2.1151613jes>.
- [78] P. Shafiei Sabet, G. Stahl, D.U. Sauer, Non-invasive investigation of predominant processes in the impedance spectra of high energy lithium-ion batteries with Nickel-Cobalt-Aluminum cathodes, *J. Power Sources* 406 (2018) 185–193, <https://doi.org/10.1016/j.jpowsour.2018.10.024>. November.
- [79] Q. Zhang, R.E. White, Calendar life study of Li-ion pouch cells, *J. Power Sources* 173 (2) (2007) 990–997, <https://doi.org/10.1016/j.jpowsour.2007.08.044>.
- [80] P. Ramadass, B. Haran, R. White, B.N. Popov, Capacity fade of Sony 18650 cells cycled at elevated temperatures: Part I. Cycling performance, *J. Power Sources* 112 (2) (2002) 606–613, [https://doi.org/10.1016/S0378-7753\(02\)00474-3](https://doi.org/10.1016/S0378-7753(02)00474-3).
- [81] Y. Zheng, Y.-B. He, K. Qian, B. Li, X. Wang, J. Li, S.W. Chiang, C. Miao, F. Kang, J. Zhang, Deterioration of lithium iron phosphate/graphite power batteries under high-rate discharge cycling, *Electrochim. Acta* 176 (2015) 270–279, <https://doi.org/10.1016/j.electacta.2015.06.096>.
- [82] Y. Zheng, K. Qian, D. Luo, Y. Li, Q. Lu, B. Li, Y.B. He, X. Wang, J. Li, F. Kang, Influence of over-discharge on the lifetime and performance of LiFePO<sub>4</sub>/graphite batteries, *RSC Adv.* 6 (36) (2016) 30474–30483, <https://doi.org/10.1039/c6ra01677d>.
- [83] V.J. Ovejas, A. Cuadras, Impedance characterization of an LCO-NMC/graphite cell: ohmic conduction, sei transport and charge-transfer phenomenon, *Batteries* 4 (3) (2018), <https://doi.org/10.3390/batteries4030043>.
- [84] R. Premanand, A. Durairajan, B. Haran, R. White, B. Popov, Studies on capacity fade of spinel-based Li-ion batteries, *J. Electrochim. Soc.* 149 (1) (2002) A54, <https://doi.org/10.1149/1.1426399>.
- [85] R. Scipioni, P.S. Jørgensen, C. Graves, J. Hjelm, S.H. Jensen, A physically-based equivalent circuit model for the impedance of a LiFePO<sub>4</sub>/graphite 26650 cylindrical cell, *J. Electrochim. Soc.* 164 (9) (2017) A2017–A2030, <https://doi.org/10.1149/2.1071709jes>.
- [86] G. Sikha, P. Ramadass, B.S. Haran, R.E. White, B.N. Popov, Comparison of the capacity fade of Sony US 18650 cells charged with different protocols, *J. Power Sources* 122 (1) (2003) 67–76, [https://doi.org/10.1016/S0378-7753\(03\)00027-2](https://doi.org/10.1016/S0378-7753(03)00027-2).
- [87] D.P. Abraham, J.L. Knuth, D.W. Dees, I. Bloom, J.P. Christoffersen, Performance degradation of high-power lithium-ion cells—electrochemistry of harvested electrodes, *J. Power Sources* 170 (2) (2007) 465–475, <https://doi.org/10.1016/j.jpowsour.2007.03.071>.
- [88] T. Momma, T. Yokoshima, H. Nara, Y. Gima, T. Osaka, Distinction of impedance responses of Li-ion batteries for individual electrodes using symmetric cells, *Electrochim. Acta* 131 (2014) 195–201, <https://doi.org/10.1016/j.electacta.2014.01.091>.
- [89] G. Nagasubramanian, Two- and three-electrode impedance studies on 18650 Li-ion cells, *J. Power Sources* 87 (1) (2000) 226–229, [https://doi.org/10.1016/S0378-7753\(99\)00469-3](https://doi.org/10.1016/S0378-7753(99)00469-3).
- [90] P. Shafiei Sabet, A.J. Warnecke, F. Meier, H. Witzenhausen, E. Martinez-Laserna, D.U. Sauer, Non-invasive yet separate investigation of anode/cathode degradation of lithium-ion batteries (nickel–cobalt–manganese vs. graphite) due to accelerated aging, *J. Power Sources* 449 (2019) 227369, <https://doi.org/10.1016/j.jpowsour.2019.227369>. July 2019.
- [91] C.H. Chen, J. Liu, K. Amine, Symmetric cell approach towards simplified study of cathode and anode behavior in lithium ion batteries, *Electrochim. Commun.* 3 (1) (2001) 44–47, [https://doi.org/10.1016/S1388-2481\(00\)00145-4](https://doi.org/10.1016/S1388-2481(00)00145-4).
- [92] R. Weber, A.J. Louli, K.P. Plucknett, J.R. Dahn, Resistance growth in lithium-ion pouch cells with LiNi0.80Coo.15Al0.05O2 positive electrodes and proposed mechanism for voltage dependent charge-transfer resistance, *J. Electrochim. Soc.* 166 (10) (2019) A1779–A1784, <https://doi.org/10.1149/2.0361910jes>.
- [93] D. Andre, M. Meiler, K. Steiner, C. Wimmer, T. Soczka-Guth, D.U. Sauer, Characterization of high-power lithium-ion batteries by electrochemical impedance spectroscopy. I. Experimental investigation, *J. Power Sources* 196 (12) (2011) 5334–5341, <https://doi.org/10.1016/j.jpowsour.2010.12.102>.
- [94] W. Waag, S. Käbitz, D.U. Sauer, Experimental investigation of the lithium-ion battery impedance characteristic at various conditions and aging states and its influence on the application, *Appl. Energy* 102 (2013) 885–897, <https://doi.org/10.1016/j.apenergy.2012.09.030>.
- [95] F. An, L. Chen, J. Huang, J. Zhang, P. Li, Rate dependence of cell-to-cell variations of lithium-ion cells, *Sci. Rep.* 6 (2016) 4–10, <https://doi.org/10.1038/srep35051>.
- [96] A.S. Kumar, T.V.S.L. Satyavani, M. Senthilkumar, Effect of temperature and charge stand on performance of lithium-ion polymer pouch cell, *J. Energy Storage* 6 (2016) 239–247, <https://doi.org/10.1016/j.est.2016.02.002>.
- [97] J.P. Fellner, G.J. Loeber, S.S. Sandhu, Testing of lithium-ion 18650 cells and characterizing/predicting cell performance, *J. Power Sources* 81–82 (1999) 867–871, [https://doi.org/10.1016/S0378-7753\(98\)00238-9](https://doi.org/10.1016/S0378-7753(98)00238-9).
- [98] M. Ecker, P. Shafiei Sabet, D.U. Sauer, Influence of operational condition on lithium plating for commercial lithium-ion batteries – electrochemical experiments and post-mortem-analysis, *Appl. Energy* 206 (August) (2017) 934–946, <https://doi.org/10.1016/j.apenergy.2017.08.034>.
- [99] V. Muenzel, A.F. Hollenkamp, A.I. Bhatt, J. De Hoog, M. Brazil, D.A. Thomas, I. Mareels, A comparative testing study of commercial 18650-format lithium-ion battery cells, *J. Electrochim. Soc.* 162 (8) (2015) A1592–A1600, <https://doi.org/10.1149/2.0721508jes>.
- [100] S.S. Zhang, The effect of the charging protocol on the cycle life of a Li-ion battery, *J. Power Sources* 161 (2) (2006) 1385–1391, <https://doi.org/10.1016/j.jpowsour.2006.06.040>.
- [101] L.R. Chen, S.L. Wu, T.R. Chen, W.R. Yang, C.S. Wang, P.C. Chen, Detecting of optimal li-ion battery charging frequency by using AC impedance technique, 2009 4th IEEE Conference on Industrial Electronics and Applications, ICIEA 1 (2009) 3378–3381, <https://doi.org/10.1109/ICIEA.2009.5138829>, 2009.
- [102] S. Guo, R. Xiong, K. Wang, F. Sun, A novel echelon internal heating strategy of cold batteries for all-climate electric vehicles application, *Appl. Energy* 219 (5) (2018) 256–263, <https://doi.org/10.1016/j.apenergy.2018.03.052>.
- [103] Q.A. Huang, Y. Shen, Y. Huang, L. Zhang, J. Zhang, Impedance characteristics and diagnoses of automotive lithium-ion batteries at 7.5% to 93.0% state of charge, *Electrochim. Acta* 219 (2016) 751–765, <https://doi.org/10.1016/j.electacta.2016.09.154>.
- [104] J. Fan, S. Tan, Studies on charging lithium-ion cells at low temperatures, *J. Electrochim. Soc.* 153 (6) (2006), <https://doi.org/10.1149/1.2190029>. A1081–A1092.
- [105] E. Barsoukov, J.H. Kim, C.O. Yoon, H. Lee, Universal battery parameterization to yield a non-linear equivalent circuit valid for battery simulation at arbitrary load, *J. Power Sources* 83 (1–2) (1999) 61–70, [https://doi.org/10.1016/S0378-7753\(99\)00257-8](https://doi.org/10.1016/S0378-7753(99)00257-8).
- [106] T. Osaka, T. Momma, D. Mukoyama, H. Nara, Proposal of novel equivalent circuit for electrochemical impedance analysis of commercially available lithium ion battery, *J. Power Sources* 205 (2012) 483–486, <https://doi.org/10.1016/j.jpowsour.2012.01.070>.
- [107] T.K. Dong, M. Montaru, A. Kirchev, M. Perrin, F. Lambert, Y. Bultel, Modeling of lithium iron phosphate batteries by an equivalent electrical circuit: Part II - model parameterization as function of power and State of Energy (SOE), *ECS Transactions* 35 (32) (2011) 229–237, <https://doi.org/10.1149/1.3655706>.
- [108] T.K. Dong, A. Kirchev, F. Mattera, Y. Bultel, Modeling of lithium iron phosphate batteries by an equivalent-electrical circuit: method of model parameterization and simulation, *ECS Transactions* 25 (35) (2010) 131–138, <https://doi.org/10.1149/1.3414011>.
- [109] A. Farnam, D.U. Sauer, Comparative study of reduced order equivalent circuit models for on-board state-of-available-power prediction of lithium-ion batteries in electric vehicles, *Appl. Energy* 225 (2018) 1102–1122, <https://doi.org/10.1016/j.apenergy.2018.05.066>. April.
- [110] E. Samadani, S. Farhad, W. Scott, M. Mastali, L.E. Gimenez, M. Fowler, R. A. Fraser, Empirical modeling of lithium-ion batteries based on electrochemical impedance spectroscopy tests, *Electrochim. Acta* 160 (2015) 169–177, <https://doi.org/10.1016/j.electacta.2015.02.021>.
- [111] S.E. Li, B. Wang, H. Peng, X. Hu, An electrochemistry-based impedance model for lithium-ion batteries, *J. Power Sources* 258 (2014) 9–18, <https://doi.org/10.1016/j.jpowsour.2014.02.045>.
- [112] T. Kalogiannis, M.S. Hosen, M.A. Sokkheh, S. Goutam, J. Jaguemont, L. Jin, G. Qiao, M. Berecibar, J. Van Mierlo, Comparative study on parameter identification methods for dual-polarization lithium-ion equivalent circuit model, *Energies* 12 (21) (2019) 1–35, <https://doi.org/10.3390/en12214031>.
- [113] M. Ecker, J.B. Gerschler, J. Vogel, S. Käbitz, F. Hust, P. Dechant, D.U. Sauer, Development of a lifetime prediction model for lithium-ion batteries based on extended accelerated aging test data, *J. Power Sources* 215 (2012) 248–257, <https://doi.org/10.1016/j.jpowsour.2012.05.012>.

- [114] T.K. Dong, A. Kirchev, F. Mattera, J. Kowal, Y. Bultel, Dynamic modeling of Li-ion batteries using an equivalent electrical circuit, *J. Electrochem. Soc.* 158 (3) (2011) 326–336, <https://doi.org/10.1149/1.3543710>.
- [115] B.Y. Liaw, G. Nagasubramanian, R.G. Jungst, D.H. Doughty, Modeling of lithium ion cells - a simple equivalent-circuit model approach, *Solid State Ionics* 175 (1–4) (2004) 835–839, <https://doi.org/10.1016/j.ssi.2004.09.049>.
- [116] M. Greenleaf, H. Li, J.P. Zheng, Application of physical electric circuit modeling to characterize Li-ion battery electrochemical processes, *J. Power Sources* 270 (2014) 113–120, <https://doi.org/10.1016/j.jpowsour.2014.07.083>.
- [117] P. Schröer, H. van Faassen, T. Nemeth, M. Kuipers, D.U. Sauer, Challenges in modeling high power lithium titanate oxide cells in battery management systems, *J. Energy Storage* 28 (2020) 101189, <https://doi.org/10.1016/j.est.2019.101189>. November 2019.
- [118] R. Gopalakrishnan, Y. Li, J. Smekens, A. Barhoum, G. Van Assche, N. Omar, J. Van Mierlo, Electrochemical impedance spectroscopy characterization and parameterization of lithium nickel manganese cobalt oxide pouch cells: dependency analysis of temperature and state of charge, *Ionics* 25 (1) (2019) 111–123, <https://doi.org/10.1007/s11581-018-2595-2>.
- [119] X. Wang, X. Wei, H. Dai, Q. Wu, State estimation of lithium ion battery based on electrochemical impedance spectroscopy with on-board impedance measurement system, in: IEEE Vehicle Power and Propulsion Conference (VPPC), IEEE, 2015, pp. 1–5, <https://doi.org/10.1109/VPPC.2015.7353021>, 2015.
- [120] H. Dai, B. Jiang, X. Wei, Impedance characterization and modeling of lithium-ion batteries considering the internal temperature gradient, *Energies* 11 (1) (2018), <https://doi.org/10.3390/en11010220>.
- [121] X. Zhu, L. Fernández Macía, J. Jaguement, J. de Hoog, A. Nikolian, N. Omar, A. Hubin, Electrochemical impedance study of commercial LiNi0.80Co0.15Al0.05O2 electrodes as a function of state of charge and aging, *Electrochim. Acta* 287 (2018) 10–20, <https://doi.org/10.1016/j.jpselectacta.2018.08.054>.
- [122] C. Pastor-Fernández, K. Uddin, G.H. Chouchelamane, W.D. Widanage, J. Marco, A comparison between electrochemical impedance spectroscopy and incremental capacity-differential voltage as Li-ion diagnostic techniques to identify and quantify the effects of degradation modes within battery management systems, *J. Power Sources* 360 (2017) 301–318, <https://doi.org/10.1016/j.jpowsour.2017.03.042>.
- [123] D.A. Howey, V. Yufit, P.D. Mitcheson, G.J. Offer, N.P. Brandon, Impedance measurement for advanced battery management systems, in: 2013 World Electric Vehicle Symposium and Exhibition, EVS, 2014, pp. 1–7, <https://doi.org/10.1109/EVS.2013.6914960>, 2014.
- [124] P. Liu, J. Wang, J. Hicks-Garner, E. Sherman, S. Soukiazian, M. Verbrugge, H. Tataria, J. Musser, P. Finamore, Aging Mechanisms of LiFePO4 batteries deduced by electrochemical and structural analyses, *J. Electrochem. Soc.* 157 (4) (2010), <https://doi.org/10.1149/1.3294790>.
- [125] J. Groot, M. Swierczynski, A.I. Stan, S.K. Kær, On the complex ageing characteristics of high-power LiFePO4/graphite battery cells cycled with high charge and discharge currents, *J. Power Sources* 286 (2015) 475–487, <https://doi.org/10.1016/j.jpowsour.2015.04.001>.
- [126] K. Goebel, B. Saha, A. Saxena, J.R. Celaya, J.P. Christophersen, Prognostics in battery health management, *IEEE Instrum. Meas. Mag.* 11 (4) (2008) 33–40, <https://doi.org/10.1109/MIM.2008.4579269>.
- [127] J. Zhu, M.S. Dewi Darma, M. Knapp, D.R. Sørensen, M. Heere, Q. Fang, X. Wang, H. Dai, L. Mereacre, A. Senyshyn, X. Wei, H. Ehrenberg, Investigation of lithium-ion battery degradation mechanisms by combining differential voltage analysis and alternating current impedance, *J. Power Sources* 448 (2020) 28–30, <https://doi.org/10.1016/j.jpowsour.2019.227575>. December 2019.
- [128] E. Cuervo-Reyes, C.P. Scheller, M. Held, U. Sennhauser, A unifying view of the constant-phase-element and its role as an aging indicator for Li-ion batteries, *J. Electrochem. Soc.* 162 (8) (2015) A1585–A1591, <https://doi.org/10.1149/2.0791508jes>.
- [129] B. Stiaszny, J.C. Ziegler, E.E. Krauß, M. Zhang, J.P. Schmidt, E. Ivers-Tiffée, Electrochemical characterization and post-mortem analysis of aged LiMn 204-NMC/graphite lithium ion batteries part II: calendar aging, *J. Power Sources* 258 (2014) 61–75, <https://doi.org/10.1016/j.jpowsour.2014.02.019>.
- [130] J.C. Burns, A. Kassam, N.N. Sinha, L.E. Downie, L. Solnickova, B.M. Way, J. R. Dahn, Predicting and extending the lifetime of Li-ion batteries, *J. Electrochem. Soc.* 160 (9) (2013) 1–5, <https://doi.org/10.1149/2.060309jes>.
- [131] A. Maheshwari, M. Heck, M. Santarelli, Cycle aging studies of lithium nickel manganese cobalt oxide-based batteries using electrochemical impedance spectroscopy, *Electrochim. Acta* 273 (2018) 335–348, <https://doi.org/10.1016/j.jpselectacta.2018.04.045>.
- [132] Y. Liu, J. Xie, Failure study of commercial LiFePO4 cells in overcharge conditions using electrochemical impedance spectroscopy, *J. Electrochem. Soc.* 162 (10) (2015) A2208–A2217, <https://doi.org/10.1149/2.0911510jes>.
- [133] Y. Zhang, Q. Tang, Y. Zhang, J. Wang, U. Stimming, A.A. Lee, Identifying degradation patterns of lithium ion batteries from impedance spectroscopy using machine learning, *Nat. Commun.* 11 (1) (2020) 1706, <https://doi.org/10.1038/s41467-020-15235-7>.
- [134] S.F. Schuster, T. Bach, E. Fleder, J. Mueller, M. Brand, G. Sextl, A. Jossen, Nonlinear aging characteristics of lithium-ion cells under different operational conditions, *J. Energy Storage* 1 (1) (2015) 44–53, <https://doi.org/10.1016/j.est.2015.05.003>.
- [135] S. Schindler, M. Bauer, M. Petzl, M.A. Danzer, Voltage relaxation and impedance spectroscopy as in-operando methods for the detection of lithium plating on graphitic anodes in commercial lithium-ion cells, *J. Power Sources* 304 (2016) 170–180, <https://doi.org/10.1016/j.jpowsour.2015.11.044>.
- [136] C. Pastor-Fernández, T.F. Yu, W.D. Widanage, J. Marco, Critical review of non-invasive diagnosis techniques for quantification of degradation modes in lithium-ion batteries, *Renew. Sustain. Energy Rev.* 109 (2019) 138–159, <https://doi.org/10.1016/j.rser.2019.03.060>. August 2018.
- [137] D. Mukoyama, T. Momma, H. Nara, T. Osaka, Electrochemical impedance analysis on degradation of commercially available lithium ion battery during chargedischarge cycling, *Chem. Lett.* 41 (4) (2012) 444–446, <https://doi.org/10.1246/cl.2012.444>.
- [138] L. Zhang, J. Jiang, W. Zhang, Capacity Decay Mechanism of the LCO + NMC532/Graphite cells combined with post-mortem technique, *Energies* 10 (8) (2017), <https://doi.org/10.3390/en10081147>.
- [139] R. Scipioni, P.S. Jørgensen, D.I. Stroe, R. Younesi, S.B. Simonsen, P. Norby, J. Hjelm, S.H. Jensen, Complementary analyses of aging in a commercial LiFePO4/graphite 26650 cell, *Electrochim. Acta* 284 (2018) 454–468, <https://doi.org/10.1016/j.selectacta.2018.07.124>.
- [140] J.H. Choi, H. Kim, J.H. Lim, S.J. Kwon, E.Y. Park, K.T. Lee, Thermal behavior of Ni-rich layered oxide cathode materials during cycling of 20 Ah-scale Li-ion batteries, *J. Electrochem. Soc.* 165 (16) (2018) A3837–A3843, <https://doi.org/10.1149/2.0501810jes>.
- [141] F. Hall, J. Touzri, S. Wübler, H. Buqa, W.G. Bessler, Experimental investigation of the thermal and cycling behavior of a lithium titanate-based lithium-ion pouch cell, *J. Energy Storage* 17 (2018) 109–117, <https://doi.org/10.1016/j.est.2018.02.012>.
- [142] A. Matasso, D. Wong, D. Wetz, F. Liu, Correlation of bulk internal pressure rise and capacity degradation of commercial LiCoO2 cells, *J. Electrochem. Soc.* 161 (14) (2014) A2031–A2035, <https://doi.org/10.1149/2.0221414jes>.
- [143] S. Saxena, Y. Xing, M. Pecht, A unique failure mechanism in the Nexus 6P lithium-ion battery, *Batteries* 11 (4) (2018), <https://doi.org/10.3390/en11040841>.
- [144] M. Petzl, M. Kasper, M.A. Danzer, Lithium plating in a commercial lithium-ion battery - a low-temperature aging study, *J. Power Sources* 275 (2015) 799–807, <https://doi.org/10.1016/j.jpowsour.2014.11.065>.
- [145] P.L. Moss, G. Au, E.J. Plichta, J.P. Zheng, Study of capacity fade of lithium-ion polymer rechargeable batteries with continuous cycling, *J. Electrochem. Soc.* 157 (1) (2010) 1–7, <https://doi.org/10.1149/1.3246001>.
- [146] H. Ishikawa, O. Mendoza, Y. Sone, M. Umeda, Study of thermal deterioration of lithium-ion secondary cell using an accelerated rate calorimeter (ARC) and AC impedance method, *J. Power Sources* 198 (2012) 236–242, <https://doi.org/10.1016/j.jpowsour.2011.09.067>.
- [147] P. Röder, B. Stiaszny, J.C. Ziegler, N. Baba, P. Lagaly, H.D. Wiemhöfer, The impact of calendar aging on the thermal stability of a LiMn 204-Li(Ni1/3Mn1/3Co 1/3)O2/graphite lithium-ion cell, *J. Power Sources* 268 (2014) 315–325, <https://doi.org/10.1016/j.jpowsour.2014.06.040>.
- [148] J. Li, J. Zhang, X. Zhang, C. Yang, N. Xu, B. Xia, Study of the storage performance of a Li-ion cell at elevated temperature, *Electrochim. Acta* 55 (3) (2010) 927–934, <https://doi.org/10.1016/j.selectacta.2009.09.077>.
- [149] K. Jalkanen, J. Karppinen, L. Skogström, T. Laurila, M. Nisula, K. Vuorilehto, Cycle aging of commercial NMC/graphite pouch cells at different temperatures, *Appl. Energy* 154 (2015) 160–172, <https://doi.org/10.1016/j.apenergy.2015.04.110>.
- [150] W. Cao, J. Li, Z. Wu, Cycle-life and degradation mechanism of LiFePO4-based lithium-ion batteries at room and elevated temperatures, *Ionics* 22 (10) (2016) 1791–1799, <https://doi.org/10.1007/s11581-016-1703-4>.
- [151] R. Genieser, S. Ferrari, M. Loveridge, S.D. Beattie, R. Beanland, H. Amari, G. West, R. Bhagat, Lithium ion batteries (NMC/graphite) cycling at 80 °C: different electrolytes and related degradation mechanism, *J. Power Sources* 373 (2018) 172–183, <https://doi.org/10.1016/j.jpowsour.2017.11.01>.
- [152] B.S. Haran, P. Ramadass, R.E. White, B.N. Popov, Capacity fade of Li-ion cells cycled at different temperatures, *Proceedings of the Annual Battery Conference on Applications and Advances January* (2002) 13–18, <https://doi.org/10.1109/BCAA.2002.986361>.
- [153] Y. Zhang, C.Y. Wang, X. Tang, Cycling degradation of an automotive LiFePO4 lithium-ion battery, *J. Power Sources* 196 (3) (2011) 1513–1520, <https://doi.org/10.1016/j.jpowsour.2010.08.070>.
- [154] T. Rauhala, K. Jalkanen, T. Romanen, E. Lust, N. Omar, T. Kallio, Low-temperature aging mechanisms of commercial graphite/LiFePO4 cells cycled with a simulated electric vehicle load profile—a post-mortem study, *J. Energy Storage* 20 (2018) 344–356, <https://doi.org/10.1016/j.est.2018.10.007>. June.
- [155] T. Matsuda, K. Ando, M. Myojin, M. Matsumoto, T. Sanada, N. Takao, H. Imai, D. Imamura, Investigation of the influence of temperature on the degradation mechanism of commercial nickel manganese cobalt oxide-type lithium-ion cells during long-term cycle tests, *J. Energy Storage* 21 (2019) 665–671, <https://doi.org/10.1016/j.est.2019.01.009>. March 2018.
- [156] Y. Wu, P. Keil, S.F. Schuster, A. Jossen, Impact of temperature and discharge rate on the aging of a LiCoO2/LiNi0.8Co0.15Al0.05O2 lithium-ion pouch cell, *J. Electrochem. Soc.* 164 (7) (2017) A1438–A1445, <https://doi.org/10.1149/2.0401707jes>.
- [157] D.N. Wong, D.A. Wetz, J.M. Heinzel, A.N. Mansour, Characterizing rapid capacity fade and impedance evolution in high rate pulsed discharged lithium iron phosphate cells for complex, high power loads, *J. Power Sources* 328 (2016) 81–90, <https://doi.org/10.1016/j.jpowsour.2016.08.013>.
- [158] Y. Leng, S. Ge, D. Marple, X.G. Yang, C. Bauer, P. Lamp, C.Y. Wang, Electrochemical cycle-life characterization of high energy lithium-ion cells with thick Li(Ni0.6Mn0.2Co0.2)O2 and graphite electrodes, *J. Electrochem. Soc.* 164 (6) (2017) A1037–A1049, <https://doi.org/10.1149/2.0451706jes>.
- [159] B. Shrestha, P.M. Novak, D.A. Wetz, A.F. Matasso, Evaluation of high C rate cycle induced aging on low impedance lithium-ion batteries using in-situ

- electrochemical impedance spectroscopy (EIS) analysis, *ECS Transactions* 58 (48) (2013) 207–222, <https://doi.org/10.1149/05848.0207ecst>.
- [160] S. Schindler, M. Bauer, H. Cheetamun, M.A. Danzer, Fast charging of lithium-ion cells: identification of aging-minimal current profiles using a design of experiment approach and a mechanistic degradation analysis, *J. Energy Storage* 19 (2018) 364–378, <https://doi.org/10.1016/j.est.2018.08.002>. March.
- [161] D. Wong, B. Shrestha, D.A. Wetz, J.M. Heinzel, Impact of high rate discharge on the aging of lithium nickel cobalt aluminum oxide batteries, *J. Power Sources* 280 (2015) 363–372, <https://doi.org/10.1016/j.jpowsour.2015.01.110>.
- [162] G. Ning, B. Haran, B.N. Popov, Capacity fade study of lithium-ion batteries cycled at high discharge rates, *J. Power Sources* 117 (1) (2003) 160–169, [https://doi.org/10.1016/S0378-7753\(03\)00029-6](https://doi.org/10.1016/S0378-7753(03)00029-6).
- [163] M. Abdel Monem, K. Trad, N. Omar, O. Hegazy, B. Mantels, G. Mulder, P. Van den Bossche, J. Van Mierlo, Lithium-ion batteries: evaluation study of different charging methodologies based on aging process, *Appl. Energy* 152 (2015) 143–155, <https://doi.org/10.1016/j.apenergy.2015.02.064>.
- [164] J. Xia, M. Nie, L. Ma, J.R. Dahn, Variation of columbic efficiency versus upper cutoff potential of Li-ion cells tested with aggressive protocols, *J. Power Sources* 306 (2016) 233–240, <https://doi.org/10.1016/j.jpowsour.2015.12.013>.
- [165] K.J. Nelson, J.E. Harlow, J.R. Dahn, A comparison of NMC/graphite pouch cells and commercially available LiCoO<sub>2</sub>/graphite pouch cells tested to high potential, *J. Electrochem. Soc.* 165 (3) (2018) A456–A462, <https://doi.org/10.1149/2.0041803jes>.
- [166] J. Liu, Q. Duan, M. Ma, C. Zhao, J. Sun, Q. Wang, Aging mechanisms and thermal stability of aged commercial 18650 lithium ion battery induced by slight overcharging cycling, *J. Power Sources* 445 (2020) 227263, <https://doi.org/10.1016/j.jpowsour.2019.227263>. July 2019.
- [167] H. Maleki, J.N. Howard, Effects of overdischarge on performance and thermal stability of a Li-ion cell, *J. Power Sources* 160 (2) (2006) 1395–1402, <https://doi.org/10.1016/j.jpowsour.2006.03.043>.
- [168] D. Kong, R. Wen, P. Ping, R. Peng, J. Zhang, G. Chen, Study on degradation behavior of commercial 18650 LiAlNiCoO<sub>2</sub> cells in over-charge conditions, *Int. J. Energy Res.* 43 (1) (2019) 552–567, <https://doi.org/10.1002/er.4302>.
- [169] Y. Zheng, Y.B. He, K. Qian, B. Li, X. Wang, J. Li, C. Miao, F. Kang, Effects of state of charge on the degradation of LiFePO<sub>4</sub>/graphite batteries during accelerated storage test, *J. Alloys Compd.* 639 (2015) 406–414, <https://doi.org/10.1016/j.jallcom.2015.03.169>.
- [170] A. Barai, K. Uddin, J. Chevalier, G.H. Chouchelamane, A. McGordon, J. Low, P. Jennings, Transportation safety of lithium iron phosphate batteries - a feasibility study of storing at very low states of charge, *Sci. Rep.* 7 (1) (2017) 1–10, <https://doi.org/10.1038/s41598-017-05438-2>.
- [171] Y. Liu, Q. Liu, Z. Li, Y. Ren, J. Xie, H. He, F. Xu, Failure study of commercial LiFePO<sub>4</sub> cells in over-discharge conditions using electrochemical impedance spectroscopy, *J. Electrochem. Soc.* 161 (4) (2014) A620–A632, <https://doi.org/10.1149/2.090404jes>.
- [172] J. Schmitt, A. Maheshwari, M. Heck, S. Lux, M. Vetter, Impedance change and capacity fade of lithium nickel manganese cobalt oxide-based batteries during calendar aging, *J. Power Sources* 353 (2017) 183–194, <https://doi.org/10.1016/j.jpowsour.2017.03.090>.
- [173] C.T. Love, K. Swider-Lyons, Impedance diagnostic for overcharged lithium-ion batteries, *Electrochim. Solid State Lett.* 15 (4) (2012) 53–56, <https://doi.org/10.1149/2.014204esl>.
- [174] R.P. Ramasamy, R.E. White, B.N. Popov, Calendar life performance of pouch lithium-ion cells, *J. Power Sources* 141 (2) (2005) 298–306, <https://doi.org/10.1016/j.jpowsour.2004.09.024>.
- [175] J. Zhu, Z. Sun, X. Wei, H. Dai, W. Gu, Experimental investigations of an AC pulse heating method for vehicular high power lithium-ion batteries at subzero temperatures, *J. Power Sources* 367 (2017) 145–157, <https://doi.org/10.1016/j.jpowsour.2017.09.063>.
- [176] J. Jiang, H. Ruan, B. Sun, L. Wang, W. Gao, W. Zhang, A low-temperature internal heating strategy without lifetime reduction for large-size automotive lithium-ion battery pack, *Appl. Energy* 230 (2018) 257–266, <https://doi.org/10.1016/j.apenergy.2018.08.070>. August.
- [177] Q. Kellner, D. Worwood, A. Barai, W.D. Widanage, J. Marco, Duty-cycle characterisation of large-format automotive lithium ion pouch cells for high performance vehicle applications, *J. Energy Storage* 19 (2018) 170–184, <https://doi.org/10.1016/j.est.2018.07.018>. May.
- [178] M. Reichert, D. Andre, A. Rösmann, P. Janssen, H.G. Bremes, D.U. Sauer, S. Passerini, M. Winter, Influence of relaxation time on the lifetime of commercial lithium-ion cells, *J. Power Sources* 239 (2013) 45–53, <https://doi.org/10.1016/j.jpowsour.2013.03.053>.
- [179] M. Spielbauer, P. Berg, M. Ringat, O. Bohlen, A. Jossen, Experimental study of the impedance behavior of 18650 lithium-ion battery cells under deforming mechanical abuse, *J. Energy Storage* 26 (November) (2019) 101039, <https://doi.org/10.1016/j.est.2019.101039>.
- [180] M.J. Brand, S.F. Schuster, T. Bach, E. Fleder, M. Stelz, S. Gläser, J. Müller, G. Sextl, A. Jossen, Effects of vibrations and shocks on lithium-ion cells, *J. Power Sources* 288 (2015) 62–69, <https://doi.org/10.1016/j.jpowsour.2015.04.107>.
- [181] J.M. Hooper, J. Marco, G.H. Chouchelamane, C. Lyness, Vibration durability testing of nickel manganese cobalt oxide (NMC) lithium-ion 18,650 battery cells, *Energies* 9 (1) (2016) 1–27, <https://doi.org/10.3390/en9010052>.
- [182] P.K.P. Ferraz, J. Kowal, A comparative study on the influence of DC/DC-converter induced high frequency current Ripple on Lithium-Ion Batteries, *Sustainability* 11 (21) (2019) 6050, <https://doi.org/10.3390/su11216050>.
- [183] A. Bessman, R. Soares, O. Wallmark, P. Svens, G. Lindbergh, Aging effects of AC harmonics on lithium-ion cells, *J. Energy Storage* 21 (2019) 741–749, <https://doi.org/10.1016/j.est.2018.12.016>. December 2018.
- [184] K. Uddin, A.D. Moore, A. Barai, J. Marco, The effects of high frequency current ripple on electric vehicle battery performance, *Appl. Energy* 178 (2016) 142–154, <https://doi.org/10.1016/j.apenergy.2016.06.033>.
- [185] M.J. Brand, M.H. Hofmann, S.S. Schuster, P. Keil, A. Jossen, The influence of current ripples on the lifetime of lithium-ion batteries, *IEEE Trans. Veh. Technol.* 67 (11) (2018) 10438–10445, <https://doi.org/10.1109/TVT.2018.2869982>.
- [186] B.V. Ratnakumar, M.C. Smart, L.D. Whitcanack, E.D. Davies, K.B. Chin, F. Deligiannis, S. Surampudi, Behavior of Li-ion cells in high-intensity radiation environments II. Sony/AEA/ComDEV cells, *J. Electrochem. Soc.* 152 (2) (2005) 357–363, <https://doi.org/10.1149/1.1848212>.
- [187] C. Mao, S.J. An, H.M. Meyer, J. Li, M. Wood, R.E. Ruther, D.L. Wood, Balancing formation time and electrochemical performance of high energy lithium-ion batteries, *J. Power Sources* 402 (2018) 107–115, <https://doi.org/10.1016/j.jpowsour.2018.09.019>.
- [188] K.W. Knehr, T. Hodson, C. Bommier, G. Davies, A. Kim, D.A. Steingart, Understanding full-cell evolution and non-chemical electrode crosstalk of Li-ion batteries, *Joule* 2 (6) (2018) 1146–1159, <https://doi.org/10.1016/j.joule.2018.03.016>.
- [189] M. Wünsch, J. Kaufman, D.U. Sauer, Investigation of the influence of different bracing of automotive pouch cells on cyclic lifetime and impedance spectra, *J. Energy Storage* 21 (2019) 149–155, <https://doi.org/10.1016/j.est.2018.11.019>. October 2018.
- [190] A. Barai, Y. Guo, A. McGordon, P. Jennings, A study of the effects of external pressure on the electrical performance of a lithium-ion pouch cell, in: *International Conference on Connected Vehicles and Expo, ICCVE 2013 - Proceedings*, 2013, pp. 295–299, <https://doi.org/10.1109/ICCVE.2013.6799809>, 2013.
- [191] Y. Olofsson, J. Groot, T. Katrašnik, G. Tavčar, Impedance spectroscopy characterisation of automotive NMC/graphite Li-ion cells aged with realistic PHEV load profile, in: *IEEE International Electric Vehicle Conference, IEVC 2014*, 2014, <https://doi.org/10.1109/IEVC.2014.7056095>, 2015.
- [192] A.S. Mussa, M. Klett, M. Behm, G. Lindbergh, R.W. Lindström, Fast-charging to a partial state of charge in lithium-ion batteries: a comparative ageing study, *J. Energy Storage* 13 (2017) 325–333, <https://doi.org/10.1016/j.est.2017.07.004>.
- [193] M. Mathew, S. Janhunen, M. Rashid, F. Long, M. Fowler, Comparative analysis of lithium-ion battery resistance estimation techniques for battery management systems, *Energies* 11 (6) (2018) 121693718, <https://doi.org/10.3390/en11061490>.
- [194] B. Liebhart, L. Komsitska, C. Endisch, Passive impedance spectroscopy for monitoring lithium-ion battery cells during vehicle operation, *J. Power Sources* 449 (2020) 227297, <https://doi.org/10.1016/j.jpowsour.2019.227297>. October 2019.
- [195] H. Zappen, F. Ringbeck, D.U. Sauer, Application of time-resolved multi-sine impedance spectroscopy for lithium-ion battery characterization, *Batteries* 4 (4) (2018) 1–18, <https://doi.org/10.3390/batteries4040064>.
- [196] N. Lohmann, P. Weßkamp, P. Haußmann, J. Melbert, T. Musch, Electrochemical impedance spectroscopy for lithium-ion cells: test equipment and procedures for aging and fast characterization in time and frequency domain, *J. Power Sources* 273 (2015) 613–623, <https://doi.org/10.1016/j.jpowsour.2014.09.132>.
- [197] X. Hong, N. Li, J. Feng, Q. Kong, G. Liu, Multi-electrode resistivity probe for investigation of local temperature inside metal shell battery cells via resistivity: experiments and evaluation of electrical resistance tomography, *Energies* 8 (2) (2015) 742–764, <https://doi.org/10.3390/en8020742>.
- [198] M. Fleckenstein, S. Fischer, O. Bohlen, B. Bäker, Thermal Impedance Spectroscopy - a method for the thermal characterization of high power battery cells, *J. Power Sources* 223 (2013) 259–267, <https://doi.org/10.1016/j.jpowsour.2012.07.144>.
- [199] E. Barsoukov, J.H. Jang, H. Lee, Thermal impedance spectroscopy for Li-ion batteries using heat-pulse response analysis, *J. Power Sources* 109 (2) (2002) 313–320, [https://doi.org/10.1016/S0378-7753\(02\)00080-0](https://doi.org/10.1016/S0378-7753(02)00080-0).
- [200] P. Keil, K. Rumpf, A. Jossen, Thermal impedance spectroscopy for Li-ion batteries with an IR temperature sensor system, *World Electric Vehicle Journal* 6 (3) (2013) 581–591, <https://doi.org/10.3390/wevj6030581>.
- [201] M. Swierczynski, D.I. Stroe, T. Stanciu, S.K. Kar, Electrothermal impedance spectroscopy as a cost efficient method for determining thermal parameters of lithium ion batteries: prospects, measurement methods and the state of knowledge, *J. Clean. Prod.* 155 (2017) 63–71, <https://doi.org/10.1016/j.jclepro.2016.09.109>.
- [202] J.P. Schmidt, A. Weber, E. Ivers-Tiffée, A novel and precise measuring method for the entropy of lithium-ion cells:  $\delta S$  via electrothermal impedance spectroscopy, *Electrochim. Acta* 137 (1) (2014) 311–319, <https://doi.org/10.1016/j.electacta.2014.05.153>.
- [203] L. Palafox, F. Raso, J. Ku, F. Overney, L. Callegaro, P. Gournay, A. Zio, J. Niissilä, G. Eklund, T. Lippert, AIM QuTE : automated impedance metrology extending the quantum toolbox for electricity, in: *16th International Congress of Metrology 11001*, 2013, pp. 1–3, <https://doi.org/10.1051/metrology/201311001>.
- [204] LiBforSecUse, Quality assessment of electric vehicle Li ion batteries for second use applications, <https://www.ptb.de/empir2018/libforsecuse/home/>.
- [205] BIPM, IEC, IFCC, LAC, IUPAC, IUPAP, ISO, OIML, The international vocabulary of metrology—basic and general concepts and associated terms (VIM). [www.bipm.org/utils/common/documents/jcgm/JCGM\\_200\\_2012.pdf](http://www.bipm.org/utils/common/documents/jcgm/JCGM_200_2012.pdf), 2012.
- [206] L. Callegaro, Traceable measurements of electrical impedance, *IEEE Instrum. Meas. Mag.* 18 (6) (2015) 42–46, <https://doi.org/10.1109/MIM.2015.7335839>.

- [207] S.A. Awan, B. Kibble, J. Schurr, Coaxial Electrical Circuits for Interference-free Measurements, IET Electrical Measurement Series, Institution of Engineering and Technology, London, United Kingdom, 2011, <https://doi.org/10.1049/PBEO13E>.
- [208] L. Callegaro, Electrical Impedance. Principles, Measurement, and Application, Series in Sensors, Taylor & Francis, 2013, <https://doi.org/10.1201/b13069>.
- [209] R.D. Cutkosky, Four-terminal-pair networks as precision admittance and impedance standards, *IEEE Transactions on Communication and Electronics* 83 (70) (1964) 19–22, <https://doi.org/10.1109/TCOME.1964.6539563>.
- [210] B. Kibble, Four terminal-pair to anything else!, in: *IEE Colloquium Interconnections from DC to Microwaves 1999*, IEE, 1999, pp. 1–6, <https://doi.org/10.1049/ic:19990102>.
- [211] B.P. Kibble, Proposals for extending traceable impedance measurements to higher frequencies, *Metrologia* 35 (1) (1998) 17–20, <https://doi.org/10.1088/0026-1394/35/1/3>.
- [212] B. Hague, T.R. Foord, *Alternating Current Bridge Methods*, Pitman Publishing, 1971.
- [213] G.H. Rayner, The derivation of resistance, inductance, and capacitance from the NPL primary standard of mutual inductance, *IRE Transactions on Instrumentation I-7* (3 & 4) (1958) 212–220, <https://doi.org/10.1109/IRE-I.1958.5006792>.
- [214] G.H. Rayner, B.P. Kibble, M.J. Swan, On obtaining the henry from the farad, *NPL Report DES 63* (1980).
- [215] A. Campbell, On a standard of mutual inductance, in: *Proceedings of the Royal Society A: Mathematical, Physical and Engineering Sciences* 79, 1907, pp. 428–435, <https://doi.org/10.1098/rspa.1907.0053>, 532.
- [216] A.M. Thompson, D. Lampard, A new theorem in electrostatics and its application to calculable standards of capacitance, *Nature* 177 (4515) (1956) 888, <https://doi.org/10.1038/177888a0>.–888.
- [217] B.N. Taylor, T.J. Witt, New international electrical reference standards based on the Josephson and quantum Hall effects, *Metrologia* 26 (1) (1989) 47–62, <https://doi.org/10.1088/0026-1394/26/1/004>.
- [218] M. Stock, R. Davis, E. de Mirandés, M.J.T. Milton, The revision of the SI—the result of three decades of progress in metrology, *Metrologia* 56 (2) (2019), 022001, <https://doi.org/10.1088/1681-7575/ab0013>.
- [219] F. Overney, B. Jeanneret, Impedance bridges: from wheatstone to Josephson, *Metrologia* 55 (5) (2018) S119–S134, <https://doi.org/10.1088/1681-7575/aacf6c>.
- [220] L. Callegaro, V. D'Elia, M. Kampik, Dan Bee Kim, M. Ortolano, F. Pourdanesh, Experiences with a two-terminal-pair digital impedance bridge, *IEEE Transactions on Instrumentation and Measurement* 64 (6) (2015) 1460–1465, <https://doi.org/10.1109/TIM.2015.2401192>.
- [221] L. Callegaro, V. D'Elia, M. Ortolano, F. Pourdanesh, A three-arm current comparator bridge for impedance comparisons over the complex plane, *IEEE Transactions on Instrumentation and Measurement* 64 (6) (2015) 1466–1471, <https://doi.org/10.1109/TIM.2015.2398953>.
- [222] F. Overney, N.E. Flowers-Jacobs, B. Jeanneret, A. Rüfenacht, A.E. Fox, J. M. Underwood, A.D. Koffman, S.P. Benz, Josephson-based full digital bridge for high-accuracy impedance comparisons, *Metrologia* 53 (4) (2016) 1045–1053, <https://doi.org/10.1088/0026-1394/53/4/1045>.
- [223] S. Mašlán, M. Šíra, T. Skalická, T. Bergsten, Four-terminal pair digital sampling impedance bridge up to 1MHz, *IEEE Transactions on Instrumentation and Measurement* 68 (6) (2019) 1860–1869, <https://doi.org/10.1109/TIM.2019.2908649>.
- [224] M. Ortolano, L. Palafox, J. Kučera, L. Callegaro, V. D'Elia, M. Marzano, F. Overney, G. Gülmез, An international comparison of phase angle standards between the novel impedance bridges of CMI, INRIM and METAS, *Metrologia* 55 (4) (2018) 499–512, <https://doi.org/10.1088/1681-7575/aabf24>.
- [225] F. Overney, B. Jeanneret, Calibration of an LCR-meter at arbitrary phase Angles using a fully automated impedance simulator, *IEEE Transactions on Instrumentation and Measurement* 66 (6) (2017) 1516–1523, <https://doi.org/10.1109/TIM.2017.2652500>.
- [226] A. Technologies, Using OPEN/SHORT/LOAD correction application note 346-3, Tech. rep (1998). <https://literature.cdn.keysight.com/litweb/pdf/5091-6553E.pdf?id=1000030303:epsg:down>. (Accessed 25 August 2020).
- [227] J.M. Torrents, R. Pallàs-Areny, Compensation of impedance meters when using an external front-end amplifier, *IEEE Transactions on Instrumentation and Measurement* 51 (2) (2002) 310–313, <https://doi.org/10.1109/19.997829>.
- [228] D.N. Homan, Applications of coaxial chokes to a-c bridge circuits, *J. Res. Natl. Bur. Stand. J. Res. Natl. Bur. Stand., Section C: Engineering and Instrumentation* 72C (2) (1968) 161, <https://doi.org/10.6028/jres.072C.011>.
- [229] H.W. Ott, *Noise Reduction Techniques in Electronic Systems*, second ed., 1988.
- [230] BioLogic, EC-Lab, Application note #49 EIS measurements: potentiometric or galvanic mode?. <https://www.biologic.net/documents/potentiometric-or-galvanic-eis-electrochemistry-battery-application-note-49/>, 2013 accessed: 2020-05-27.
- [231] Gamry Application Note, EIS measurement of a very low impedance lithium ion battery. [www.gamry.com/application-notes/EIS/eis-measurement-of-a-very-low-impedance-lithium-ion-battery/](http://www.gamry.com/application-notes/EIS/eis-measurement-of-a-very-low-impedance-lithium-ion-battery/), 2016.
- [232] L. Deleebeck, S. Veltzé, Electrochemical impedance spectroscopy study of commercial Li-ion phosphate batteries : a metrology perspective, *Int. J. Energy Res.* (2020) 1–25, <https://doi.org/10.1002/er.5350>.
- [233] T. Stanciu, D.I. Stroe, R. Teodorescu, M. Swierczynski, Extensive EIS characterization of commercially available lithium polymer battery cell for performance modelling, in: 2015 17th European Conference on Power Electronics and Applications, EPE-ECCE Europe 2015, 2015, pp. 1–10, <https://doi.org/10.1109/EPE.2015.7309443>.
- [234] M. Oldenburger, B. Bedürftig, A. Gruhle, F. Grimsmann, E. Richter, R. Findeisen, A. Hintennach, Investigation of the low frequency Warburg impedance of Li-ion cells by frequency domain measurements, *J. Energy Storage* 21 (2019) 272–280, <https://doi.org/10.1016/j.est.2018.11.029>, December 2018.
- [235] M. Messing, T. Shoa, S. Habibi, Lithium-Ion Battery Relaxation Effects, ITEC 2019 - 2019 IEEE Transportation Electrification Conference and Expo, 2019, <https://doi.org/10.1109/ITEC.2019.8790449>.
- [236] F.M. Kindermann, A. Noel, S.V. Erhard, A. Jossen, Long-term equalization effects in Li-ion batteries due to local state of charge inhomogeneities and their impact on impedance measurements, *Electrochim. Acta* 185 (2015) 107–116, <https://doi.org/10.1016/j.electacta.2015.10.108>.
- [237] J.P. Schmidt, E. Ivers-Tiffée, Pulse-fitting - a novel method for the evaluation of pulse measurements, demonstrated for the low frequency behavior of lithium-ion cells, *J. Power Sources* 315 (2016) 316–323, <https://doi.org/10.1016/j.jpowsour.2016.03.026>.
- [238] Y. Fernández Pulido, C. Blanco, D. Anseán, V.M. García, F. Ferrero, M. Valledor, Determination of suitable parameters for battery analysis by electrochemical impedance spectroscopy, *Measurement*, *Journal of the International Measurement Confederation* 106 (1) (2017) 1–11, <https://doi.org/10.1016/j.measurement.2017.04.022>.
- [239] A. Barai, G.H. Chouchelamane, Y. Guo, A. McGordon, P. Jennings, A study on the impact of lithium-ion cell relaxation on electrochemical impedance spectroscopy, *J. Power Sources* 280 (2015) 74–80, <https://doi.org/10.1016/j.jpowsour.2015.01.097>.
- [240] Y. Troxler, B. Wu, M. Marinescu, V. Yufit, Y. Patel, A.J. Marquis, N.P. Brandon, G. J. Offer, The effect of thermal gradients on the performance of lithium-ion batteries, *J. Power Sources* 247 (2014) 1018–1025, <https://doi.org/10.1016/j.jpowsour.2013.06.084>.
- [241] X. Wang, H. Dai, B. Jiang, Research on impedance and nonlinear characteristics of lithium-ion batteries, in: *IEEE Vehicle Power and Propulsion Conference, VPPC 2018 - Proceedings*, 2018, pp. 1–6, <https://doi.org/10.1109/VPPC.2018.8604963>, 2019.
- [242] J. Huang, H. Ge, Z. Li, J. Zhang, Dynamic electrochemical impedance spectroscopy of a three-electrode lithium-ion battery during pulse charge and discharge, *Electrochim. Acta* 176 (2015) 311–320, <https://doi.org/10.1016/j.electacta.2015.07.017>.
- [243] J. Huang, Z. Li, J. Zhang, Dynamic electrochemical impedance spectroscopy reconstructed from continuous impedance measurement of single frequency during charging/discharging, *J. Power Sources* 273 (2015) 1098–1102, <https://doi.org/10.1016/j.jpowsour.2014.07.067>.
- [244] S. Ernst, T.P. Heins, N. Schlüter, U. Schröder, Capturing the current-overpotential nonlinearity of lithium-ion batteries by nonlinear electrochemical impedance spectroscopy (NLEIS) in charge and discharge direction, *Frontiers in Energy Research* 7 (2019) 1–13, <https://doi.org/10.3389/fenrg.2019.00151>, December.
- [245] Z. Stoynov, Nonstationary impedance spectroscopy, *Electrochim. Acta* 38 (14) (1993) 1919–1922, [https://doi.org/10.1016/0013-4686\(93\)80315-Q](https://doi.org/10.1016/0013-4686(93)80315-Q).
- [246] M. Itagaki, N. Kobari, S. Yotsuda, K. Watanabe, S. Kinoshita, M. Ue, In situ electrochemical impedance spectroscopy to investigate negative electrode of lithium-ion rechargeable batteries, *J. Power Sources* 135 (1) (2004) 255–261, <https://doi.org/10.1016/j.jpowsour.2004.04.004>.
- [247] M. Itagaki, N. Kobari, S. Yotsuda, K. Watanabe, S. Kinoshita, M. Ue, LiCoO<sub>2</sub> electrode/electrolyte interface of Li-ion rechargeable batteries investigated by in situ electrochemical impedance spectroscopy, *J. Power Sources* 148 (2005) 78–84, <https://doi.org/10.1016/j.jpowsour.2005.02.007>.
- [248] N. Harting, N. Wolff, U. Kreuer, Identification of lithium plating in lithium-ion batteries using nonlinear frequency response analysis (NFRA), *Electrochim. Acta* 281 (2018) 378–385, <https://doi.org/10.1016/j.electacta.2018.05.139>.
- [249] D.A. Howey, P.D. Mitcheson, S. Member, V. Yufit, G.J. Offer, N.P. Brandon, Online measurement of battery impedance using motor controller excitation, *IEEE Transaction on Vehicular Technology* 63 (6) (2014) 2557–2566, <https://doi.org/10.1109/TVT.2013.2293597>.
- [250] P.T. Wojcik, P. Agarwal, M.E. Orazem, A method for maintaining a constant potential variation during galvanostatic regulation of electrochemical impedance measurements, *Electrochim. Acta* 41 (7) (1996) 977–983, [https://doi.org/10.1016/0013-4686\(95\)00428-9](https://doi.org/10.1016/0013-4686(95)00428-9).
- [251] B. Stiaszny, J.C. Ziegler, E.E. Krauß, J.P. Schmidt, E. Ivers-Tiffée, Electrochemical characterization and post-mortem analysis of aged LiMn<sub>204</sub>-Li(Ni<sub>0.5</sub>Mn<sub>0.3</sub>Co<sub>0.2</sub>O<sub>2</sub>)<sub>2</sub>/graphite lithium ion batteries. Part I: cycle aging, *J. Power Sources* 251 (2014) 439–450, <https://doi.org/10.1016/j.jpowsour.2013.11.080>.
- [252] M.D. Murbach, V.W. Hu, D.T. Schwartz, Nonlinear electrochemical impedance spectroscopy of lithium-Ion batteries: experimental approach, analysis, and initial findings, *J. Electrochim. Soc.* 165 (11) (2018) A2758–A2765, <https://doi.org/10.1149/2.0711811jes>.
- [253] M. Kiel, O. Bohlen, D.U. Sauer, Harmonic analysis for identification of nonlinearities in impedance spectroscopy, *Electrochim. Acta* 53 (25) (2008) 7367–7374, <https://doi.org/10.1016/j.electacta.2008.01.089>.
- [254] J.J. Giner-Sanz, E.M. Ortega, V. Pérez-Herranz, Total harmonic distortion based method for linearity assessment in electrochemical systems in the context of EIS, *Electrochim. Acta* 186 (2015) 598–612, <https://doi.org/10.1016/j.electacta.2015.10.152>.
- [255] Y. Firouz, R. Relan, J.M. Timmermans, N. Omar, P. Van den Bossche, J. Van Mierlo, Advanced lithium ion battery modeling and nonlinear analysis based on robust method in frequency domain: nonlinear characterization and non-parametric modeling, *Energy* 106 (2016) 602–617, <https://doi.org/10.1016/j.energy.2016.03.028>.

- [256] N. Harting, N. Wolff, F. Röder, U. Krewer, Nonlinear frequency response analysis (NFRA) of lithium-ion batteries, *Electrochim. Acta* 248 (2017) 133–139, <https://doi.org/10.1016/j.electacta.2017.04.037>.
- [257] N. Wolff, N. Harting, M. Heinrich, U. Krewer, Nonlinear frequency response analysis on lithium-ion batteries: process identification and differences between transient and steady-state behavior, *Electrochim. Acta* 298 (2019) 788–798, <https://doi.org/10.1016/j.electacta.2018.12.107>.
- [258] N. Wolff, N. Harting, M. Heinrich, F. Röder, U. Krewer, Nonlinear frequency response analysis on lithium-ion batteries: a model-based assessment, *Electrochim. Acta* 260 (2018) 614–622, <https://doi.org/10.1016/j.electacta.2017.12.097>.
- [259] N. Harting, N. Wolff, F. Röder, U. Krewer, State-of-health diagnosis of lithium-ion batteries using nonlinear frequency response analysis, *J. Electrochim. Soc.* 166 (2) (2019) A277–A285, <https://doi.org/10.1149/2.1031902jes>.
- [260] F. Fasmin, R. Srinivasan, Review—nonlinear electrochemical impedance spectroscopy, *J. Electrochim. Soc.* 164 (7) (2017) H443–H455, <https://doi.org/10.1149/2.0391707jes>.
- [261] M. Heinrich, N. Wolff, N. Harting, V. Laue, F. Röder, S. Seitz, U. Krewer, Physico-chemical modeling of a lithium-ion battery: an ageing study with electrochemical impedance spectroscopy, *Batteries and Supercaps* 2 (1) (2019) 530–540, <https://doi.org/10.1002/batt.201900011>.
- [262] E. Ivers-Tiffée, A. Weber, Evaluation of electrochemical impedance spectra by the distribution of relaxation times, *J. Ceram. Soc. Jpn.* 125 (4) (2017) 193–201, <https://doi.org/10.2109/jcersj2.16267>.
- [263] D. Klotz, M. Schönleber, J.P. Schmidt, E. Ivers-Tiffée, New approach for the calculation of impedance spectra out of time domain data, *Electrochim. Acta* 56 (24) (2011) 8763–8769, <https://doi.org/10.1016/j.electacta.2011.07.096>.
- [264] R. Mingant, J. Bernard, V. Sauvant-Meynot, Novel state-of-health diagnostic method for Li-ion battery in service, *Appl. Energy* 183 (2016) 390–398, <https://doi.org/10.1016/j.apenergy.2016.08.118>.
- [265] Gamry Application Note,™ OptiEIS, A Multisine Implementation, 2016.
- [266] BioLogic, EC-Lab, Application note #19 2010 EIS measurements with multisine I – introduction. <https://www.biologic.net/documents/eis-multisine-electrochemistry-battery-corrosion-application-note-19/>, 2010 accessed: 2020-05-27.
- [267] K. Takano, K. Nozaki, Y. Saito, K. Kato, A. Negishi, Impedance spectroscopy by voltage-step chronoamperometry using the Laplace transform method in a lithium-ion battery, *J. Electrochim. Soc.* 147 (3) (2000) 922–929, <https://doi.org/10.1149/1.1393293>.
- [268] J. Sihvo, T. Messo, T. Roinila, R. Luhtala, Online internal impedance measurements of Li-ion battery using PRBS broadband excitation and fourier techniques: methods and injection design, in: International Power Electronics Conference, IPEC-Niigata - ECCE Asia 2018 vol. 0, 2018, pp. 2470–2475, <https://doi.org/10.23919/IPEC.2018.8507565>, 1) (2018).
- [269] N. Lohmann, P. Haussmann, P. Wesskamp, J. Melbert, T. Musch, Employing real automotive driving data for electrochemical impedance spectroscopy on lithium-ion cells, *SAE International Journal of Alternative Powertrains* 4 (2) (2015) 308–317, <https://doi.org/10.4271/2015-01-1187>.
- [270] A. Mertens, I.G. Vinke, H. Tempel, H. Kungl, L.G.J. De Haart, R.A. Eichel, J. Granwehr, Quantitative analysis of time-domain supported electrochemical impedance spectroscopy data of Li-ion batteries: reliable activation energy determination at low frequencies, *J. Electrochim. Soc.* 163 (7) (2016) H521–H527, <https://doi.org/10.1149/2.0511607jes>.
- [271] T. Tanaka, S. Ito, M. Muramatsu, T. Yamada, H. Kamiko, N. Kakimoto, Y. Inui, Accurate and versatile simulation of transient voltage profile of lithium-ion secondary battery employing internal equivalent electric circuit, *Appl. Energy* 143 (2015) 200–210, <https://doi.org/10.1016/j.apenergy.2015.01.028>.
- [272] N.S. Spinner, C.T. Love, S.L. Rose-Pehrsson, S.G. Tuttle, Expanding the operational limits of the single-point impedance diagnostic for internal temperature monitoring of lithium-ion batteries, *Electrochim. Acta* 174 (2015) 488–493, <https://doi.org/10.1016/j.electacta.2015.06.003>.
- [273] R. Srinivasan, B.G. Carkhuff, M.H. Butler, A.C. Baisden, Instantaneous measurement of the internal temperature in lithium-ion rechargeable cells, *Electrochim. Acta* 56 (17) (2011) 6198–6204, <https://doi.org/10.1016/j.electacta.2011.03.136>.
- [274] R. Srinivasan, P.A. Demirev, B.G. Carkhuff, Rapid monitoring of impedance phase shifts in lithium-ion batteries for hazard prevention, *J. Power Sources* 405 (August) (2018) 30–36, <https://doi.org/10.1016/j.jpowsour.2018.10.014>.
- [275] R.R. Richardson, P.T. Ireland, D.A. Howey, Battery internal temperature estimation by combined impedance and surface temperature measurement, *J. Power Sources* 265 (2014) 254–261, <https://doi.org/10.1016/j.jpowsour.2014.04.129>.
- [276] C.T. Love, M.B.V. Virji, R.E. Rocheleau, K.E. Swider-Lyons, State-of-health monitoring of 18650 4S packs with a single-point impedance diagnostic, *J. Power Sources* 266 (2014) 512–519, <https://doi.org/10.1016/j.jpowsour.2014.05.033>.
- [277] A. Chu, P. Braatz, Comparison of commercial supercapacitors and high-power lithium-ion batteries for power-assist applications in hybrid electric vehicles: I. Initial characterization, *J. Power Sources* 112 (1) (2002) 236–246, [https://doi.org/10.1016/S0378-7753\(02\)00364-6](https://doi.org/10.1016/S0378-7753(02)00364-6).
- [278] H.G. Schweiger, O. Obeidi, O. Komesker, A. Raschke, M. Schiemann, C. Zehner, M. Gehnen, M. Keller, P. Birke, Comparison of several methods for determining the internal resistance of lithium ion cells, *Sensors* 10 (6) (2010) 5604–5625, <https://doi.org/10.3390/s100605604>.
- [279] IEC 62660-1, Secondary Lithium-Ion Cells for the Propulsion of Electric Road Vehicles – Part 1: Performance Testing, International Standard, International Electrotechnical Commission, Geneva, Switzerland, 2012.
- [280] Electrically propelled road vehicles, Test Specification for Lithium-Ion Traction Battery Systems – Part 2: High Energy Applications, International Standard, British Standards Institution, 2012.
- [281] J.P. Christoffersen, Battery test manual for electric vehicles, ReVision 3 (2015), <https://doi.org/10.2172/1186745>.
- [282] J.P. Meyers, M. Doyle, R.M. Darling, J. Newman, The impedance response of a porous electrode composed of intercalation particles, *J. Electrochim. Soc.* 147 (8) (2000) 2930, <https://doi.org/10.1149/1.1393627>.
- [283] M. Doyle, J.P. Meyers, J. Newman, Computer simulations of the impedance response of lithium rechargeable batteries, *J. Electrochim. Soc.* 147 (1) (2000) 99, <https://doi.org/10.1149/1.1393162>.
- [284] G. Sikha, R.E. White, Analytical expression for the impedance response of an insertion electrode cell, *J. Electrochim. Soc.* 154 (1) (2007) A43, <https://doi.org/10.1149/1.2372695>.
- [285] G. Sikha, R.E. White, Analytical expression for the impedance response for a lithium-ion cell, *J. Electrochim. Soc.* 155 (12) (2008) A893, <https://doi.org/10.1149/1.2976359>.
- [286] J. Huang, J. Zhang, Theory of impedance response of porous electrodes: simplifications, inhomogeneities, non-stationarities and applications, *J. Electrochim. Soc.* 163 (9) (2016) A1983–A2000, <https://doi.org/10.1149/2.0901609jes>.
- [287] A. Zaban, E. Zinigrad, D. Aurbach, Impedance spectroscopy of Li electrodes. 4. A general simple model of the Li-solution interphase in polar aprotic systems, *J. Phys. Chem.* 100 (8) (1996) 3089–3101, <https://doi.org/10.1021/jp9514279>.
- [288] E.R.v. Schweidler, Studien über die Anomalien im Verhalten der Dielektrika, *Ann. Phys.* 329 (14) (1907) 711–770, <https://doi.org/10.1002/andp.19073291407>.
- [289] K.W. Wagner, Zur Theorie der unvollkommenen Dielektrika, *Ann. Phys.* 345 (5) (1913) 817–855, <https://doi.org/10.1002/andp.19133450502>.
- [290] H. Schichlein, A.C. Müller, M. Voigts, A. Krügel, E. Ivers-tiffe, Deconvolution of electrochemical impedance spectra for the identification of electrode reaction mechanisms in solid oxide fuel cells, *J. Appl. Electrochim.* 32 (2002) 875–882, <https://doi.org/10.1020599525160>.
- [291] J.P. Schmidt, P. Berg, M. Schönleber, A. Weber, E. Ivers-Tiffée, The distribution of relaxation times as basis for generalized time-domain models for Li-ion batteries, *J. Power Sources* 221 (2013) 70–77, <https://doi.org/10.1016/j.jpowsour.2012.07.100>.
- [292] J. Illig, T. Chrobak, M. Ender, J.P. Schmidt, D. Klotz, E. Ivers-Tiffée, Studies on LiFePO<sub>4</sub> as cathode material in Li-ion batteries, *ECS Transactions* 28 (30) (2010) 3–17, <https://doi.org/10.1149/1.3505456>.
- [293] MATLAB, Version 7.10.0, The MathWorks Inc., Natick, Massachusetts, 2019, 2019.
- [294] Matlab Optimization Toolbox, the MathWorks, Natick, MA, USA, 2019.
- [295] T.H. Wan, M. Saccoccia, C. Chen, F. Ciucci, Influence of the discretization methods on the distribution of relaxation times deconvolution: implementing radial basis functions with DRTtools, *Electrochim. Acta* 184 (2015) 483–499, <https://doi.org/10.1016/j.electacta.2015.09.097>.
- [296] E. Barsoukov, D.H. Kim, H.S. Lee, H. Lee, M. Yakovleva, Y. Gao, J.F. Engel, Comparison of kinetic properties of LiCoO<sub>2</sub> and LiTi<sub>0.05</sub>Mg<sub>0.05</sub>Ni<sub>0.7</sub>Coo<sub>2</sub>O<sub>2</sub> by impedance spectroscopy, *Solid State Ionics* 161 (1–2) (2003) 19–29, [https://doi.org/10.1016/S0167-2738\(03\)00150-4](https://doi.org/10.1016/S0167-2738(03)00150-4).
- [297] J. Moskon, S.D. Talian, R. Dominik, M. Gaberšček, Advances in understanding Li battery mechanisms using impedance spectroscopy, *J. Electrochim. Sci. Eng.* 10 (2020), <https://doi.org/10.2298/JSC1002120575>.
- [298] F. Dion, A. Lasia, The use of regularization methods in the deconvolution of underlying distributions in electrochemical processes, *J. Electroanal. Chem.* 475 (1) (1999) 28–37, [https://doi.org/10.1016/S0022-0728\(99\)00334-4](https://doi.org/10.1016/S0022-0728(99)00334-4).
- [299] F. Ciucci, C. Chen, Analysis of electrochemical impedance spectroscopy data using the distribution of relaxation times: a Bayesian and hierarchical Bayesian approach, *Electrochim. Acta* 167 (2015) 439–454, <https://doi.org/10.1016/j.electacta.2015.03.123>.
- [300] H. Qu, J. Kafle, J. Harris, D. Zheng, J. Koshina, D. Boone, A.M. Drake, C. J. Abegglen, D. Qu, Application of ac impedance as diagnostic tool – low temperature electrolyte for a Li-ion battery, *Electrochim. Acta* 322 (2019), <https://doi.org/10.1016/j.electacta.2019.134755>.
- [301] A.L. Gavriluk, D.A. Osinkin, D.I. Bronin, The use of Tikhonov regularization method for calculating the distribution function of relaxation times in impedance spectroscopy, *Russ. J. Electrochim.* 53 (6) (2017) 575–588, <https://doi.org/10.1134/S1023193517060040>.
- [302] M. Hahn, S. Schindler, L.C. Trieb, M.A. Danzer, Optimized process parameters for a reproducible distribution of relaxation times analysis of electrochemical systems, *Batteries* 5 (2) (2019), <https://doi.org/10.3390/batteries5020043>.
- [303] M.A. Danzer, Generalized distribution of relaxation times analysis for the characterization of impedance spectra, *Batteries* 5 (3) (2019) 1–16, <https://doi.org/10.3390/batteries5030053>.
- [304] J. Song, M.Z. Bazant, Electrochemical impedance imaging via the distribution of diffusion times, *Phys. Rev. Lett.* 120 (11) (2018) 116001, <https://doi.org/10.1103/PhysRevLett.120.116001>.
- [305] M.D. Murbach, D.T. Schwartz, Analysis of li-ion battery electrochemical impedance spectroscopy data: an easy-to-implement approach for physics-based parameter estimation using an open-source tool, *J. Electrochim. Soc.* 165 (2) (2018) A297–A304, <https://doi.org/10.1149/2.1021802jes>.
- [306] A. Eddahech, O. Briat, J.M. Vinassa, Performance comparison of four lithium-ion battery technologies under calendar aging, *Energy* 84 (2015) 542–550, <https://doi.org/10.1016/j.energy.2015.03.019>.
- [307] C. Fleischer, W. Waag, H.M. Heyn, D.U. Sauer, On-line adaptive battery impedance parameter and state estimation considering physical principles in

- reduced order equivalent circuit battery models: Part 1. Requirements, critical review of methods and modeling, *J. Power Sources* 260 (2014) 276–291, <https://doi.org/10.1016/j.jpowsour.2014.01.129>.
- [308] F. Kohlrausch, W.A. Nippoldt, Über die Gültigkeit der Ohm'schen Gesetze für Electrolyte und eine numerische Bestimmung des Leitungs widerstandes der verdünnten Schwefelsäure durch alternirende Ströme, *Ann. Phys.* 214 (10) (1869) 280–289.
- [309] O. Heaviside, *Electromagnetic Theory*, Macmillan & Co., London, 1894.
- [310] E. Warburg, Ueber das Verhalten sogenannter unpolarisirbarer Elektroden gegen Wechselstrom, *Ann. Phys.* 303 (3) (1899) 493–499, <https://doi.org/10.1002/andp.18993030302>.
- [311] J.E.B. Randles, Kinetics of rapid electrode reactions, *Discuss. Faraday Soc.* 1 (1947) 11–19, <https://doi.org/10.1039/DF9470100011>.
- [312] C. Ho, I. Raistrick, R. Huggins, Application of a-c techniques to the study of lithium diffusion in tungsten trioxide thin films, *J. Electrochem. Soc.* 127 (2) (1980) 343–350, <https://doi.org/10.1149/1.2129668>.
- [313] R. De Levie, On porous electrodes in electrolyte solutions: I. capacitance effects, *Electrochim. Acta* 8 (10) (1963) 751–780, [https://doi.org/10.1016/0013-4686\(63\)80042-0](https://doi.org/10.1016/0013-4686(63)80042-0).
- [314] R. De Levie, On porous electrodes in electrolyte solutions—iv, *Electrochim. Acta* 9 (9) (1964) 1231–1245, [https://doi.org/10.1016/0013-4686\(64\)85015-5](https://doi.org/10.1016/0013-4686(64)85015-5).
- [315] H. Gerischer, Wechselstrompolarisation von Elektroden mit einem potentialbestimmenden Schritt beim Gleichgewichtspotential II, *Z. Phys. Chem.* 201 (1) (1952) 55–67, <https://doi.org/10.1515/zpch-1952-20105>.
- [316] J. Bisquert, Influence of the boundaries in the impedance of porous film electrodes, *Phys. Chem. Chem. Phys.* 2 (18) (2000) 4185–4192, <https://doi.org/10.1039/B001708F>.
- [317] J. Bisquert, F. Fabregat-Santiago, *Impedance spectroscopy: a general introduction and application to dye-sensitized solar cells*, in: *Dye-sensitized Solar Cells*, EPFL Press, 2010, pp. 477–574.
- [318] E.C. Shin, J. Ma, P.A. Ahn, H.H. Seo, D.T. Nguyen, J.S. Lee, Deconvolution of four transmission-line-model impedances in Ni-YSZ/YSZ/LSM solid oxide cells and mechanistic insights, *Electrochim. Acta* 188 (2016) 240–253, <https://doi.org/10.1016/j.electacta.2015.11.118>.
- [319] H.T. Nguyen, T.L. Tran, D.T. Nguyen, E.-C. Shin, S.-H. Kang, J.-S. Lee, Full parametric impedance analysis of photoelectrochemical cells: case of a  $\text{TiO}_2$  photoanode, *J. Kor. Chem. Soc.* 55 (3) (2018) 244–260, <https://doi.org/10.4191/kcers.2018.55.3.11>.
- [320] H. Seo, K. Jin, S. Park, K.H. Cho, H. Ha, K.G. Lee, Y.H. Lee, D.T. Nguyen, H. Randriamahazaka, J.S. Lee, K.T. Nam, Mechanistic investigation with kinetic parameters on water oxidation catalyzed by manganese oxide nanoparticle film, *ACS Sustain. Chem. Eng.* 7 (12) (2019) 10595–10604, <https://doi.org/10.1021/acssuschemeng.9b01159>.
- [321] ZView 3.5, Impedance/gain Phase Graphing and Analysis Software, Scribner Ass. Inc., 2020 accessed, <http://www.scribner.com/software/68-general-electrochem-mistr36-zview-for-windows/>, 05-27.
- [322] K.S. Cole, R.H. Cole, Dispersion and absorption in dielectrics i. alternating current characteristics, *J. Chem. Phys.* 9 (4) (1941) 341–351, <https://doi.org/10.1063/1.1750906>.
- [323] P. Vyroubal, T. Kazda, Equivalent circuit model parameters extraction for lithium ion batteries using electrochemical impedance spectroscopy, *J. Energy Storage* 15 (2018) 23–31, <https://doi.org/10.1016/j.est.2017.10.019>.
- [324] Q.K. Wang, Y.J. He, J.N. Shen, X.S. Hu, Z.F. Ma, State of charge-dependent polynomial equivalent circuit modeling for electrochemical impedance spectroscopy of lithium-ion batteries, *IEEE Trans. Power Electron.* 33 (10) (2018) 8449–8460, <https://doi.org/10.1109/TPEL.2017.2780184>.
- [325] W. Choi, H.-C. Shin, J.M. Kim, J.-Y. Choi, W.-S. Yoon, Modeling and applications of electrochemical impedance spectroscopy (eis) for lithium-ion batteries, *Journal of Electrochemical Science and Technology* 11 (1) (2020) 1–13, <https://doi.org/10.33961/jecst.2019.00528>.
- [326] Y. Zhang, R. Zhao, J. Dubie, T. Jahns, L. Juang, Investigation of current sharing and heat dissipation in parallel-connected lithium-ion battery packs, *ECCE 2016 - IEEE Energy Conversion Congress and Exposition, Proceedings* (2016) 1, <https://doi.org/10.1109/ECCE.2016.7855217>.
- [327] S. Buteau, J.R. Dahn, Analysis of thousands of electrochemical impedance spectra of lithium-ion cells through a machine learning inverse model, *J. Electrochem. Soc.* 166 (8) (2019), <https://doi.org/10.1149/2.1051908jes>. A1611–A1622.
- [328] H.C. Shin, W.I. Cho, H. Jang, Electrochemical properties of the carbon-coated LiFePO<sub>4</sub> as a cathode material for lithium-ion secondary batteries, *J. Power Sources* 159 (2) (2006) 1383–1388, <https://doi.org/10.1016/j.jpowsour.2005.12.043>.
- [329] J. Xia, F. Zhu, L. Wang, G. Wang, Y. Meng, Y. Zhang, In situ coating on LiFePO<sub>4</sub> with ionic liquid as carbon source for high-performance lithium batteries, *J. Nanoparticle Res.* 20 (7) (2018), <https://doi.org/10.1007/s11051-018-4298-z>.
- [330] C. Zou, L. Zhang, X. Hu, Z. Wang, T. Wik, M. Pecht, A review of fractional-order techniques applied to lithium-ion batteries, lead-acid batteries, and supercapacitors, *J. Power Sources* 390 (2018) 286–296, <https://doi.org/10.1016/j.jpowsour.2018.04.033>. February.
- [331] J. Huang, Z. Li, B.Y. Liaw, J. Zhang, Graphical analysis of electrochemical impedance spectroscopy data in Bode and Nyquist representations, *J. Power Sources* 309 (2016) 82–98, <https://doi.org/10.1016/j.jpowsour.2016.01.073>.
- [332] S. Buller, *Impedance-Based Simulation Models for Energy Storage Devices in Advanced Automotive Power Systems*, Shaker Verlag GmbH, 2003.
- [333] J. Song, M.Z. Bazant, Effects of nanoparticle geometry and size distribution on diffusion impedance of battery electrodes, *J. Electrochim. Soc.* 160 (1) (2013) A15–A24, <https://doi.org/10.1149/2.023301jes>.
- [334] J. Song, M.Z. Bazant, Electrochemical impedance of a battery electrode with anisotropic active particles, *Electrochim. Acta* 131 (2014) 214–227, <https://doi.org/10.1016/j.electacta.2014.03.013>.
- [335] J. Illig, M. Ender, A. Weber, E. Ivers-Tiffée, Modeling graphite anodes with serial and transmission line models, *J. Power Sources* 282 (2015) 335–347, <https://doi.org/10.1016/j.jpowsour.2015.02.038>.
- [336] J. Landesfeind, J. Hattendorff, A. Ehrl, W.A. Wall, H.A. Gasteiger, Tortuosity determination of battery electrodes and separators by impedance spectroscopy, *J. Electrochim. Soc.* 163 (7) (2016) A1373–A1387, <https://doi.org/10.1149/2.1141607jes>.
- [337] J. Bisquert, G. Garcia-Belmonte, F. Fabregat-Santiago, N.S. Ferriols, P. Bogdanoff, E.C. Pereira, Doubling exponent models for the analysis of porous film electrodes by impedance. relaxation of  $\text{TiO}_2$  nanoporous in aqueous solution, *J. Phys. Chem. B* 104 (10) (2000) 2287–2298, <https://doi.org/10.1021/jp993148h>.
- [338] CNLS (Complex Nonlinear Least Squares), Immittance, Inversion, and Simulation Fitting Programs, J. R. MacDonald, 2020 accessed, [https://grossmacdonald.com/l\\_evmlevmw/](https://grossmacdonald.com/l_evmlevmw/), 05-27.
- [339] MEISP 3.0:Multiple Electrochemical Impedance Spectra Parameterization, Korea Kumho Petrochemical Co., <http://impedance0.tripod.com/#3>.
- [340] Python-assisted physics-based electrochemical impedance spectroscopy. <https://github.com/thulylinhpham/PyPhyEIS>.
- [341] E. Barsoukov, J.H. Kim, K.S. Hwang, D.H. Kim, C.O. Yoon, H. Lee, Parametric analysis of electrical storage materials: new concept and application, *Synth. Met.* 117 (1–3) (2001) 53–59, [https://doi.org/10.1016/S0379-6779\(00\)00538-5](https://doi.org/10.1016/S0379-6779(00)00538-5).
- [342] J. Bisquert, V.S. Vikhrenko, Analysis of the kinetics of ion intercalation. two state model describing the coupling of solid state ion diffusion and ion binding processes, *Electrochim. Acta* 47 (24) (2002) 3977–3988, [https://doi.org/10.1016/S0013-4686\(02\)00372-9](https://doi.org/10.1016/S0013-4686(02)00372-9).
- [343] D. Aurbach, M.D. Levi, E. Levi, A review on the solid-state ionics of electrochemical intercalation processes: how to interpret properly their electrochemical response, *Solid State Ionics* 179 (21–26) (2008) 742–751, <https://doi.org/10.1016/j.jssi.2007.12.070>.
- [344] R. Huggins, *Advanced Batteries: Materials Science Aspects*, Springer Science & Business Media, 2008, <https://doi.org/10.1007/978-0-387-76424-5>.
- [345] T. Jacobsen, K. West, Diffusion impedance in planar, cylindrical and spherical symmetry, *Electrochim. Acta* 40 (2) (1995) 255–262, [https://doi.org/10.1016/0013-4686\(94\)E0192-3](https://doi.org/10.1016/0013-4686(94)E0192-3).
- [346] S.D. Talian, J. Moskón, R. Dominko, M. Gabersček, Impedance response of porous carbon cathodes in polysulfide redox system, *Electrochim. Acta* 302 (2019) 169–179, <https://doi.org/10.1016/j.electacta.2019.02.037>.
- [347] R. Kronig, On the theory of dispersion of X-rays, *J. Opt. Soc. Am.* 12 (6) (1926) 547, <https://doi.org/10.1364/JOSA.12.000547>.
- [348] M.H.A. Kramers, La diffusion de la lumière par les atomes, *Trans. Volta Centenary Congr* 2 (1927) 545–557.
- [349] C.F. Bohren, What did Kramers and Kronig do and how did they do it? *Eur. J. Phys.* 31 (3) (2010) 573–577, <https://doi.org/10.1088/0143-0807/31/3/014>.
- [350] C.W. Peterson, B.W. Knight, Causality calculations in the time domain: an efficient alternative to the Kramers-Kronig method\*, *J. Opt. Soc. Am.* 63 (10) (1973) 1238, <https://doi.org/10.1364/josa.63.001238>.
- [351] P. Agarwal, M.E. Orazem, L.H. Garcia-Rubio, Measurement models for electrochemical impedance spectroscopy: I. Demonstration of applicability, *J. Electrochim. Soc.* 139 (7) (1992) 1917–1927, <https://doi.org/10.1149/1.2069522>.
- [352] B.A. Boukamp, A linear kronig-kramers transform test for immittance data validation, *J. Electrochim. Soc.* 142 (6) (1995) 1885–1901, <https://doi.org/10.1149/1.2044210>.
- [353] M. Schönleber, D. Klötz, E. Ivers-Tiffée, A method for improving the robustness of linear kramers-kronig validity tests, *Electrochim. Acta* 131 (2014) 20–27, <https://doi.org/10.1016/j.electacta.2014.01.034>.
- [354] O. Alao, P. Barendse, Online condition monitoring of sealed lead acid lithium nickel-cobalt-manganese oxide batteries using broadband impedance spectroscopy, *IEEE Energy Conversion Congress and Exposition, ECCE 2018* (2018) 2026–2032, <https://doi.org/10.1109/ECCE.2018.8558352>, 2018.
- [355] X. Han, L. Lu, Y. Zheng, X. Feng, Z. Li, J. Li, M. Ouyang, A review on the key issues of the lithium ion battery degradation among the whole life cycle, *eTransportation* 1 (2019) 100005, <https://doi.org/10.1016/j.etran.2019.100005>.
- [356] T. Waldmann, A. Iturrondebeitia, M. Kasper, N. Ghanbari, F. Agusse, E. Bektaert, L. Daniel, S. Genies, I.J. Gordon, M.W. Löble, E.D. Vito, M. Wohlfahrt-Mehrens, Review - post-mortem analysis of aged lithium-ion batteries: disassembly methodology and physico-chemical analysis techniques, *J. Electrochim. Soc.* 163 (10) (2016) A2149–A2164, <https://doi.org/10.1149/2.1211609jes>.
- [357] A. Pfarrang, A. Kersys, A. Kriston, D.U. Sauer, C. Rahe, S. Käbitz, E. Figgemeier, Long-term cycling induced jelly roll deformation in commercial 18650 cells, *J. Power Sources* 392 (2018) 168–175, <https://doi.org/10.1016/j.jpowsour.2018.03.065>.
- [358] J. Lamb, C.J. Orendorff, Evaluation of mechanical abuse techniques in lithium ion batteries, *J. Power Sources* 247 (2014) 189–196, <https://doi.org/10.1016/j.jpowsour.2013.08.066>.
- [359] M. Dubarry, V. Svoboda, R. Hwu, B.Y. Liaw, A roadmap to understand battery performance in electric and hybrid vehicle operation, *J. Power Sources* 174 (2) (2007) 366–372, <https://doi.org/10.1016/j.jpowsour.2007.06.237>.
- [360] D. Aurbach, B. Markovsky, A. Radzin, M. Cojocaru, E. Levi, H.-J. Kim, An analysis of rechargeable lithium-ion batteries after prolonged cycling, *Electrochim. Acta* 47 (12) (2002) 1899–1911, [https://doi.org/10.1016/S0013-4686\(02\)00013-0](https://doi.org/10.1016/S0013-4686(02)00013-0).
- [361] A. Pfarrang, F.D. Persio, A. Kriston, N. Lebedeva, V. Ruiz, D. Dams, T. Kosmidou, J. Ungeheuer, I. Adanouj, L. Boon-Brett, *Battery Testing Methods Assessed from a*

- Policy-Making Perspective: Battery Materials and Cell Performance Testing, EVS30 Symposium, 2017.**
- [362] N.P. Lebedeva, F.D. Persio, T. Kosmidou, D. Dams, A. Pfhang, A. Kersys, L. Boon-Brett, Amount of free liquid electrolyte in commercial large format Prismatic Li-Ion battery cells, *J. Electrochem. Soc.* 166 (4) (2019) A779–A786, <https://doi.org/10.1149/2.1151904jes>.
- [363] A.W. Golubkov, D. Fuchs, J. Wagner, H. Wiltsche, C. Stangl, G. Fauler, G. Voitic, A. Thaler, V. Hacker, Thermal-runaway experiments on consumer Li-ion batteries with metal-oxide and olivine-type cathodes, *RSC Adv.* 4 (7) (2014) 3633–3642, <https://doi.org/10.1039/C3RA45748F>.
- [364] L. Somerville, J. Bareño, P. Jennings, A. McGordon, C. Lyness, I. Bloom, The effect of pre-analysis washing on the surface film of graphite electrodes, *Electrochim. Acta* 206 (2016) 70–76, <https://doi.org/10.1016/j.electacta.2016.04.133>.
- [365] M. Klett, R. Eriksson, J. Groot, P. Svens, K. Ciosek Höglström, R.W. Lindström, H. Berg, T. Gustafson, G. Lindbergh, K. Edström, Non-uniform aging of cycled commercial LiFePO<sub>4</sub>/graphite cylindrical cells revealed by post-mortem analysis, *J. Power Sources* 257 (2014) 126–137, <https://doi.org/10.1016/j.jpowsour.2014.01.105>.
- [366] H. Liu, Z. Li, A. Grenier, G.E. Kamm, L. Yin, G.S. Mattei, M.R. Cosby, P. G. Khalilah, P.J. Chupas, K.W. Chapman, Best practices for operando depth-resolving battery experiments, *J. Appl. Crystallogr.* 53 (1) (2020) 133–139, <https://doi.org/10.1107/S1600576719016315>.
- [367] M. Morcrette, Y. Chabre, G. Vaughan, G. Amatucci, J.-B. Leriche, S. Patoux, C. Masquelier, J.-M. Tarascon, In situ X-ray diffraction techniques as a powerful tool to study battery electrode materials, *Electrochim. Acta* 47 (19) (2002) 3137–3149, [https://doi.org/10.1016/S0013-4686\(02\)00233-5](https://doi.org/10.1016/S0013-4686(02)00233-5).
- [368] P. Barpanda, G. Rousse, T. Ye, C.D. Ling, Z. Mohamed, Y. Klein, A. Yamada, Neutron diffraction study of the Li-ion battery cathode Li<sub>2</sub>FeP2O<sub>7</sub>, *Inorg. Chem.* 52 (6) (2013) 3334–3341, <https://doi.org/10.1021/ic302816w>.
- [369] W.K. Pang, V.K. Peterson, A custom battery for operando neutron powder diffraction studies of electrode structure, *J. Appl. Crystallogr.* 48 (1) (2015) 280–290, <https://doi.org/10.1107/S1600576715000679>.
- [370] M. Balasubramanian, X. Sun, X.Q. Yang, J. McBreen, In situ X-ray diffraction and X-ray absorption studies of high-rate lithium-ion batteries, *J. Power Sources* 92 (1) (2001) 1–8, [https://doi.org/10.1016/S0378-7753\(00\)00493-6](https://doi.org/10.1016/S0378-7753(00)00493-6).
- [371] U.W. Arndt, D.C. Creagh, R.D. Deslattes, J.H. Hubbell, P. Indelicato, E.G.K. Jr., E. Lindroth, *International Tables for Crystallography* 4.2 (2006).
- [372] T. Zhang, H. Zhou, A reversible long-life lithium-air battery in ambient air, *Nat. Commun.* 4 (1) (2013) 1817, <https://doi.org/10.1038/ncomms2855>.
- [373] J. Zheng, M.H. Engelhard, D. Mei, S. Jiao, B.J. Polzin, J.-G. Zhang, W. Xu, Electrolyte additive enabled fast charging and stable cycling lithium metal batteries, *Nature Energy* 2 (3) (2017) 17012, <https://doi.org/10.1038/nenergy.2017.12>.
- [374] I. Buchberger, S. Seidlmaier, A. Pokharel, M. Piana, J. Hattendorff, P. Kudejova, R. Gilles, H.A. Gasteiger, Aging analysis of graphite/LiNi<sub>1/3</sub>Mn<sub>1/3</sub>Co<sub>1/3</sub>O<sub>2</sub> cells using XRD, PGAA, and AC impedance, *J. Electrochem. Soc.* 162 (14) (2015) A2737–A2746, <https://doi.org/10.1149/2.0721514jes>.
- [375] Y. Su, Y. Yang, L. Chen, Y. Lu, L. Bao, G. Chen, Z. Yang, Q. Zhang, J. Wang, R. Chen, S. Chen, F. Wu, Improving the cycling stability of Ni-rich cathode materials by fabricating surface rock salt phase, *Electrochim. Acta* 292 (2018) 217–226, <https://doi.org/10.1016/j.electacta.2018.09.158>.
- [376] X. Zhang, W.J. Jiang, A. Mauger, Qilu, F. Gendron, C.M. Julien, Minimization of the cation mixing in Li<sub>1+x</sub>(NMC)<sub>1-x</sub>O<sub>2</sub> as cathode material, *J. Power Sources* 195 (5) (2010) 1292–1301, <https://doi.org/10.1016/j.jpowsour.2009.09.029>.
- [377] H.M. Rietveld, Line profiles of neutron powder-diffraction peaks for structure refinement, *Acta Crystallogr.* 22 (1) (1967) 151–152, <https://doi.org/10.1107/S0365110X67000234>.
- [378] H.M. Rietveld, A profile refinement method for nuclear and magnetic structures, *J. Appl. Crystallogr.* 2 (2) (1969) 65–71, <https://doi.org/10.1107/S002188969006558>.
- [379] F. Lin, I.M. Markus, D. Nordlund, T.-C. Weng, M.D. Asta, H.L. Xin, M.M. Doeff, Surface reconstruction and chemical evolution of stoichiometric layered cathode materials for lithium-ion batteries, *Nat. Commun.* 5 (1) (2014) 3529, <https://doi.org/10.1038/ncomms4529>.
- [380] C.S. Johnson, N. Li, C. Lefief, J.T. Vaughney, M.M. Thackeray, Synthesis, characterization and electrochemistry of lithium battery electrodes: xLi<sup>2</sup>MnO<sup>3(1-x)</sup>LiMn<sup>0.333</sup>Ni<sup>0.333</sup>Co<sup>0.333</sup>O<sup>2</sup> (0≤x≤0.7), *Chem. Mater.* 20 (19) (2008) 6095–6106, <https://doi.org/10.1021/cm801245r>.
- [381] E. Meza, J. Ortiz, D. Ruiz-León, J.F. Marco, J.L. Gautier, Lithium-nickel cobalt oxides with spinel structure prepared at low temperature. XRD, XPS, and EIS measurements, *Mater. Lett.* 70 (2012) 189–192, <https://doi.org/10.1016/j.materlet.2011.11.108>.
- [382] D. Mohanty, S. Kalnaus, R.A. Meisner, K.J. Rhodes, J. Li, E.A. Payzant, D.L. Wood, C. Daniel, Structural transformation of a lithium-rich Li<sub>1.2</sub>Co<sub>0.1</sub>Mn<sub>0.55</sub>Ni<sub>0.15</sub>O<sub>2</sub> cathode during high voltage cycling resolved by in situ X-ray diffraction, *J. Power Sources* 229 (2013) 239–248, <https://doi.org/10.1016/j.jpowsour.2012.11.144>.
- [383] Y. Li, M. Bettge, B. Polzin, Y. Zhu, M. Balasubramanian, D.P. Abraham, Understanding long-term cycling performance of Li<sub>1.2</sub>Ni<sub>0.15</sub>Mn<sub>0.55</sub>Co<sub>0.1</sub>O<sub>2</sub>-graphite lithium-ion cells, *J. Electrochem. Soc.* 160 (5) (2013) A3006–A3019, <https://doi.org/10.1149/2.002305jes>.
- [384] F. Friedrich, B. Strehle, A.T.S. Freiberg, K. Kleiner, S.J. Day, C. Erk, M. Piana, H. A. Gasteiger, Capacity fading mechanisms of NCM-811 cathodes in lithium-ion batteries studied by X-ray diffraction and other diagnostics, *J. Electrochem. Soc.* 166 (15) (2019) A3760–A3774, <https://doi.org/10.1149/2.0821915jes>.
- [385] D. Saurel, J. Segalini, M. Jauregui, A. Pendasheth, B. Daffos, P. Simon, M. Casas-Cabanás, A SAXS outlook on disordered carbonaceous materials for electrochemical energy storage, *Energy Storage Materials* 21 (2019) 162–173, <https://doi.org/10.1016/j.ensm.2019.05.007>.
- [386] M. Povia, J. Sottmann, G. Portale, K.D. Knudsen, S. Margadonna, S. Sartori, Operando SAXS/WAXS on the a-P/C as the anode for Na-ion batteries, *J. Phys. Chem. C* 122 (11) (2018) 5917–5923, <https://doi.org/10.1021/acs.jpcc.7b12825>.
- [387] T.-G. Jeong, J. Chun, B.-W. Cho, J. Lee, Y.-T. Kim, Enhanced performance of sulfur-infiltrated bimodal mesoporous carbon foam by chemical solution deposition as cathode materials for lithium sulfur batteries, *Sci. Rep.* 7 (1) (2017) 42238, <https://doi.org/10.1038/srep42238>.
- [388] J. McBreen, The application of synchrotron techniques to the study of lithium-ion batteries, *J. Solid State Electrochem.* 13 (7) (2009) 1051–1061, <https://doi.org/10.1007/s10008-008-0685-1>.
- [389] M. Hirayama, H. Ido, K. Kim, W. Cho, K. Tamura, J. Mizuki, R. Kanno, Dynamic structural changes at LiMn<sub>2</sub>O<sub>4</sub>/electrolyte interface during lithium battery reaction, *J. Am. Chem. Soc.* 132 (43) (2010) 15268–15276, <https://doi.org/10.1021/ja105389t>.
- [390] N. Yamakawa, M. Jiang, B. Key, C.P. Grey, Identifying the local structures formed during lithiation of the conversion material, iron fluoride, in a Li ion battery: a solid-state NMR, X-ray diffraction, and pair distribution function analysis study, *J. Am. Chem. Soc.* 131 (30) (2009) 10525–10536, <https://doi.org/10.1021/ja902639w>.
- [391] B. Key, M. Morcrette, J.-M. Tarascon, C.P. Grey, Pair distribution function analysis and solid state NMR studies of silicon electrodes for lithium ion batteries: understanding the (De)lithiation mechanisms, *J. Am. Chem. Soc.* 133 (3) (2011) 503–512, <https://doi.org/10.1021/ja108085d>.
- [392] D. Zeng, J. Cabana, J. Bréger, W.-S. Yoon, C.P. Grey, Cation ordering in Li<sub>x</sub>Ni<sub>1-x</sub>Mn<sub>x</sub>Co<sub>1-2x</sub>O<sub>2</sub>-layered cathode materials: a nuclear magnetic resonance (NMR), pair distribution function, X-ray absorption spectroscopy, and electrochemical study, *Chem. Mater.* 19 (25) (2007) 6277–6289, <https://doi.org/10.1021/cm702241a>.
- [393] J. Wu, M. Fenech, R.F. Webster, R.D. Tilley, N. Sharma, Electron microscopy and its role in advanced lithium-ion battery research, *Sustainable Energy and Fuels* 3 (7) (2019) 1623–1646, <https://doi.org/10.1039/c9se00038k>.
- [394] M. Koltypin, D. Aurbach, L. Nazar, B. Ellis, More on the performance of LiFePO<sub>4</sub> electrodes-The effect of synthesis route, solution composition, aging, and temperature, *J. Power Sources* 174 (2) (2007) 1241–1250, <https://doi.org/10.1016/j.jpowsour.2007.06.045>.
- [395] N. Dupré, J.F. Martin, J. Degryse, V. Fernandez, P. Soudan, D. Guyomard, Aging of the LiFePO<sub>4</sub> positive electrode interface in electrolyte, *J. Power Sources* 195 (21) (2010) 7415–7425, <https://doi.org/10.1016/j.jpowsour.2010.05.042>.
- [396] K. Amine, J. Liu, J. Belharouak, High-temperature storage and cycling of C-LiFePO<sub>4</sub>/graphite Li-ion cells, *Electrochim. Commun.* 7 (7) (2005) 669–673, <https://doi.org/10.1016/j.elecom.2005.04.018>.
- [397] K. Striebel, J. Shim, A. Sierra, H. Yang, X. Song, R. Kostecki, K. McCarthy, The development of low cost LiFePO<sub>4</sub>-based high power lithium-ion batteries, *J. Power Sources* 146 (1–2) (2005) 33–38, <https://doi.org/10.1016/j.jpowsour.2005.03.119>.
- [398] G. Zampardi, F. La Mantia, Solid-Electrolyte Interphase at the Positive Electrodes in High Energy Li-ion Batteries: Current Understanding and Analytical Tools, *Batteries & Supercaps* 3 (8) (2020) 672–697, <https://doi.org/10.1002/batt.201900177>.
- [399] J.Y. Song, H.H. Lee, Y.Y. Wang, C.C. Wan, Two- and three-electrode impedance spectroscopy of lithium-ion batteries, *J. Power Sources* 111 (2) (2002) 255–267, [https://doi.org/10.1016/S0378-7753\(02\)00310-5](https://doi.org/10.1016/S0378-7753(02)00310-5).
- [400] C.H. Chen, J. Liu, K. Amine, Symmetric cell approach and impedance spectroscopy of high power lithium-ion batteries, *J. Power Sources* 96 (2) (2001) 321–328, [https://doi.org/10.1016/S0378-7753\(00\)00666-2](https://doi.org/10.1016/S0378-7753(00)00666-2).
- [401] R. Raccichini, L. Furness, J.W. Dibden, J.R. Owen, N. García-Aráez, Impedance characterization of the transport properties of electrolytes contained within porous electrodes and separators useful for Li-S batteries, *J. Electrochim. Soc.* 165 (11) (2018) A2741–A2749, <https://doi.org/10.1149/2.0631811jes>.
- [402] C.-H. Chen, F. Planella, K. O'Regan, D. Gastol, D. Widanagea, E. Kendrick, Development of experimental techniques for parameterization of multi-scale lithium-ion battery models, *J. Electrochim. Soc.* 167 (2020), 080534, <https://doi.org/10.1149/1945-7111/ab9050>.
- [403] B.N. Popov, A. Durairajan, Y. Podrazhansky, R.C. Cope, Capacity fade of Li-ion cells: comparison of DC and ENREV charging protocols, in: Proceedings of the Annual Battery Conference on Applications and Advances 2000-Janua (Dmc), 2000, pp. 185–191, <https://doi.org/10.1109/BAAA.2000.838402>.